




2018

Comparison Between the Structure-Function Relationship in the Wild Type G α i1 Protein and Its Oncogenic Mutant

Jesse Lee Goossens

Follow this and additional works at: https://ecommons.luc.edu/luc_diss

 Part of the [Biochemistry, Biophysics, and Structural Biology Commons](#)

Recommended Citation

Goossens, Jesse Lee, "Comparison Between the Structure-Function Relationship in the Wild Type G α i1 Protein and Its Oncogenic Mutant" (2018). *Dissertations*. 2957.

https://ecommons.luc.edu/luc_diss/2957

This Dissertation is brought to you for free and open access by the Theses and Dissertations at Loyola eCommons. It has been accepted for inclusion in Dissertations by an authorized administrator of Loyola eCommons. For more information, please contact ecommons@luc.edu.



This work is licensed under a [Creative Commons Attribution-NonCommercial-No Derivative Works 3.0 License](#).
Copyright © 2018 Jesse Lee Goossens

LOYOLA UNIVERSITY CHICAGO

COMPARISON BETWEEN THE STRUCTURE-FUNCTION RELATIONSHIP IN THE WILD TYPE $G_{\alpha 1}$
PROTEIN AND IN ONE OF ITS ONCOGENIC MUTANTS

A DISSERTATION SUBMITTED TO
THE FACULTY OF THE GRADUATE SCHOOL
IN CANDIDACY FOR THE DEGREE OF
DOCTOR OF PHILOSOPHY

PROGRAM IN CHEMISTRY

BY

JESSE L GOOSSENS

CHICAGO, IL

AUGUST 2018

Copyright by Jesse Goossens, 2018
All rights reserved.

ACKNOWLEDGMENTS

I am exceedingly grateful to all the people who have helped make this dissertation possible. Firstly, my graduate advisor, Prof. Duarte Mota de Freitas, for training me to think critically to design meaningful experiments, the thoroughness to properly analyze data, and the skills necessary to convey results to others, which are some of the most important qualities of conducting great research.

I would also like to thank Prof. Dali Liu and Prof. Ken Olsen for the time they have dedicated as committee members and their contributions to my project have been invaluable. I would also like to thank Prof. Miguel Ballicora for the help and support he has given me throughout my graduate career both in and out of the classroom.

Brian Levenson and the other graduate students in the chemistry department have been wonderful to work with and have become good friends that I hope to get the opportunity to work with again in the future.

My mother, father, and brother have been an incredible support system and have never stopped believing in me. Their support has been invaluable in my endeavors.

Finally, I would like to thank my wife Andrea for her overwhelming support throughout this very long and sometimes difficult time in my life. At times, it seemed it would never end but she always had faith in me and gave me the motivation necessary to lift my morale and help me

to continue. She was willing to put her dreams on hold so I can accomplish mine out of pure selflessness and love. I could not have gotten this far without her.

For my children, Mason and Isla

TABLE OF CONTENTS

ACKNOWLEDGMENTS.....	iii
LIST OF TABLES	viii
LIST OF FIGURES	ix
LIST OF ABBREVIATIONS	xi
ABSTRACT	xvi
CHAPTER ONE: INTRODUCTION	1
Cell Signaling and the History of G-proteins.....	1
Heterotrimeric G-proteins.....	1
The α Subunit	2
Mechanism of GTP Hydrolysis	7
The $\beta\gamma$ Heterodimer	8
The Adenylate Cyclase Effector	9
Folding of G-Proteins and Disease States	10
Folding Overview	10
Spectroscopic Techniques Used for Studying G_{α} Proteins.....	13
Fluorescence Spectroscopy.....	13
Ultraviolet/Visible Spectroscopy.....	20
Circular Dichroism Spectrophotometry.....	21
Project Aims	24
CHAPTER TWO: COMPARISON OF THE STRUCTURE-FUNCTION RELATIONSHIPS IN WILD-TYPE $G_{\alpha i1}$ AND IN ITS R208Q MUTANT	27
Introduction	27
Materials and Methods	30
Cloning and Mutagenesis	30
Expression, Purification, and Preparation of G_{α} proteins.....	30
Crystallization Conditions, Data Collection and Structure Determination	32
Fluorescence Activity Assays.....	31
Malachite Green Assay	31
Molecular Dynamics Simulations	32
Results and Discussion.....	33
Fluorescence Changes Resulting from Nucleotide Exchange.....	33
Fluorescence Changes Resulting from GTP Hydrolysis.....	36
Structure of the R208Q $G_{\alpha i1}$ mutant	38
Computer Modeling of Intermolecular Interactions	42
Conclusion.....	50

CHAPTER THREE: PROTEIN FOLDING OF THE R208Q MUTANT	52
Introduction	52
Materials and Methods	54
Expression and Protein Purification.....	54
Fluorescence Monitored GTP γ S Exchange	55
Fluorescence-Measured Protein Denaturation.	55
UV/Vis-Measured Protein Denaturation	56
CD-Measured Protein Denaturation.....	56
Results and Discussion.....	57
The π -Cation interaction in G α Subunits.....	57
Temperature Denaturation of G α Proteins.....	62
Solvent Exposure of Trp residues.....	63
Solvent Exposure of Tyr residues and temperature dependence of secondary structure.....	66
Secondary Structure Content.....	67
Conclusion	69
APPENDIX A EFFECT OF A DOUBLE MUTANT ON THE SWITCH II REGION	71
APPENDIX B GLYCOGEN SYNTHASE KINASE 3 β	81
REFERENCES	89
VITA.....	103

LIST OF TABLES

Table 1. Families of G_{α} subunits and their effects on cell signaling	4
Table 2. Pseudo first-order rate constants for GTP γ S exchange and GTP hydrolysis.....	38
Table 3. Refinement statistics of R208Q $G_{\alpha i1}$ crystal structure	40
Table 4. Interaction energies and distances between residues involved in GTP hydrolysis.....	46
Table 5. Calculated interaction energies within residues from the WT $G_{\alpha i1}$ and Arg mutants.....	60
Table 6. Change in SASA exposure of W residues in WT $G_{i\alpha 1}$ and R208Q Mutant	61
Table 7. Estimated melting temperature G_{α} WT and mutant proteins.....	64
Table 8. T_m estimates of WT $G_{\alpha i1}$ and mutant inGDP, AMF, and GTP γ S conformations	80

LIST OF FIGURES

Figure 1. Schematic representation of G-protein coupled receptor signaling.	3
Figure 2. Crystal structure of WT $G_{\alpha i1}$ •GTP γ S superimposed on $G_{\alpha t}$ •GDP	5
Figure 3. Key interactions that facilitate GTP hydrolysis.....	8
Figure 4. Schematic representation of the energy landscape during folding.....	13
Figure 5. Jablonsky diagram outlining the process of fluorescence.....	15
Figure 6. Charge distribution in π -cation interactions	19
Figure 7. Crystal structure of $G_{\alpha i1}$ •GTP γ S depicting key for spectral analysis	22
Figure 8. Principles of circular dichroism	23
Figure 9. Changes in fluorescence resulting from exchange of GDP for GTP γ S	35
Figure 10. GTP hydrolysis monitored by time-based fluorescence emission	37
Figure 11. Structure of R208Q $G_{\alpha i1}$ •GTP γ S (teal) superimposed on WT $G_{\alpha i1}$ •GTP γ S	41
Figure 12. Superposition of the WT and mutant nucleotide binding sites after simulation.....	45
Figure 13. SASA of the residues that interact with the C1 domain of AC	49
Figure 14. Interaction energies between $G_{\alpha s}$ and AC.....	50
Figure 15. Crystal structure of WT $G_{s\alpha}$ •GTP γ S.....	54
Figure 16. The hydrophobicity of the microenvironment surrounding W211	58
Figure 17. Normalized emission spectra of WT $G_{\alpha s}$ •GDP•Mg ²⁺	59
Figure 18. Temperature variation of the difference between the λ_{max} values.....	61

Figure 19. Movement of residues interaction in WT $G_{\alpha 1}$ R208Q.....	62
Figure 20. Emission Spectra of WT and R208Q $G_{\alpha 1}$ proteins in the GTPyS conformations.....	63
Figure 21. Temperature dependence of fluorescence emission.....	65
Figure 22. Intrinsic Trp fluorescence of WT and R208Q $G_{\alpha 1}$ proteins	68
Figure 23. Calculated % secondary structure	69
Figure 24. WT $G_{\alpha 1}$ structure causing a red shift.....	73
Figure 25: Activation with AlF_4^- of WT $G_{\alpha 1}$, R208Q $G_{\alpha 1}$ proteins, and the R205A/R208Q double mutant	75
Figure 26. Shift in maximal wavelength at 20 °C λ_{max} vs temp	76
Figure 27. Trypsin digest of G_{α} proteins in the inactive and active conformations.....	78
Figure 28. Crystal structure of GSK-3 β	84
Figure 29. PCR analysis of bacterial colonies.....	86
Figure 30. Transfected Sf-9 Cells under a light microscope.....	87
Figure 31. Western blot analysis of GSK-3 in Sf-9 whole cell lysate	88

LIST OF ABBREVIATIONS

2XYT	2X yeast extract tryptone
A	Alanine
AC	Adenylyl Cyclase
ADP	Adenosine 5' –diphosphate
ATP	Adenosine 5' –triphosphate
AlCl ₃	Aluminum chloride
AlF ₄ ⁻	Tetrafluoroaluminate (III)
AMF	Aluminum magnesium fluoride
(NH ₄) ₂ SO ₃	Ammonium sulfite
ANS	8-Anilinonaphthalene-1-sulfonic acid
BSA	Bovine Serum Albumin
<i>c</i>	Speed of light constant
C-terminus	Carboxyl terminus
cAMP	3',5' -cyclic adenosine monophosphate
C _α	Alpha carbon
Ca ²⁺	Calcium ion
CD	Circular dichroism
cGMP	3',5' -cyclic Guanosine monophosphate

ΔE	Change in energy
$\Delta\lambda_{\max}$	Change in wavelength at maximal absorbance
DTT	Dithiothreitol
ϵ	Extinction coefficient
E	Glutamate
E_i	Interaction Energy
EDTA	Ethylenediaminetetraacetic acid
EGTA	Ethylene glycol – bis (β – aminoethylether) – N,N,N',N' – tetra acetic acid
EPAC	Exchange factor directly activated by cAMP I
FPLC	Fast performance liquid chromatography
G	Glycine
GAP	GTPase activating protein
GDP	Guanosine 5'-diphosphate
$GDP \bullet AlF_4^-$	Guanosine 5'-diphosphate tetrafluoroaluminate complex
G_α	α subunit of a heterotrimeric G protein
$G_{\alpha 12}$	α subunit of the heterotrimeric G protein 12 subfamily
$G_{\alpha 13}$	α subunit of the heterotrimeric G protein 13 subfamily
$G_{\alpha i 1}, G_{\alpha i 2}, G_{\alpha i 3}$	Isoforms of α subunits of the inhibitory G protein of AC
$G_{\alpha i} \bullet AMF$	Activated α subunit complexed with AlF_4^-
$G_{\alpha i 1} \bullet GDP$	Inactive α subunit complexed with GDP

$G_{\alpha i1} \bullet GTP\gamma S$	Activated α subunit complexed with $GTP\gamma S$
$G_{\alpha olf}$	α subunit of the stimulatory G protein of AC in olfactory cells
$G_{\alpha q}$	α subunit of the stimulatory G protein that activates PLC
$G_{\alpha s}$	α subunit of the stimulatory G protein of AC
$G_{\alpha t}$	α subunit of the transducin heterotrimeric G protein
G_{β}	β subunit of a heterotrimeric G protein
G_{γ}	γ subunit of a heterotrimeric G protein
GPCR	G-protein coupled receptor
GRIN1	Glutamate [NMDA] receptor subunit zeta-1
GRIN2	Glutamate [NMDA] receptor subunit zeta-2
GSK3 β	Glycogen Synthase Kinase 3 β
GTP	Guanosine 5'-triphosphate
$GTP\gamma S$	Guanosine 5'-[γ -thio]triphosphate
HCl	Hydrochloric acid
I	Isoleucine
h	Planck's constant
HEPES	4-(2-hydroxyethyl)-1-piperazineethanesulfonic acid
His ₆ - $G_{\alpha i1}$	N – terminus hexahistidine tagged $G_{\alpha i1}$ protein
iNOS	Inducible nitric oxide synthases
K	Lysine
k	Rate constant

λ_{\max}	Wavelength at maximal absorbance
L	Leucine
M	Molar
Mg^{2+}	Magnesium ion
MgCl_2	Magnesium chloride
MgSO_4	Magnesium Sulfate
MOI	Multiplicity of Infection
Mol	Mole
N	Asparagine
ν	Frequency
N-terminus	Amino terminus
NaCl	Sodium chloride
NaF	Sodium fluoride
NaH_2PO_4	Sodium dihydrogen phosphate
NAMD	Nanoscale Molecular Dynamics
NaOH	Sodium hydroxide
NO	Nitric oxide
OD	Optical density
PDE	Phosphodiesterase
pfu	Plaque forming units
P_i	Inorganic phosphate

PKA	Protein kinase A
PLC	Phospholipase C
PLD	Phospholipase D
PP _i	Pyrophosphate
PDB	Protein data bank
Q	Glutamine
R	Arginine
RAP1	Ras related protein 1
RGS	Regulator of G-protein signaling
RMSD	Root mean square deviation
SASA	Surface accessible surface area
SDS	Sodium dodecyl sulfate
SDS – PAGE	Sodium dodecyl sulfate polyacrylamide gel electrophoresis
T	Threonine
t _{1/2}	Half-life
Tris – Cl	Tris(hydroxymethyl)amino methane
UV/Vis	Ultraviolet visible spectrophotometry
VMD	Visual Molecular Dynamics
W	Tryptophan
WT	Wild-Type

ABSTRACT

Many signal transduction pathways are regulated by guanine nucleotide-binding (G_{α}) proteins, which function as molecular switches fluctuating between active and inactive conformations. Proper function depends on three flexible switch regions that are involved in the relatively slow hydrolysis of GTP. Deep sequencing studies have found mutations in the *GNAS* and *GNAI1* genes involved in tumorigenesis, among which include a mutation corresponding to a highly conserved arginine residue in the switch II region. A mutation in *GNAI1* encoding an R208Q change in $G_{\alpha i1}$ has been linked to intestinal cancers. We investigated the molecular basis of oncogenesis of this mutant by studying the kinetics of nucleotide binding and single-turnover GTP hydrolysis. We demonstrated that, relative to the corresponding wild-type proteins, this mutation hindered nucleotide exchange; however, the rate of GTP hydrolysis was lower in R208Q $G_{\alpha i1}$. The R208Q $G_{\alpha i1}$ mutant was crystallized and its X-ray structure was compared to that of the wild-type protein and was also used to conduct molecular dynamics simulations. These studies suggested that changes in the rates of hydrolysis can be attributed to alterations in the microenvironments of the nucleotide binding site which seemingly destabilize the switch II region but do not perturb the surface of the protein. The mutation presumably results in a decrease in the production of the secondary messenger cAMP *via* its interaction with the effector adenylyl cyclase that might promote oncogenesis in tumor cells. Furthermore, we investigated the folding and structural integrity of the protein with three spectroscopic

techniques. We showed that for the mutant, both the active and inactive conformations have similar melting temperatures, which are comparable to the inactive conformation of the wild-type protein but lower relative to the active conformation.

CHAPTER ONE

CELL SIGNALING AND THE HISTORY OF G-PROTEINS

Complex organisms are composed of a remarkably complex network of individual cells working harmoniously to form what we know as life. Cell signaling is central for survival and is the relay of messages between cells, which are involved in everything from cell division to apoptosis. A signaling molecule, such as a hormone or a neurotransmitter, binds to an extracellular receptor. It then transmits the signal to the inside of the cell using a variety of intermediary proteins that function as binary switches, alternating between “on” and “off” states that propagate the signal via secondary messengers. Guanine nucleotide-binding proteins (G-proteins) are among the most common signal transducing proteins found in the cell.

Alfred Gilman and Martin Rodbell conducted the initial landmark studies on G-proteins. Their work was deemed so important that they received the Nobel Prize in 1994 in Physiology or Medicine (1-3). All G-proteins are involved in signaling but differ in their mechanisms and are classified as either monomeric small GTPases, such as the Ras superfamily, or larger heterotrimeric membrane-bound proteins (4). This study will focus on the latter.

Heterotrimeric G-proteins

Heterotrimeric G-proteins are comprised of an α (G_α), β (G_β), and a γ (G_γ), subunit and work synergistically with a heptahelical transmembrane receptor protein, a G-protein coupled receptor (GPCR) (4). In the resting state, the GDP-bound $G_{\alpha\beta\gamma}$ trimer interacts with a GPCR. When

the GPCR becomes stimulated, a conformational change in the G_{α} subunit occurs that causes it to release GDP and bind GTP, which further leads to the dissociation from the $G_{\beta\gamma}$ subunits and the receptor (Figure 1). The active $G_{\alpha}\cdot\text{GTP}$ diffuses along the membrane until it reaches an effector, which then uses secondary messengers to induce a response inside the cell. The signal terminates when the bound GTP hydrolyzes to GDP at which point the $G_{\alpha\beta\gamma}$ complex is reformed (Figure 1). GTPase activity, which requires a Mg^{2+} cofactor, is relatively inefficient to permit adequate signal propagation. Therefore, the intensity of the signal is dependent on the time it takes G_{α} to hydrolyze GTP to GDP (4-6).

Humans have roughly 865 different GPCRs that elicit different cellular responses using relatively few G-protein complexes (7). There are 16 G_{α} genes that encode 23 different proteins, 5 G_{β} genes that encode 6 proteins and 12 G_{γ} genes (7). G_{α} proteins vary widely in their function and expression patterns and are classified into four subfamilies according to sequence homology: $G_{\alpha s}$, $G_{\alpha i}$, $G_{\alpha q}$, $G_{\alpha 12}$ (Table 1) (4, 8-11). $G_{\alpha i1}$ (and to a lesser extent $G_{\alpha s}$) are the primary focus of this research.

The α Subunit

G_{α} proteins are highly conserved and found in almost all eukaryotes (12). Sequence similarity between G_{α} proteins vary between 35% and 95% but all are composed of two domains: a GTPase domain and a α -helical domain (Figure 2). The GTPase domain is structurally and mechanistically similar to the small monomeric GTPase family of G-proteins and is comprised of five α -helices surrounding six-stranded β -sheets at the core (5). Beginning at the N-terminus, each individual α -helix are numbered $\alpha 1$ - $\alpha 5$ and each β -sheet as $\beta 1$ - $\beta 6$ (Figure 2).

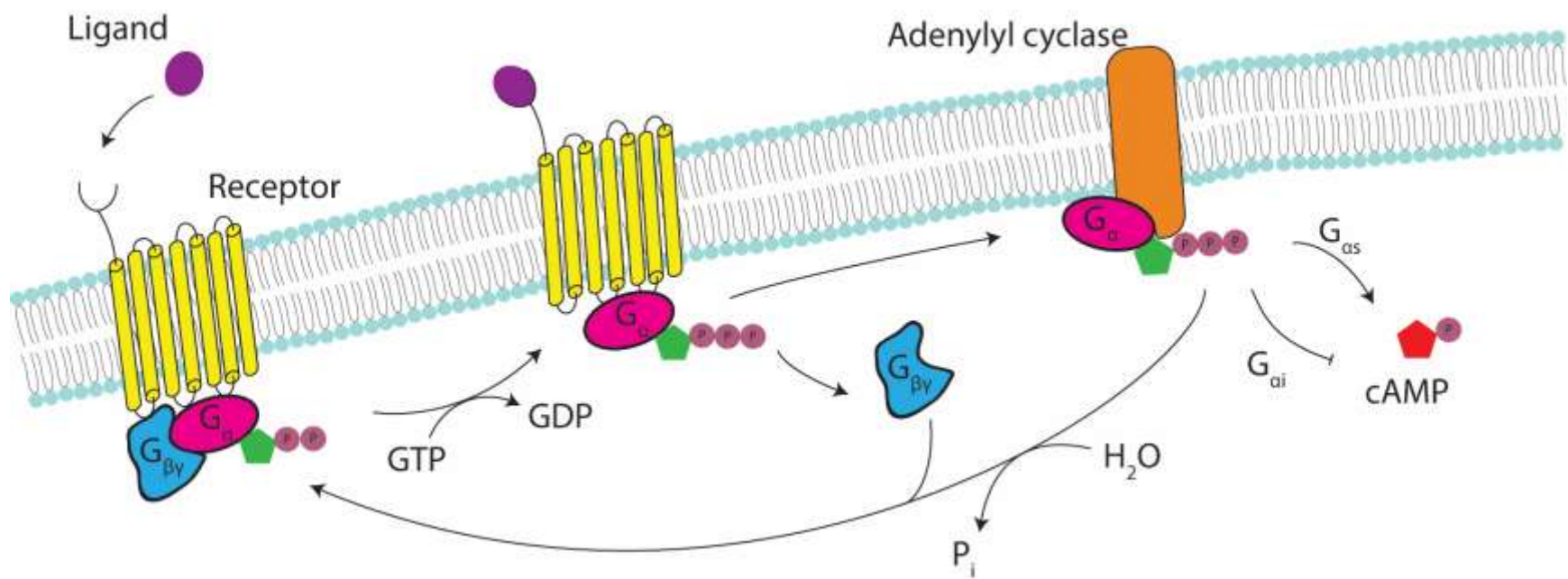


Figure 1. Schematic representation of the pathway of G-protein coupled receptor signaling.

Table 1. Families of G α subunits and their effects on cell signaling. For further detail see (4).

G α protein	Expression	Receptor(s) for	Effector(s)	Cellular Response
G α_s - subfamily				
G α_s (S, L)	Universal	Adrenalin, noradrenalin, dopamine, glucagon	Adenylyl Cyclase	cAMP \uparrow
G α_{olf}	Olfactory cells	Odorants	Adenylyl Cyclase	cAMP \uparrow
G α_i - subfamily				
G α_{i1}	Neuronal cells	Noradrenalin, prostaglandins, opiates	Adenylyl Cyclase	cAMP \downarrow
G α_{i2}	Universal Nonneuronal	Noradrenalin, prostaglandins, opiates	Rap1, GAP	cGMP \downarrow
G α_{i3}	cells	Noradrenalin, prostaglandins, opiates	GRIN1, GRIN2	cGMP \downarrow
G α_{t1}	Rods	Photons	cGMP-PDE	cGMP \downarrow
G α_{t2}	Cones	Photons	cGMP-PDE	cGMP \downarrow
G α_q - subfamily				
G α_q	Universal	Acetylcholine, serotonin, vasopressin, epinephrine	PLC	Ca $^{2+}$ \uparrow
G α_{12} - subfamily				
G α_{12}	Universal	LPA, thrombin	PLD	NO \uparrow
G α_{13}	Universal	LPA, thrombin	iNOS	NO \uparrow

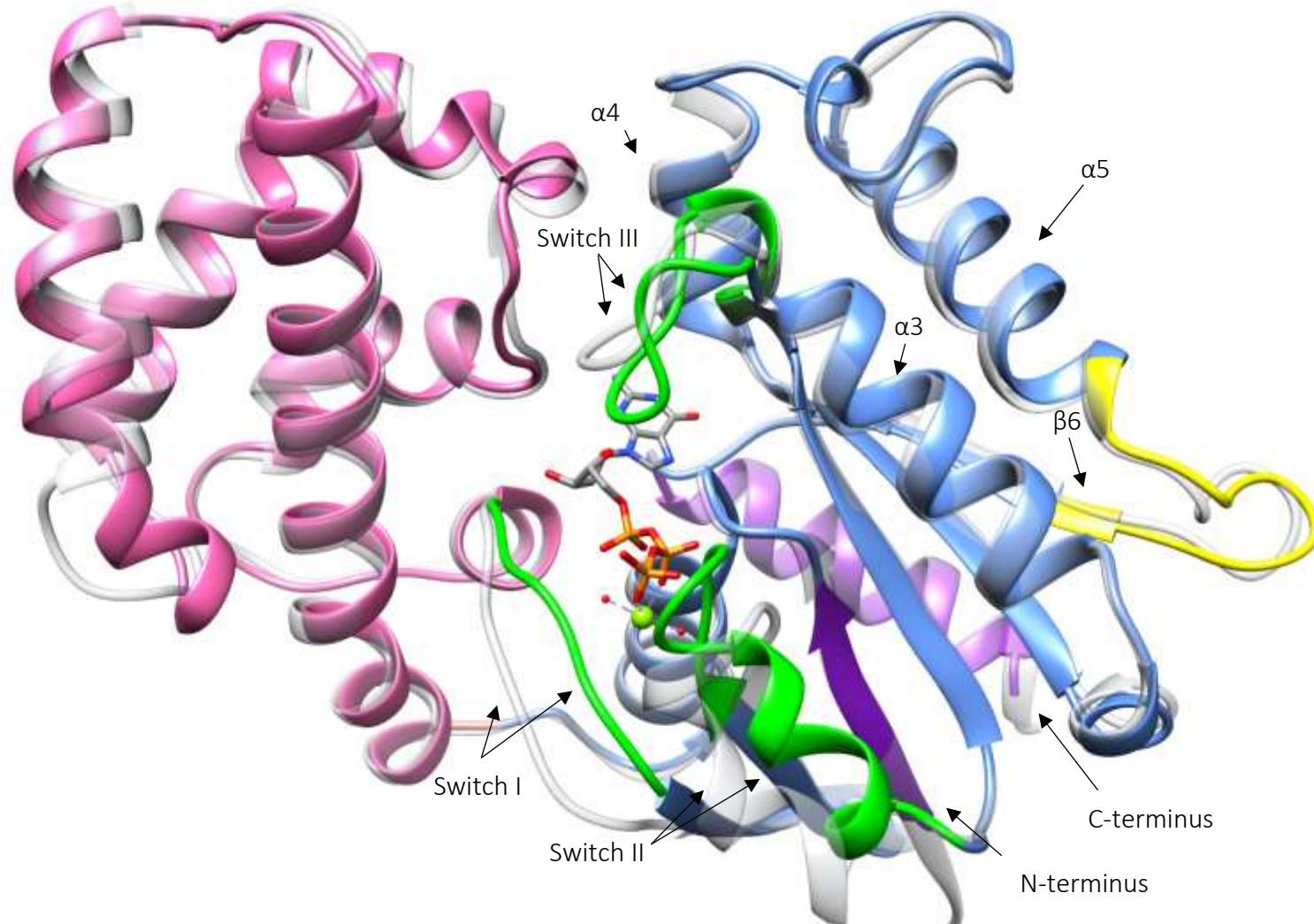


Figure 2. Crystal structure of WT $G_{\alpha i1} \cdot GTP\gamma S$ (colored [PDB ID: 1GIA]) superimposed on $G_{\alpha t} \cdot GDP$ (gray [1TAG]) to illustrate the structural differences between the active and inactive conformations. $G_{\alpha i1} \cdot GDP$ is disordered in the switch II region. $G_{\alpha t} \cdot GDP$ closely resembles $G_{\alpha i1} \cdot GDP$ and is used in place of $G_{\alpha i1}$ to illustrate the differences in the switch II region. The GTPase domain (blue) contains the active site in which the switch regions are located (green). The amino and carboxyl termini (purple) and the adenylyl cyclase binding site (yellow and switch II) are also in the GTPase domain. The α -helical domain denoted in pink.

The GTPase domain contains the active site where there are five highly conserved sequences necessary for binding of the nucleotide and the cofactor. The diphosphate binding P-loop (GXGESGKS) and the guanine ring binding motifs (NKXD) and (TCAT) bind the guanine nucleotide while two conserved motifs (RXXTXGI) and (DXXG) anchor the Mg^{2+} cofactor (4, 5).

Also of importance in the GTPase domain are the three flexible regions known as switches I, II, and III. The switches are the most dynamic regions of the protein and reside near the γ - phosphate of GTP; their positioning is dependent on the type of nucleotide that is bound (Figure 2 shown in green). In the inactive conformation, the switches are unordered which allows for GDP to escape the active site (13, 14) but upon binding to GTP, switches II and III become more rigid and form a lid over the nucleotide (15, 16). Switches I and II are also important interfaces with G_{β} for the formation of the heterotrimer (17), and interact with effectors in some instances (18-20). Finally, the N-terminus in the GTPase domain also undergoes a post-translational modification and becomes lipidated. $G_{\alpha i1}$ becomes myristoylated by myristoyl CoA while $G_{\alpha s}$ becomes palmitoylated by palmitoyl CoA (21-23). In the case of $G_{\alpha i1}$, the N-terminus is unordered but upon myristoylation, forms an ordered α -helix (21, 22, 24). The myristol group, a 14-carbon fatty acid, attaches to a glycine residue at the N-terminus *via* an amide bond, which allows the G_{α} subunit to interact with the $G_{\beta\gamma}$ complex via the G_{γ} subunit and anchor the complex to the membrane (21, 24-26).

The α -helical domain contains six α -helices designated by letters A through F with A being closer to the N – terminus and F being near the C – terminus (5). Interestingly, there is less homology amongst G_{α} proteins in the α helical domain, which enhances the specificity of G_{α}

proteins to distinct receptors and effectors (27, 28). The α helical domain also gives the G-protein an increased affinity for guanine nucleotides (29, 30).

GTPase activating proteins (GAPs) are proteins that add an additional layer of regulation. The binding of a GAP (such as regulator of G – protein signaling 4 [RGS4]) to a G_{α} protein enhances the GTPase activity and promotes GTP hydrolysis (31, 32). GTPase rates can be as much as 1000 fold higher when a GAP is present (33).

Mechanism of GTP Hydrolysis

Conceptualizing a mechanism for GTP hydrolysis has proven to be challenging. G_{α} proteins contain highly conserved catalytic residues that act to stabilize charge build-up around GTP. Furthermore, $G_{\alpha i1}$ proteins properly position a water molecule for a nucleophilic attack near the γ – phosphate of GTP (Figure 3). The transition state of GTP during its hydrolysis is not well understood due to the presence of d orbitals on the phosphorous atom of the γ -phosphate. Furthermore, it is not known if the mechanism of hydrolysis is associative, dissociative, or a combination thereof (34, 35). An associative transition state would utilize a base that would remove a proton from a molecule of H_2O at the active site, priming it for a nucleophilic attack on the γ – phosphate. Conversely, a dissociative mechanism would involve bond cleavage between the terminal phosphates resulting in a shift in negative charge from the γ to the β phosphate causing the γ – phosphate to become a stable leaving group (35). There are two highly conserved residues in the switch II region of G_{α} proteins that could accomplish this (6). In wild-type $G_{\alpha i1}$ ($WTG_{\alpha i1}$), Glutamine (Q) 204 and the carbonyl functional group of glycine (G) 203 are in a

position to facilitate such a mechanism. Similarly, arginine (R) 187 in the switch I region has been shown to be critical for catalytic activity (36-38).

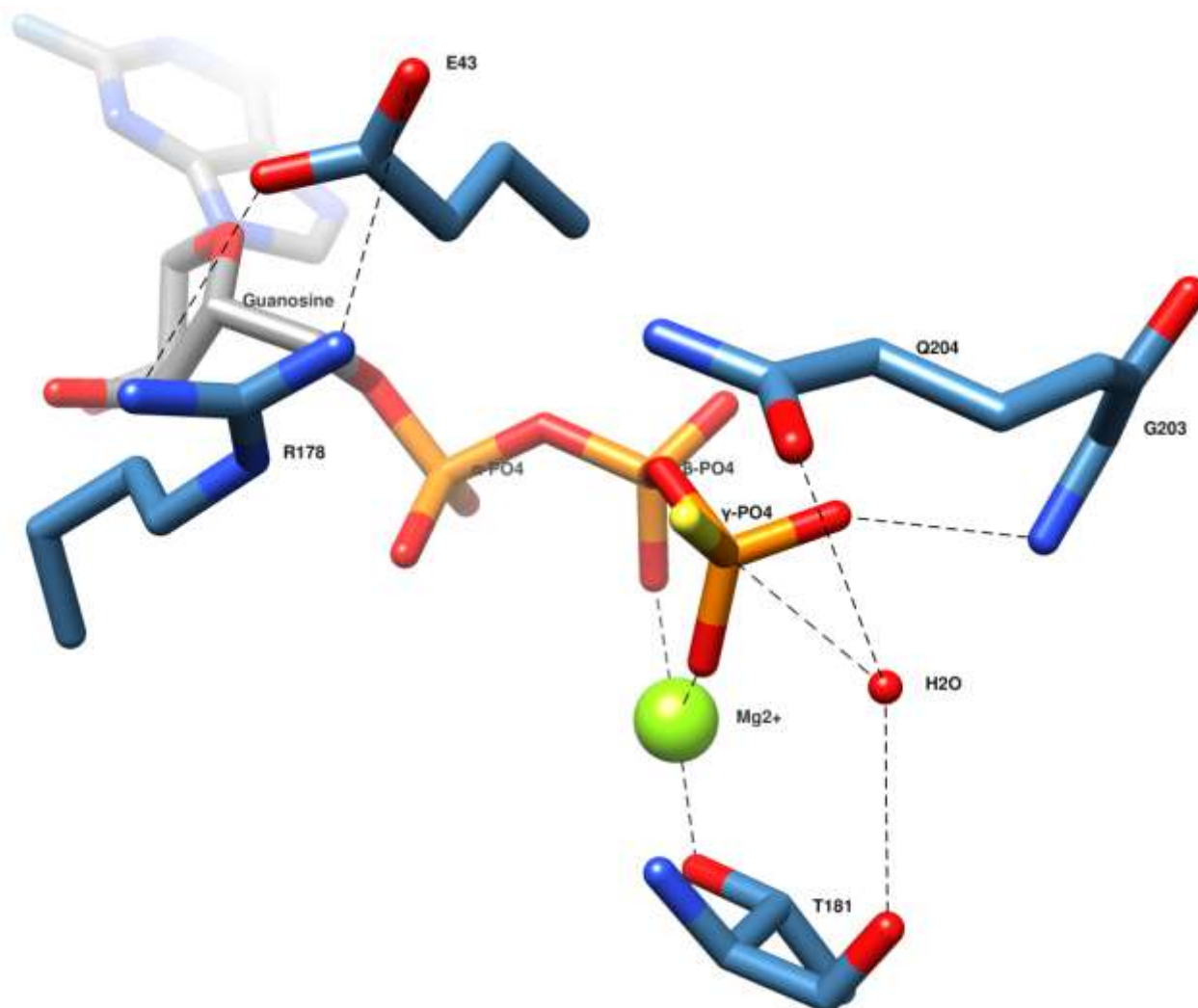


Figure 3. Key interactions that facilitate GTP hydrolysis.

The $\beta\gamma$ Heterodimer

The G _{β} and the G _{γ} subunits are always complexed together, as there are no known instances in which they are separated. There are five known G _{β} isoforms numbered 1-5, and each is composed of seven β -sheets oriented in the shape of a propeller, and an α -helix at the N-

terminus. There exist 12 G_γ isoforms, numbered 1-12, that consist of two α -helices connected by a loop (39, 40). The G_β and G_γ subunits have two points of contact: 1) at their N-terminal, helices as well as an interaction between $\beta 5/\beta 6$ of the G_β subunit, and 2) at the C-terminal, the α -helix of the G_γ subunit. Many possible combinations between G_β and G_γ subunits are possible (41). Specificity is dictated by regions on the G_γ subunit as small as 14 residues (42). Upon activation of the G-protein, the G_α separates from the $G_{\beta\gamma}$ complex and, similarly to the G_α subunit, continues to relay the signal through interactions with effectors (39).

The Adenylate Cyclase Effector

Each cell relies on a myriad of signaling pathways to incite changes within the cell to an ever-changing environment. Effectors are responsible for the production of a secondary messenger necessary to invoke a response to an extracellular stimulus. A common effector acted on by both the G_α subunit and the $G_{\beta\gamma}$ complex is adenylyl cyclase (AC). AC is a membrane-bound protein that catalyzes the conversion of adenosine triphosphate (ATP) to cyclic adenosine monophosphate (cAMP) and pyrophosphate (PP_i) which acts as a secondary messenger. To propagate the signal, cAMP activates protein kinase A (PKA), which in turn promotes glucose metabolism (43, 44). Alternatively, cAMP will bind exchange factor directly activated by cAMP I (EPAC) which has many intracellular targets involved in cell proliferation (45-49). There are 10 known isoforms of AC, each of which is composed of two pseudo-symmetrical transmembrane domains referred to as C1 and C2 (50).

AC is a unique effector in that it is both activated (G_{α_s}) and inhibited ($G_{\alpha_{i1}}$) by a G_α protein. Both G_α subunits are structurally similar and a comparison of the two crystal structures

results in a 1.07 Å root mean square deviation (RMSD) between the C_{α} atoms (22). It is therefore surprising that G_{α_s} and $G_{\alpha_{i1}}$ interact with different AC subunits using distinctly different motifs and have opposite effects on the activity of AC. Scanning mutagenesis of G_{α_s} identified important residues for the activation of AC located on the switch II and $\alpha 4\beta 6$ loop (51). Further studies that solved the crystal structure of active G_{α_s} complexed with AC and the non-hydrolyzable GTP analog GTP γ S (G_{α_s} •GTP γ S•AC) revealed that the interaction occurs between the switch II region of G_{α_s} and the C2 domain of AC. The interface between G_{α_s} and AC includes the following residues: leucine (L) 272, asparagine (N) 279, arginine (R)280, tryptophan (W) 281, L282, R283, threonine (T) 284, R231, R232, glutamine (Q) 236, and N239 (52). To date, crystallization of the $G_{\alpha_{i1}}$ •GTP γ S•AC complex has not been reported. Unlike G_{α_s} , $G_{\alpha_{i1}}$ requires the post-translational addition of a myristoyl fatty acid in order to bind AC, making it more difficult to crystallize. Nonetheless, evidence suggests that $G_{\alpha_{i1}}$ interacts exclusively with C1 of AC while G_{α_s} interacts solely with C2 (22). Because of the structural similarity between G_{α_s} and $G_{\alpha_{i1}}$, it is reasonable to presume that $G_{\alpha_{i1}}$ switch II and $\alpha 4\beta 6$ loop regions interact with the AC C1 domain in a similar manner. Point of contact residues between $G_{\alpha_{i1}}$ and AC have been experimentally determined as: arginine (R) 208, lysine (K) 209, isoleucine (I) 212, K312, R313, K314, K315, T316, and glutamate (E)318 as the residues involved in binding to AC (52-54).

Folding of G-Proteins and Disease States

Folding Overview

Eukaryotic organisms rely on intercellular signaling for all biological processes, including growth, senescence and apoptosis. Aberrations in proteins involved in signal transduction can

affect protein folding, catalytic function, or protein-protein interactions. This can lead to aberrant cellular signaling, which is the basis for several human diseases.

Folding is crucial for the structural integrity of proteins and directly responsible for their physiological function. Protein folding is an elegant process in which a nascent protein co-translationally folds into a higher order structure. Although it is not fully understood, it is thought to proceed through an energy landscape that includes multiple pathways with a variety of intermediates, or molten globules, each one with progressively lower free energy (55-57). The native structure at the end of the path has the lowest free energy and is, therefore, the most stable (Figure 4). Under denaturing conditions, a protein will unfold, altering the secondary structure and revert to a molten globule state, which may retain some activity (58, 59). Furthermore, molten globules that are high in β -sheet content pose an increased risk for aggregating and amyloid fibril formation, which are described in many devastating diseases such as Alzheimer's and Huntington's disease (60-62). *In vitro* studies using thermal or chemical denaturants are physiologically unrealistic, but suitable methods for the investigation of the relative stability of a wild-type protein compared to a mutant as the non-covalent interactions are altered, causing different unfolding properties for each protein (63, 64).

G-Proteins and Cancer

Cancer is the second most common cause of death in the US and ranks similarly across the rest of the developed world (65). Neoplastic disease is defined as the uncontrolled growth of cells and can occur in nearly every tissue type. Tumorigenesis starts in cells carrying a repertoire of genetic alterations that lead to aberrant cellular signaling. This aberrant signaling will often result

in accelerated growth and inhibition of apoptosis signaling, allowing diseased cells to be further propagated. Furthermore, since several of these genetic alterations result in inactivation for DNA repair pathways, diseased cells accumulate additional genetic changes with time, which is thought to be one mechanism of multidrug resistance. Some genetic changes are germline, i.e., inherited and therefore exist in every cell in the body. However, the vast majority of genetic alterations are somatic, as they originate in a single cell after birth.

Cancer-related, genetically-altered genes can affect tumorigenesis or tumor progression and are classified as being either oncogenes or tumor suppressor genes. When oncogenes become mutated, they are endowed with a gain of function to often evade inhibitory signals and are aberrantly activated. Tumor suppressor genes are genes involved in the suppression of growth and the promotion of senescence and apoptosis. These genes are mutationally inactivated or deleted in cancers (66, 67).

GNAI1 and *GNAS* are two oncogenes that encode the $G_{\alpha i1}$ and $G_{\alpha s}$ proteins, respectively (68). The R208Q mutation in the switch II region of $G_{\alpha i1}$ has been associated with colorectal cancer (68). The corresponding mutation in $G_{\alpha s}$ is R231H, which has been linked with neuroectodermal tumors (68). G-proteins have been implicated in various diseases, including bipolar disorder (69-71) and McCune-Albright syndrome (72) but are one of the most highly targeted protein families in drug design because of their association with human cancers (68, 73-77).

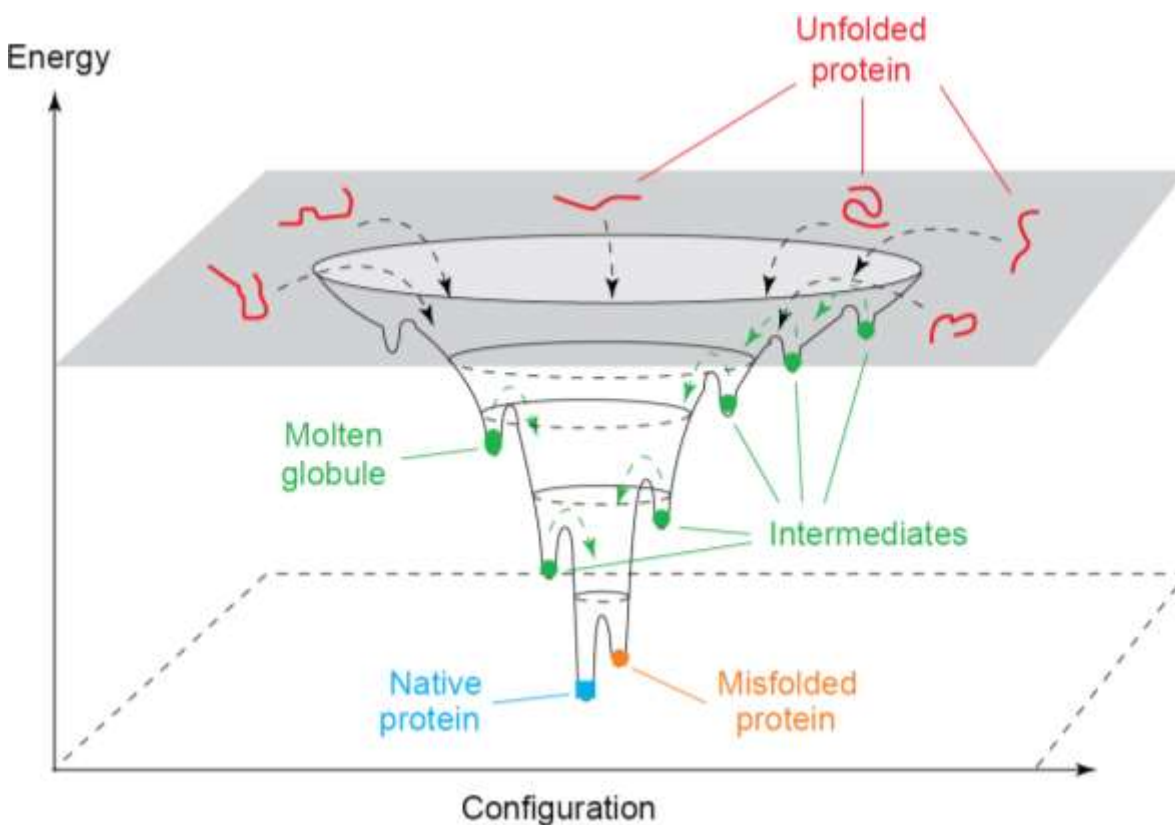


Figure 4. Schematic representation of the energy landscape during folding. Reused with permission from (57).

Spectroscopic Techniques Used for Studying G_α Proteins

Fluorescence Spectroscopy

Fluorescence is a radiative decay process in which an excited molecule releases a photon as it returns from the ground vibrational level of the first excited state to the ground state (Figure 5A). The energy difference between the excited state and the ground state is quantized and governed according to the equation: $\Delta E = h \cdot \nu$ where ΔE is the energy change, h is Planck's constant and ν is the frequency. A more convenient expression to relate ΔE to the wavelength (λ) utilizes the speed of light constant (c): $\Delta E = h \cdot c \cdot \lambda^{-1}$. Not every molecule has this ability, but the ones that do are considered fluorophores.

Fluorophores are typically organic compounds that contain conjugated π -bonds. In 1954, Weber and Laurence studied the environmental effects on fluorescence intensity (78). Their work involved many polycyclic organic compounds. They found that, in water, they did not fluoresce, but became fluorescent upon the addition of serum albumin. Their work paved the way for small molecule fluorescent dyes and one of the dyes they worked with was 8-anilinonaphthalene-1-sulfonic acid (ANS) (Figure 5B, inset). Weber and Laurence found that the quantum yield and the Stoke's shift were dependent on the polarity of the solvent. A less-polar solvent such as octanol caused the maximal wavelength (λ_{\max}) to become shorter, creating a blue shift while increasing the quantum yield (79). The opposite is true for ANS in a more polar solvent such as ethylene glycol (Figure 5B). The shift in the wavelength at maximal absorbance ($\Delta\lambda_{\max}$) is explained by comparing the dipole moment of the excited state versus the ground state. The dipole moment of the excited state can be considerably different from the ground state due to distinct electron distributions. Typically, the excited state has a larger dipole moment causing it to become more polar relative to the ground state. In a hydrophobic solvent, this leads to a disruption of the dynamics within the solvent's environment, rendering it less stable, thereby increasing the energy gap between the excited state and the ground state (Figure 5A).

The effects of solvent on quantum yield (i.e. fluorescence intensity) are a result of intersystem crossing. Electrons in the ground state are paired with opposite spins. When an electron becomes excited, it retains its spin initially and is in a singlet state. Polar environments interact more with the excited state and facilitate a spin conversion to the triplet state resulting

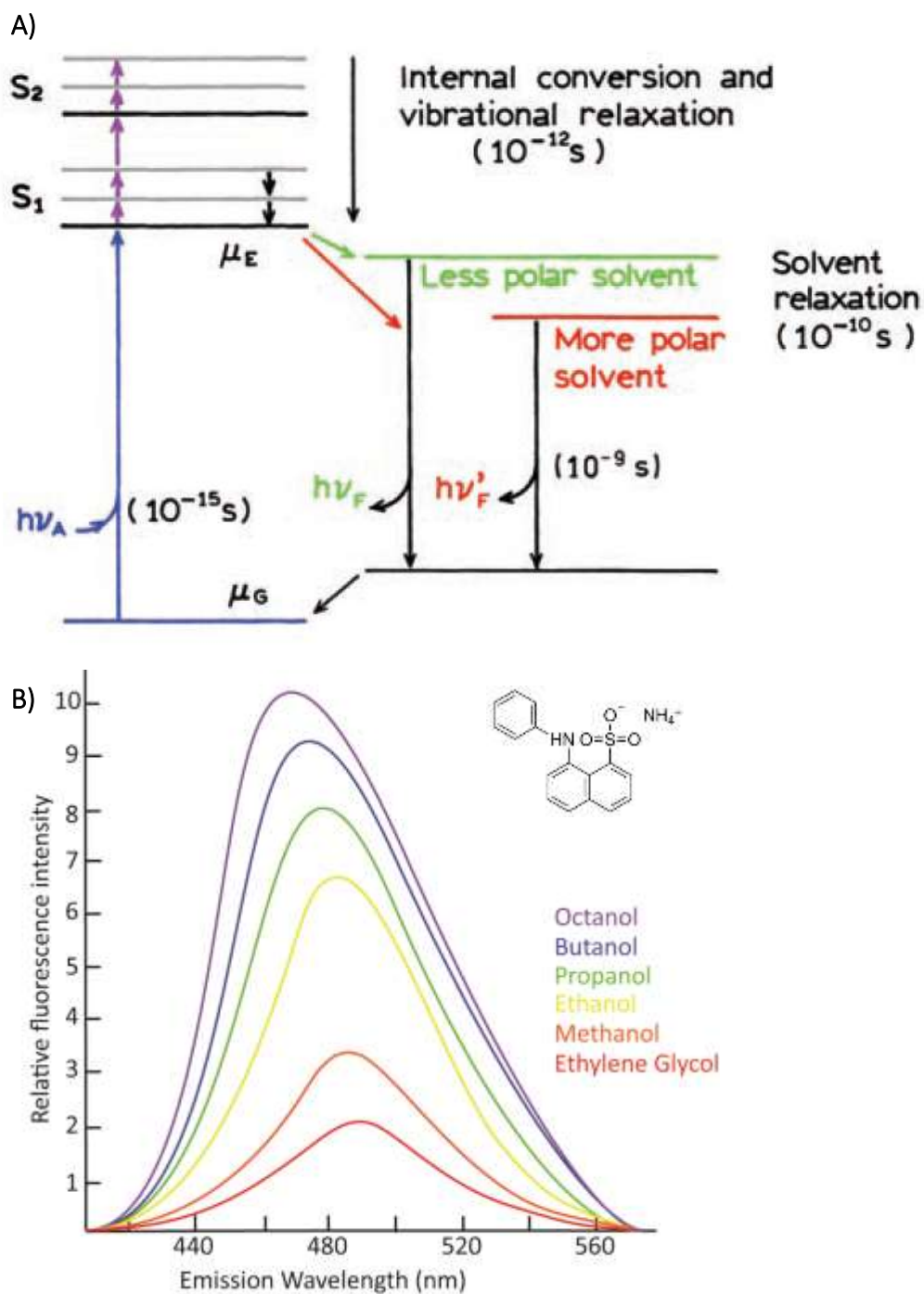


Figure 5. Jablonsky diagram outlining the process of fluorescence. **A)** A fluorophore is excited at a given wavelength (blue arrow) and emission occurs at a lower wavelength (green and red arrows). The solvent can affect the energy of the photon. Used with permission from (79). **B)** The wavelength is blue shifted and the intensity increases as the fluorophore (ANS – structure shown in top right of diagram) is placed in different solvents of decreasing polarity. Recreated from (78).

in unpaired electrons. A transition from the triplet state to the ground state is forbidden, resulting in a slower internal conversion to the ground state without the emission of a photon causing a lower fluorescence intensity.

Gilman and coworkers used these phenomena to obtain an indirect measurement of G-protein activity by monitoring the intrinsic tryptophan fluorescence following the addition of GTP γ S, a non-hydrolyzable analog of GTP (80, 81). Tryptophan (W) is a highly conjugated residue that contains a large degree of overlap between its p-orbitals, rendering it a fluorophore. As the protein moves into the active conformation, the W microenvironments change to become more hydrophobic and the intensity increases as a result (82). G $_{\alpha}$ proteins are not consistent with the number of tryptophan residues they contain. For example, G $_{\alpha t}$ contains two tryptophan residues while G $_{\alpha i1}$ and G $_{\alpha s}$ have three and four, respectively. While tryptophan residues are generally seen at the core of the protein, they are distributed around the protein at various frequencies and therefore, do not equally contribute to the change in the overall fluorescence.

Chabre et al. (83) determined that G $_{\alpha t}$ could be placed in an active conformation by the addition of tetrafluoroaluminate (III) (AlF $_4^-$) and that this method of activation was a zero order reaction. The AlF $_4^-$ mimics the γ phosphate so the GDP is left in place and the rate is not dependent on the exchange, unlike activation with GTP γ S. Henceforth, activation using AlF $_4^-$ and Mg $^{2+}$ will be referred to as AMF activation. Additionally, Chabre (84) investigated the contribution of the two-tryptophan residues in G $_{\alpha t}$ towards the overall fluorescence in the protein. Using tryptophan mutants, Chabre found that W207, rather than W127, was primarily responsible for the change in fluorescence (in G $_{\alpha t}$, W207 is in the switch II region, but W127 is

not). Furthermore, activated $G_{\alpha t} \bullet \text{AMF}$ and $G_{\alpha t} \bullet \text{GTP}\gamma\text{S}$ exhibited an increase in fluorescence intensity vs $G_{\alpha t} \bullet \text{GDP}$ that was accompanied by a red shift of λ_{max} (83, 84).

Using intrinsic tryptophan fluorescence, Hamm and co-workers (85) found $G_{\alpha i 1} \bullet \text{AMF}$ also exhibited a red shift. Analysis of crystal structures of $G_{\alpha i 1} \bullet \text{GDP}$ (86) and $G_{\alpha i 1} \bullet \text{AMF}$ (16) reveals that W211 is a part of the switch II region that moves from an unordered state to an ordered state upon binding of AlF_4^- . The new environment is more hydrophobic, which would normally coincide with a blue shift. Therefore, this observation was unexpected. It was later determined that the red shift arises from the formation of a π – cation interaction between W211 and R208 in the active conformation (85). Electrostatic interactions can form within a protein between residues bearing a positive charge (such as lysine and arginine) and ones with π – electron systems (such as phenylalanine, tyrosine, and tryptophan). The electrons are distributed more with the sp^2 -hybridized carbons of a ring structure, creating a partial negative charge toward the interior of the ring and a partial positive charge around the edge (Figure 6) (87-90). The strength of this interaction is dependent on the distance and the angle between the residues, and typically range from 1 – 5 $\text{kcal} \cdot \text{mol}^{-1}$ (91). Other interactions such as π – π stacking between π – electrons of nearby residues interact with each other (92), and less common, π – anion interactions have also been described (93, 94), in which a negatively charged residue such as aspartate or glutamate interacts with the π – electrons of a nearby residue.

Najor et al. (95) determined the contribution of each of the three-tryptophan residues in $G_{\alpha i 1}$ to the overall change in fluorescence. $G_{\alpha i 1}$ contains three tryptophan residues: W131 in the α -helical domain, W211 in the switch II region, and W258 in the GTPase domain. They found that

the W211F mutant abolishes the change in fluorescence while the W131F mutant showed an increase in the change of fluorescence. The W258F mutant had a change in fluorescence similar to WT (95).

Fluorescence is a useful technique for studying G_{α} proteins because it offers a tool to probe both structural and functional characteristics. The overall structure can be monitored during thermal denaturation as the fluorescence signal decreases and eventually disappears when the protein is fully unfolded. Similarly, by monitoring the red shift, the π -cation interaction reveals information about the structural integrity. Functionally, the changes in conformation from the inactive to active correlate to the changes in fluorescence intensity.

Ultraviolet/Visible Spectroscopy

Ultraviolet/visible (UV/Vis) spectroscopy is a commonly used technique for studying proteins and quantifying protein concentrations. UV/Vis spectroscopy is similar in theory to fluorescence spectroscopy. While fluorescence spectroscopy considers the relaxation of an excited electron to the ground state, UV/Vis spectroscopy focuses on the transition from the ground state to the excited state and measures the absorption of light at a given wavelength within the ultraviolet-visible light spectrum. Similar to fluorescence, the difference in energy is given by the equation: $\Delta E = h \cdot c \cdot \lambda^{-1}$ while the absorbance is given by the Beer-Lambert Law: $A = \epsilon \cdot c \cdot l$ where ϵ is the molar extinction coefficient, c is the concentration, and l is the path length. Although the wavelength of a photon that a molecule can absorb is quantized, broad peaks in a UV/Vis spectrum are common that arise from different vibrational and rotational states that change the energy difference.

Three amino acid residues contain conjugated structures that absorb light in the UV/Vis region and therefore can act as chromophores: tryptophan (W), tyrosine (Y), and phenylalanine (F). Phenylalanine shows the lowest absorption and absorbs at a wavelength of 260 nm with an extinction coefficient of $125 \text{ M}^{-1} \cdot \text{cm}^{-1}$. Tryptophan and tyrosine both absorb at 280 nm but tryptophan has a higher extinction coefficient ($5690 \text{ M}^{-1} \cdot \text{cm}^{-1}$ vs $1280 \text{ M}^{-1} \cdot \text{cm}^{-1}$) and therefore absorbs more light than tyrosine. Although tryptophan absorbs more light, they are relatively uncommon relative to the frequency of tyrosine residues making the latter more relevant. The extinction coefficient of a polypeptide can be estimated simply from the sum of multiplying the

number of tryptophan and tyrosine residues by their respective extinction coefficient. $G_{\alpha 1}$ has an extinction coefficient of $36,495 \text{ M}^{-1} \cdot \text{cm}^{-1}$ (96).

$G_{\alpha 1}$ has thirteen Y residues and three W residues (Figure 7). Unfolding a protein causes the chromophore residues to become more exposed, allowing them to absorb more light leading to a hyperchromic effect. Melting temperatures (T_m) can be deduced from the midpoint of the change in absorption as the protein unfolds.

Circular Dichroism Spectrophotometry

Circular dichroism (CD) uses circularly polarized light to determine the secondary structure of a polypeptide. Light consists of the sum of an electric and a magnetic component. Polarization occurs when each of the two components is limited to one respective plane normal to each other. Most common is linear polarization, which occurs when the two wave functions are in phase with each other. Circular polarization is when one of the wave functions is out of phase by 90° (Figure 8A). Circular dichroism results from a chiral molecule (e.g. polypeptide) interacting with one polarized state more than the other. CD is affected by the overall structure of the macromolecule, rather than the individual chiral centers, and each secondary structure has a signature pattern. An α -helix has a high absorption at 190 nm and then goes into a valley and creates a double hump between 210 nm and 230 nm. In contrast, a β -sheet starts out at a much lower absorption and decreases into a single hump (Figure 8B and C).

Quantifying the concentration of each type of secondary structure species requires the aid of computer algorithms that use a set of reference proteins of known structure to analyze

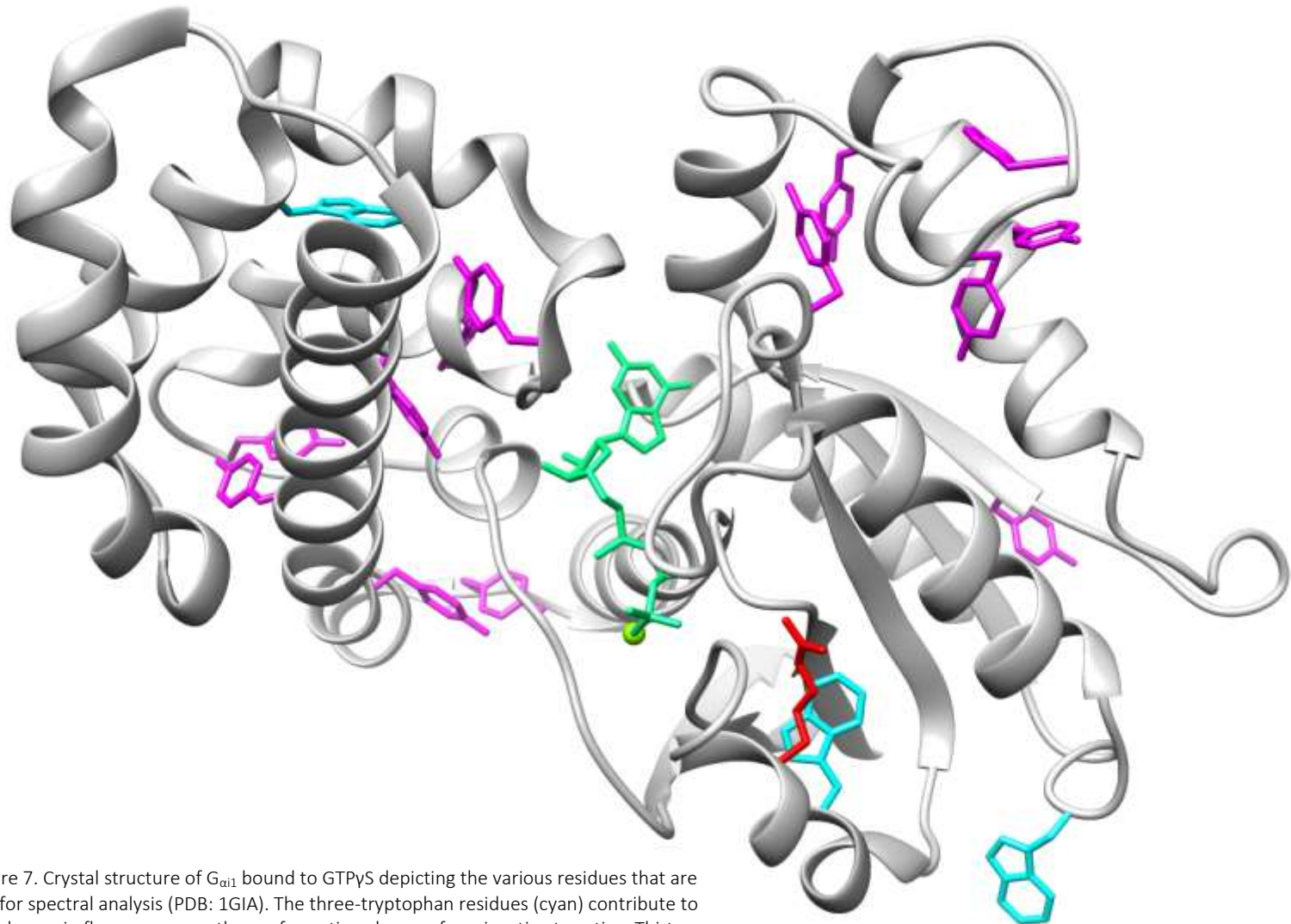


Figure 7. Crystal structure of $G_{\alpha i1}$ bound to $GTP\gamma S$ depicting the various residues that are key for spectral analysis (PDB: 1GIA). The three-tryptophan residues (cyan) contribute to the change in fluorescence as the conformation changes from inactive to active. Thirteen tyrosine residues are used in UV/Vis (pink).

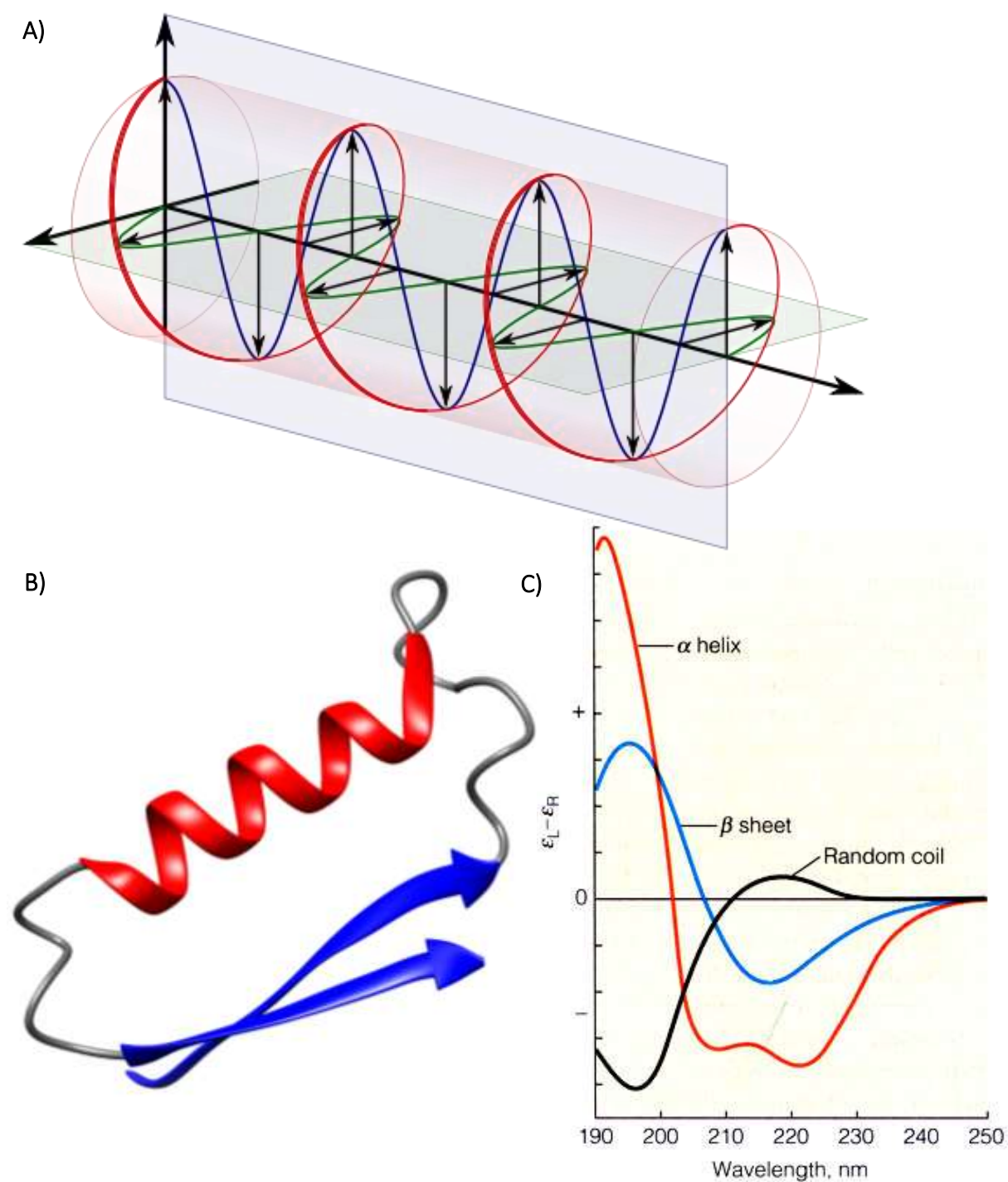


Figure 8. **A)** Schematic representation depicting the vertical and horizontal phases of a wave to illustrate circularly polarized light. **B)** Common secondary structures in proteins. **C)** The α -helix (red) produces a signature double hump pattern in a CD spectrum while a β -sheet (blue) shows only a single hump. Random coils (black) start with a negative ellipticity that then turns positive.

the spectrum (97). This approach is necessary for determining the secondary structure content of WT G_{α} proteins and mutants at different stages of unfolding.

Project Aims

The overall goal of this research is to gain insight into why the R208Q mutation in $G_{\alpha 1}$ promotes tumor growth. A better understanding of the biology of this mutant protein may lead to better therapeutic options for patients whose cancers harbor mutations in this gene (68). The specific aims addressed in this dissertation are as follows: 1) structural analysis of the R208Q mutant and comparison with the WT protein; 2) determination of functional activity of the R208Q mutant and how the mutation affects the rate of GTP hydrolysis vs WT; and 3) elucidation of mechanistic consequences of the R208Q mutation.

We began by studying the structural properties of wild-type (WT) and mutant $G_{\alpha 1}$, with the ultimate goal of gaining insight into how changes in the structural properties of the mutant proteins promotes neoplastic disease.

We used several biophysical techniques to study the WT and the R208Q mutant of $G_{\alpha 1}$ in three conformations ($G_{\alpha 1} \bullet \text{GDP}$, $G_{\alpha 1} \bullet \text{AMF}$, $G_{\alpha 1} \bullet \text{GTPyS}$) to better understand the global structures of these proteins. Fluorescence spectroscopy is able to take advantage of the relatively uncommon tryptophan residues at the core of the protein, as it can be used for monitoring the conformation of the protein as it transforms from the inactive to the active conformation. We further used UV/Vis spectroscopy to study protein unfolding, by monitoring the absorbance of tyrosine residues on the surface of the protein. In order to obtain an appreciation for the global structural changes, we turned to CD, as it monitors the types of

secondary structures present in the protein. Taken together, these three techniques offer a glimpse into the structural integrity of the protein characterized by melting temperatures (T_m).

G_α proteins hydrolyze GTP at an inefficient rate with turnover times that are exponentially slower than other enzymes. In this respect, G_α proteins are not considered enzymes but have evolved with this trait to provide time to propagate their signal. In the case of $G_{\alpha 1}$, the duration in the active state is directly related to the cellular concentrations of the secondary messenger cAMP. Studying the rates of GTP hydrolysis is necessary to determine downstream effects of the R208Q mutation. Fluorescence spectroscopy can be used to monitor the conformation as the protein goes from the inactive conformation to the active GTP-bound conformation and back as it hydrolyzes GTP. Malachite green is a dye that binds inorganic phosphate (P_i) that results from GTP hydrolysis, and is quantifiable *via* UV/Vis spectroscopy as the bound and free malachite green absorb light at different wavelengths. The combination of these techniques offers a parallel analysis of GTP hydrolysis and are used in conjunction to determine a more accurate rate of GTP hydrolysis.

We turned to *in silico* computational analysis to study the interactions within the protein to investigate the consequences of the R208Q mutation on an internal relay between key residues involved in normal function. This approach has been an invaluable resource for integrating the structural data with the functional GTP hydrolysis results.

Cancer is a complicated disease, with each patient harboring a unique milieu of genetic alterations leading to aberrant cellular function. Modern cancer therapies exploit unique protein

products or signaling properties of diseased genes. Because of the large variety of genetic alterations, there is a constant need to better understand the biology of mutant proteins found in cancer. By comparing the differences between the wild-type and R208Q versions of $G_{\alpha 1}$, we are able to better understand the altered G-protein signaling and attempt to elucidate a mechanism for cancer progression associated with this mutant protein. We hope these results will be useful for designing treatments for people with mutations in these genes and will expand our knowledge of cell signaling, which can be translated to other systems or cancers.

CHAPTER TWO

COMPARISON OF THE STRUCTURE-FUNCTION RELATIONSHIPS IN WILD-TYPE $G_{\alpha i1}$ AND IN ITS R208Q MUTANT

Heterotrimeric G proteins are composed of α , β , and γ subunits that act as binary switches oscillating between “on” and “off” states, amplifying extracellular signals into the cytoplasm in the form of secondary messengers. G-proteins work synergistically with receptors at the surface of the cell. In the inactive conformation, complexes are formed between G-protein coupled receptors (GPCR) and a GDP-bound heterotrimer. When an extracellular ligand binds to a specific receptor, a conformational change ensues, causing the G_{α} subunit to exchange GDP for GTP, and release the receptor and the $G_{\beta\gamma}$ subunit. The G_{α} protein further relays the signal through direct interactions with effector proteins until GTP is hydrolyzed, which results in a return to the inactive state (5, 6).

Folding in G_{α} proteins is highly conserved and consist of two domains: an α helical domain and a GTPase domain (6). The former is composed of six α helices and is important for effector and regulator selectivity (6). The GTPase domain is similar in structure and function to those of the Ras superfamily and contains six β sheets at the core surrounded by five α helices (31). This domain houses the nucleotide binding site, which contains a Mg^{2+} cofactor, and is surrounded by three flexible switch regions designated switch I through III. The switch regions

contain many conserved residues that are oriented around the γ -phosphate of GTP and are crucial for GTP hydrolysis (98).

G_{α} proteins have a relatively slow turnover rate compared to most enzymes (81, 99). The ability to remain active for a longer period is important to allow for appropriate signal propagation through interactions with an effector. The extent to which the cell responds to stimuli is dependent on the time the G_{α} subunit is in the active conformation, which in turn is dictated by the rate of GTP hydrolysis. Homeostasis relies on a delicate equilibrium that can be deleterious. Therefore, cellular signaling must be highly regulated.

Mutations in genes that encode G_{α} proteins have been shown to be involved in several diseases, including cancer (68, 74, 100). Admittedly, cancer is not the result of any single mutated gene and there are a plethora of tissue-specific permutations that can give rise to cancer (101). Although cancer can arise from improper regulation of pathways involving many G_{α} proteins, this study focuses on the cAMP pathway, which is stimulated by G_{α_s} and inhibited by G_{α_i1} through interactions with AC (6). Cyclic nucleotides are secondary messengers commonly associated with tumor progression and have been found to be either upregulated or downregulated, depending on the type of cancer (102).

The R231H G_{α_s} and the corresponding R208Q G_{α_i1} mutations have been reported in tumors of the central nervous system and large intestine, respectively (68, 103, 104). This highly conserved arginine is located in the switch II region, which contains residues critical for GTP hydrolysis. To investigate the effects of these mutations on the function of each G_{α} protein, GTP

hydrolysis studies were conducted. $G_{\alpha 1}$ and $G_{\alpha s}$ contain Trp residues, which upon activation, move into more hydrophobic environments. As a result, the increase in fluorescence intensity can be used as an indirect measurement of protein activity (80). This phenomenon is primarily due to the movement of the switch II Trp residue (W211 in $G_{\alpha 1}$ and W234 in $G_{\alpha s}$). Exchange of GDP for GTP is accompanied by an increase in fluorescence which returns to the original intensity at a rate proportional to GTP hydrolysis (81). The steady-state rate of GTP hydrolysis is determined by the rate of GDP release. For obtaining the time the protein is in an active conformation, which is more biologically relevant when studying effects downstream in the signaling pathway (36), fluorescence measurements were used to calculate single turnover rates under conditions of pre-steady state kinetics. Malachite green was also used for measuring the increase in the concentration of inorganic phosphate (P_i) that was released during the course of a single turnover of the enzyme (105, 106).

We investigated how the functional differences observed by fluorescence and malachite green assays for WT G_{α} proteins and their corresponding mutants could be rationalized in terms of structure. To determine if differences in the active conformation exist between WT $G_{\alpha 1}$ and its oncogenic mutant, we solved the X-ray structure R208Q $G_{\alpha 1}$ protein bound to GTP γ S (a non-hydrolyzable GTP analog) and compared it with that of the published WT $G_{\alpha 1}$ •GTP γ S (16). Furthermore, to probe the microenvironments in the vicinity of the mutations that are located in the flexible switch II region, molecular dynamics (MD) simulations were conducted on both R208Q and R231H mutants, as well as on WT $G_{\alpha 1}$ and WT $G_{\alpha s}$ proteins. We found that a network of molecular interactions was disrupted as a result of the mutations in the switch II region, which

propagated to other local motifs within the protein. In the case of $G_{\alpha i1}$, catalytic residues involved in Mg^{2+} binding and in the orientation of a nucleophilic water moved away from the nucleotide binding site, while the opposite was seen in the simulated $G_{\alpha s}$ mutant. Interestingly, the residues involved in binding to AC were left mostly unchanged for both WT $G_{\alpha i1}$ and $G_{\alpha s}$ and their respective mutants.

Using a combination of spectroscopic and *in silico* techniques, we were able to elucidate the functional consequences of oncogenic mutations in the switch II regions of $G_{\alpha s}$ and $G_{\alpha i1}$. We propose that both mutants result in lower cellular concentrations of cAMP as a result of altered GTP hydrolysis.

Materials and Methods

Cloning and Mutagenesis

Wild-type $G_{\alpha i1}$ -C-His6x from rat and wild-type bovine $G_{\alpha s}$ -C-His6x have previously been cloned into *DpnI* in the pQE-60 vector (Qiagen) *via* restriction sites and co-transformed into BL21 E. coli with the pREP4 repressor plasmid. Site-directed mutagenesis was performed to create the R208Q $G_{\alpha i1}$ point mutation using the QuikChange II kit (Agilent) and the forward, 5''- GCC CAG AGA TCA GAG CAG AAG TGG ATT CAC -3'', and the reverse, 5''- GTG AAT CAA CTT CTG CTC TGA TCT CTG GCC -3'', primers, which introduces a c.G623A mutation. The R231H $G_{\alpha s}$ mutant plasmid was purchased from Bio Basic in the pQE-60 vector and was subcloned into BL21 E. coli cells containing a pREP4 repressor plasmid.

Expression, Purification, and Preparation of G α proteins

Recombinant proteins were expressed and purified as described (107) to a purity of \geq 95% and stored at -80 °C. All purified proteins were subject to a time - based fluorescent emission assay to ensure proper activity prior to any further functional assays.

Mg²⁺-free G α •GTP γ S proteins were prepared by dialysis for six hours in 50.0 mM TrisCl pH 8.0, 0.005 % n-octyl- β -D-glucopyranoside, 1.0 mM EDTA, and 10.0 mM DTT, and again in 50.0 mM TrisCl pH 8.0, 0.01 mM GTP γ S, and 10.0 mM DTT for an additional six hours.

Fluorescence Assays for Nucleotide Binding and Hydrolysis

Experiments were performed with a PTI QuantaMaster fluorimeter (Photon Technologies, Inc., Mirmingham, NJ). Time-based assays were conducted with excitation and emission wavelengths set at 280 nm and 340 nm, respectively. Apo G α •GDP was incubated with 20.0 μ M GTP for 3 hours at 20.0 °C to exchange GDP for GTP.

Malachite Green Assay

Malachite green (Abcam) assays were performed on a Biotek ELx808 microplate reader OD. An aliquot of 10.0 μ M Apo G α •GDP was incubated with 5.0 μ M GTP for three hours at 4°C (50.0 mM HEPES pH 7.4, 2.0 mM EDTA, 100.0 μ M GTP, 1.0mM DTT, and 0.2 mg*mL⁻¹ BSA). Following GTP exchange, 1.0 mM MgSO₄, and 40.0 μ M GTP γ S were added to the reaction mixture. After 10 minutes, the reaction was quenched with 30.0 μ L malachite green and protected from light for 30 min. P_i was then determined by addition of 230.0 μ L to a 96 – well plate using phosphate standards.

Crystallization Conditions, Data Collection and Structure Determination

Purified R208Q G_{α1}•GTPγS was crystallized by using the hanging drop vapor diffusion method under slightly modified conditions (108). The total drop size of 6.00 μL was composed of 4.80 μL protein solution (7.0 mg*mL⁻¹ G_{α1}•GTPγS, 80.0 mM HEPES pH 7.4, 120.0 mM succinic acid, 8.0 mM DTT, 1.0 mM GTPγS, and 25.0 mM MgSO₄) and 1.20 μL reservoir solution (2.0 M (NH₄)₂SO₃ pH 8.0). Aliquots of 1.0 mL reservoir solution were placed in each well of a 24 – well plate (VDX). Crystals formed after six days at 20 °C. The R208Q G_{α1}•GTPγS crystals with the best morphology were transferred into a cryo-protectant (well solution supplemented with 25% (v/v) glycerol) before being flash cooled in liquid nitrogen.

Monochromatic data sets were collected at the LS-CAT, Advanced Photon Source (APS) at Argonne National Laboratory (ANL). Diffraction data was collected at a wavelength of 0.98 Å at 100K using a Dectris Eigen 9M detector. All data sets were indexed and integrated using HKL2000 . The best data set was processed to a resolution of 2.07Å. Data collection statistics are summarized in Table 3.

The structure of R208Q G_{α1}•GTPγS was solved by molecular replacement using PHASER in the Phenix software suit (109). The initial search model was based on a previously published structure of WT G_{α1}•GTPγS (PDB code: 1GIA). Model building was performed using Coot and refined using Phenix and the structure was analyzed using Coot and UCSF Chimera (110). Final refinement statistics are presented in Table X (PDB code: XXXX). Structural figures were created using UCSF Chimera (110).

Molecular Dynamics Simulations

The coordinates of $G_{\alpha 1}$ •GDP (PDB ID: 1BOF,(86)) and $G_{\alpha 1}$ •GTP γ S (PDB ID: 1GIA, (16)) were downloaded from the Protein Data Bank (PDB, (111)). Missing loops in the $G_{\alpha 1}$ structures were modeled using Swiss-Model (112) and the corresponding transducin structures (PDB ID: 1TAG,(13), 1TAD, (113) and 1TND,(15)). The simulations were done using procedures previously described (95). Unrestrained dynamics were run for 14 ns before the data were acquired for an additional 1 ns. The simulations were done at 37 °C (310 K) and 50 °C (328 K). These data were then used in the analyses. The R231H point mutation models were generated using VMD (114) and subjected to the same equilibration procedure as the wild-type structures. All molecular graphics diagrams were generated using UCSF Chimera (110). Pairwise Van der Waals and electrostatic interaction energies were calculated using nanoscale molecular dynamics (NAMD) (115). The solvent accessible surface area (SASA) was measured with the SASA routine in VMD. The values presented in Table 4 and in Figure 13 and Figure 14 were calculated for the final 1 ns in each simulation and then averaged. The simulation was equilibrated for 15 ns, and the interaction energy (E_i) between networking residues were calculated using NAMD.

Results and Discussion

Fluorescence Changes Resulting from Nucleotide Exchange

To determine if the oncogenic mutations affected GTP binding, we measured the rates of GDP exchange for GTP γ S (a non-hydrolyzable GTP analog) in WT and mutant proteins. Time-based intrinsic tryptophan fluorescence is a surrogate measure of G_{α} protein activity (80). Activation with nucleotide triphosphate results in an increase in fluorescence intensity

emanating from a change in the environment surrounding tryptophan residues to one that is more hydrophobic. Upon the addition of GTP γ S, both WT G $_{\alpha 1}$ and WT G $_{\alpha s}$ showed an increase in fluorescence intensity of approximately 35-40 % over a 100 min timespan (Figure 9A and B), which is within the expected range of 30-35 % for GTP γ S activation reported in the literature (80). The mutants showed impaired increases in fluorescence intensity compared to their respective WT counterparts: the R208Q G $_{\alpha 1}$ mutant exhibited an approximate increase of 20 % (Figure 9A), while the R231H G $_{\alpha s}$ mutant showed a 25 % increase (Figure 9B). W211 in G $_{\alpha 1}$ and W234 in G $_{\alpha s}$ are the major contributors toward the intrinsic fluorescence of these proteins (95). The differences in the maximal fluorescence intensities between the WT proteins and their respective mutants can be attributed to these specific Trp residues moving into environments with different levels of hydrophobicity.

The pseudo first-order rate of GTP γ S exchange is limited by the rate of dissociation of GDP (k_{app}) (116). Using a similar analysis for the rate of change in fluorescence that was previously described (83, 117), the calculated k_{app} values for WT G $_{\alpha 1}$ was 0.03 min $^{-1}$ and 0.02 min $^{-1}$ for the R208Q mutant (Table 2). Under the same conditions, the WT G $_{\alpha s}$ showed a GTP γ S exchange rate of 0.52 min $^{-1}$ whereas, for the R231H mutant, k_{app} was 0.27 min $^{-1}$ (Figure 9). Although the k_{app} values previously reported for G $_{\alpha s}$ are approximately two-fold higher, 0.28 min $^{-1}$ vs our observed 0.13 min $^{-1}$, respectively (118)), their ratio is similar to that in our study, which might be due to the different methodology used and experimental conditions. In conclusion, both G $_{\alpha}$ mutants showed a decreased nucleotide exchange rate, but they were still able to bind GTP and attain the active conformation.

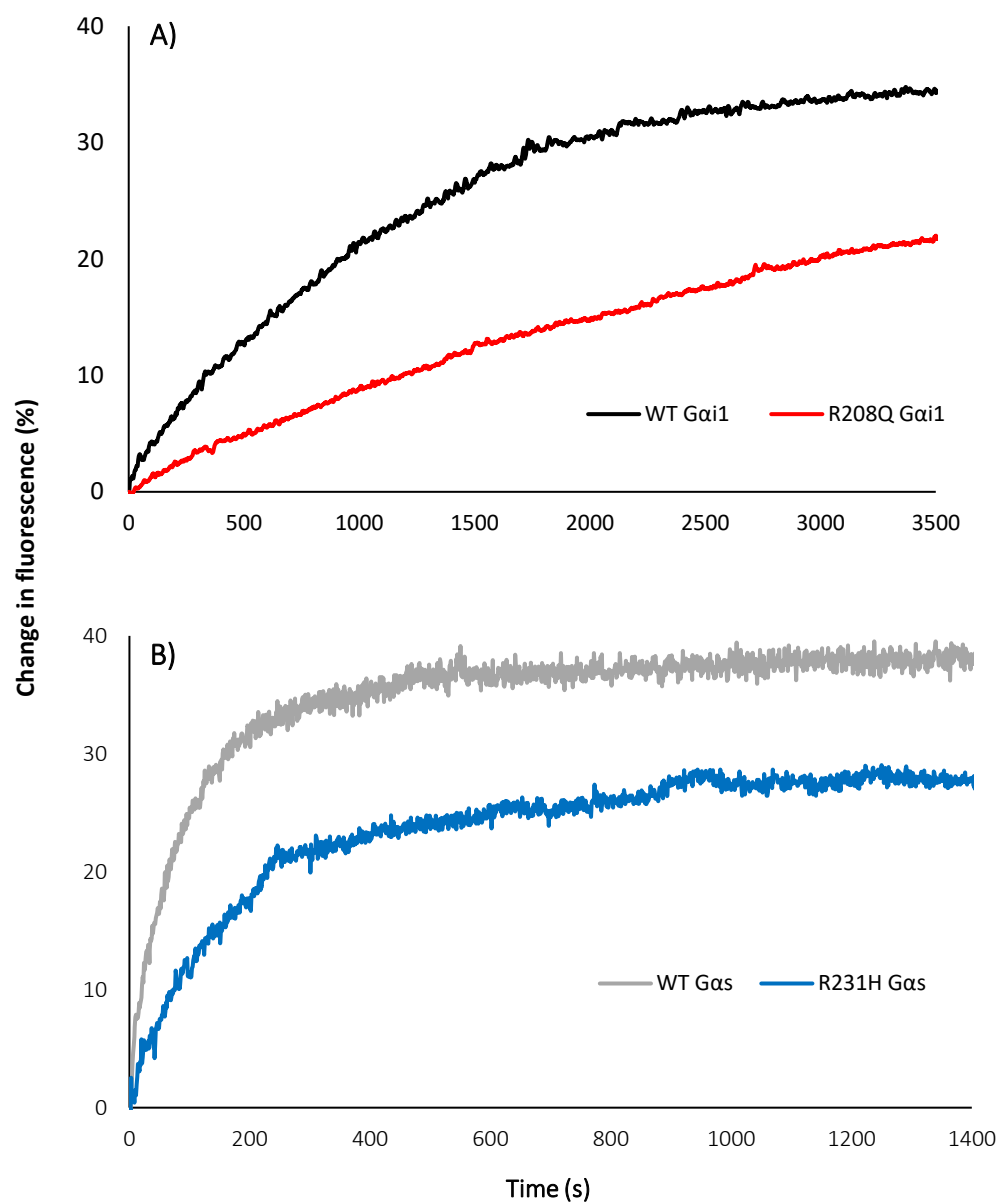


Figure 9. Changes in time-based fluorescence emission resulting from exchange of GDP for GTP γ S bound to G α proteins. Fluorescence intensities were normalized to zero upon nucleotide addition. **(A)** WT G α i1 (black) vs R208Q G α i1 (red). **(B)** WT G α s (gray) vs the R231H mutant (blue).

Fluorescence Changes Resulting from GTP Hydrolysis

G-proteins function as molecular switches that turn on or off cellular responses. Therefore, the rate of GTP hydrolysis is what dictates the magnitude of the cellular response. Because the rate for nucleotide exchange is much slower than for hydrolysis, the steady-state turnover rate is largely determined by the release of GDP (81). All GTPases require a Mg^{2+} cofactor to function, and a highly conserved Ser is critical for Mg^{2+} coordination and holding it in the nucleotide binding site (13). In the GTP γ S conformation, Mg^{2+} has an octahedral geometry and in addition to a Ser residue, is coordinated to a Thr residue, the β and γ phosphates of the nucleotide, and two water molecules. Uncoupling the conformational change from GTPase activity is critical for investigating the time the protein remains in the active state because it bypasses the much slower rate of nucleotide exchange (36).

The single turnover rate of GTP hydrolysis was measured using two indirect, pre-steady-state techniques. The fluorescence approach that was first used monitored the change in the hydrophobicity of key tryptophan residues that track conformational changes. As Mg^{2+} was added to apo G_{α} •GTP, the fluorescence intensity increased as a result of burial of Trp residues in the active state, but it quickly returned to zero as the bound GTP was hydrolyzed to GDP and inorganic phosphate (P_i) (Figure 10A, inset) (81). The half-life ($t_{1/2}$) of the decay process was found to be 13.9 s for WT $G_{\alpha i1}$ (Figure 10A) and 11.9 s for WT $G_{\alpha s}$ (Figure 10B). From $t_{1/2}$, k_{cat} values were calculated from the equation: $k_{cat} = \ln(2) * t_{1/2}^{-1}$, resulting in a k_{cat} of $2.9 \pm 0.2 \text{ min}^{-1}$ for WT $G_{\alpha i1}$ and $3.4 \pm 0.5 \text{ min}^{-1}$ for WT $G_{\alpha s}$ (Table 2).

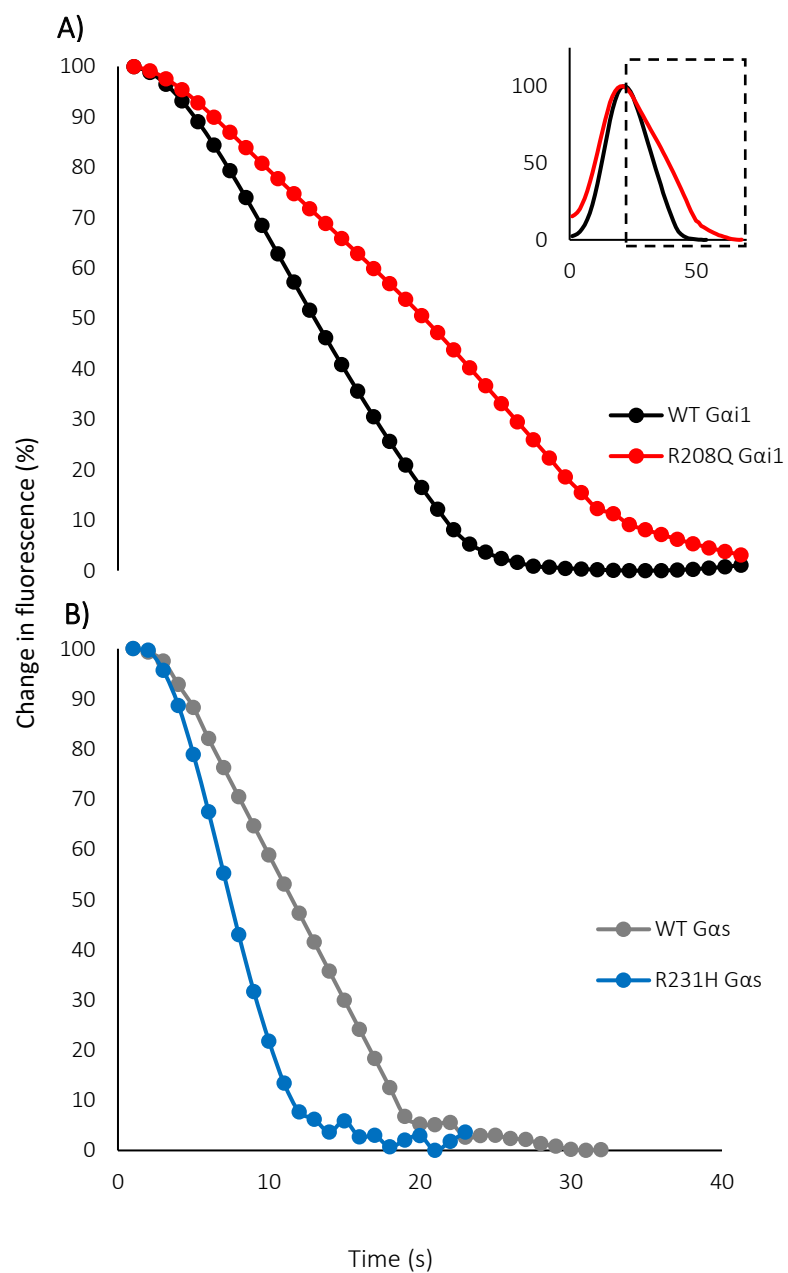


Figure 10. GTP hydrolysis monitored by time-based fluorescence emission. Due to differences in Trp environments, the maximal fluorescence intensities of WT and mutant proteins were different. The decays were therefore normalized to a range of 0 to 100. The assay was initiated by addition of Mg^{2+} at time zero (inset). **(A)** WT $G_{\alpha i1}$ (black) vs R208Q $G_{\alpha i1}$ (red). **(B)** WT $G_{\alpha s}$ (gray) vs R231H $G_{\alpha s}$ (blue).

Previous research showed the rate of hydrolysis for WT $G_{\alpha 1}$ to be 0.42 min^{-1} (36, 119), but upon the addition of RGS4, a GTPase activating protein (GAP), it was found to increase from 2.0 to 4.0 min^{-1} *via* stabilization of the transition state (116, 119-121). WT $G_{\alpha s}$ shows a turnover rate comparable to $G_{\alpha 1}$ at $3.4 \pm 0.5 \text{ min}^{-1}$ (Table 2), and with the value that was previously reported, 3.5 min^{-1} (122). A malachite green assay was also used to confirm the fluorescence measurements. With this technique, the k_{cat} value for P_i formation resulting from GTP hydrolysis was found to be $3.0 \pm 0.1 \text{ min}^{-1}$ for WT $G_{\alpha 1}$ while for WT $G_{\alpha s}$ it was $3.6 \pm 0.2 \text{ min}^{-1}$ (Table 2). The R208Q $G_{\alpha 1}$ showed lower k_{cat} values by both methods: $1.5 \pm 0.3 \text{ min}^{-1}$ using fluorescence spectroscopy and $1.9 \pm 0.3 \text{ min}^{-1}$ with malachite green, indicating that the mutant has diminished hydrolytic activity. Conversely, the R231H mutant showed higher rates of GTP hydrolysis compared to WT $G_{\alpha s}$ with k_{cat} values of $4.8 \pm 0.2 \text{ min}^{-1}$ and $4.4 \pm 0.9 \text{ min}^{-1}$ for the fluorescence and malachite green assays, respectively (Table 2).

Table 2. Pseudo first-order rate constants for GTP γ S exchange and GTP hydrolysis.

Protein	GTP exchange	GTP hydrolysis	P_i formation
WT $G_{i\alpha 1}$	0.03 ± 0.01	2.9 ± 0.2	3.0 ± 0.1
R208Q $G_{i\alpha 1}$	0.02 ± 0.01	1.5 ± 0.3	1.9 ± 0.3
WT $G_{s\alpha}$	0.52 ± 0.03	3.4 ± 0.5	3.6 ± 0.2
R231H $G_{s\alpha}$	0.27 ± 0.02	4.8 ± 0.2	4.4 ± 0.9

Rate constants given in units of min^{-1}

Errors reported as standard deviations, $n \geq 3$

Structure of the R208Q $G_{\alpha 1}$ mutant

The R208Q $G_{\alpha 1}$ structure was solved by molecular replacement using a previously published structure of the WT $G_{\alpha 1} \bullet \text{GTP}\gamma\text{S}$ (PDB code: 1GIA) (Figure 11)). The data was processed in the space group P 32 2 1, refined to a final $R_{\text{work}}/R_{\text{free}}$ (%) 16.8/19.7 and, to a

resolution of 2.07 Å. The final refinement statistics were done by Dr. Mascarenhas and are shown in Table 3. The X-ray crystal structure of the R208Q $G_{\alpha 1}$ mutant closely resembles the previously solved WT $G_{\alpha 1}$ structure (PDB entry 1GIA (16)). The most pronounced changes occur within the switch II region where the mutation is located. Arg is a longer residue than Gln, as shown by the electron density in the R208Q mutant, which properly correlates to a Gln residue length at the 208 position. In the WT protein, R208 forms a salt bridge with E245 of the $\alpha 3$ helix but because Gln is not charged, E245 in the R208Q mutant is only capable of hydrogen bonding with E245, thereby weakening the interaction between the switch II and $\alpha 3$ helix (Figure 11). Furthermore, R208 of the WT protein forms a hydrogen bond with R205 (also in the switch II region), constraining it away from the nucleotide binding site. Because Q208 is shorter, this hydrogen bond is not possible, allowing R205 to freely rotate. Compared to the WT $G_{\alpha 1}$ protein, the R208Q mutation causes the C_{α} of the Q208 residue to move slightly toward the $\alpha 3$ helix by approximately 0.7 Å.

Superimposition of the WT $G_{\alpha 1} \cdot \text{GTP}\gamma\text{S}$ and the R208Q $G_{\alpha 1} \cdot \text{GTP}\gamma\text{S}$ structures revealed a root mean square deviation (RMSD) of 0.632 Å at the site of the mutation, but only 0.255 Å between 345 aligned alpha carbons (C_{α}) in the overall proteins. However, the functionally important motifs saw relatively more deviation from the WT. The RMSD of the switch I region (residues 177-183) is approximately 70% greater (0.367 Å). Focusing only on the switch II motif (residues 202-215), the RMSD drastically increases to 0.453 Å. The switch III region (residues 232-240) experiences a minor increase with an RMSD of 0.292 Å. The $\alpha 4$ - $\beta 6$ loop, which is important for effector binding and is located near the posterior surface relative to the nucleotide

binding site, has an RMSD value of 0.244 Å. These calculations suggest that the microenvironments in the immediate vicinity of the mutation are altered while the distal motifs are left unperturbed. Given that the mutation is located on the flexible switch II region and is positioned near the similarly flexible switch I region, these results are not surprising. Because we were unable to obtain crystals for R231H G_{αs}, a similar analysis was not possible.

Table 3. Refinement statistics of R208Q G_{αi1} crystal structure

Data Processing	
Space group	P 32 2 1
Cell dimension	
α, β, γ (deg)	90.0, 90.0, 120.0
a, b, c (Å)	79.5, 79.5, 105.4
Resolution (Å)	2.07
R _{merge} ^a (%)	7.4(65.0) ^b
I/σ (I)	33.1 (2.8)
R _{pim} ^c (%)	2.2(22.9)
CC ½ ^d	0.999(0.871)
Completeness (%)	100.0(100.0)
Multiplicity	10.7(8.0)
No. Reflections	258246
No. Unique Reflections	24084
Refinement	
R _{work} ^e /R _{free} ^f (%)	16.8/19.7
No. of Atoms	
protein	2565
ligand	32
water	207
B factors	
protein	28.9
RMSD	
bond lengths (Å)	0.002
bond angles (deg)	0.476
Ramachandran plot (%)	
most favored	98.4
allowed	1.6
outliers	0

^aR_{merge} = $\sum |I_{obs} - I_{avg}| / \sum I_{avg}$.

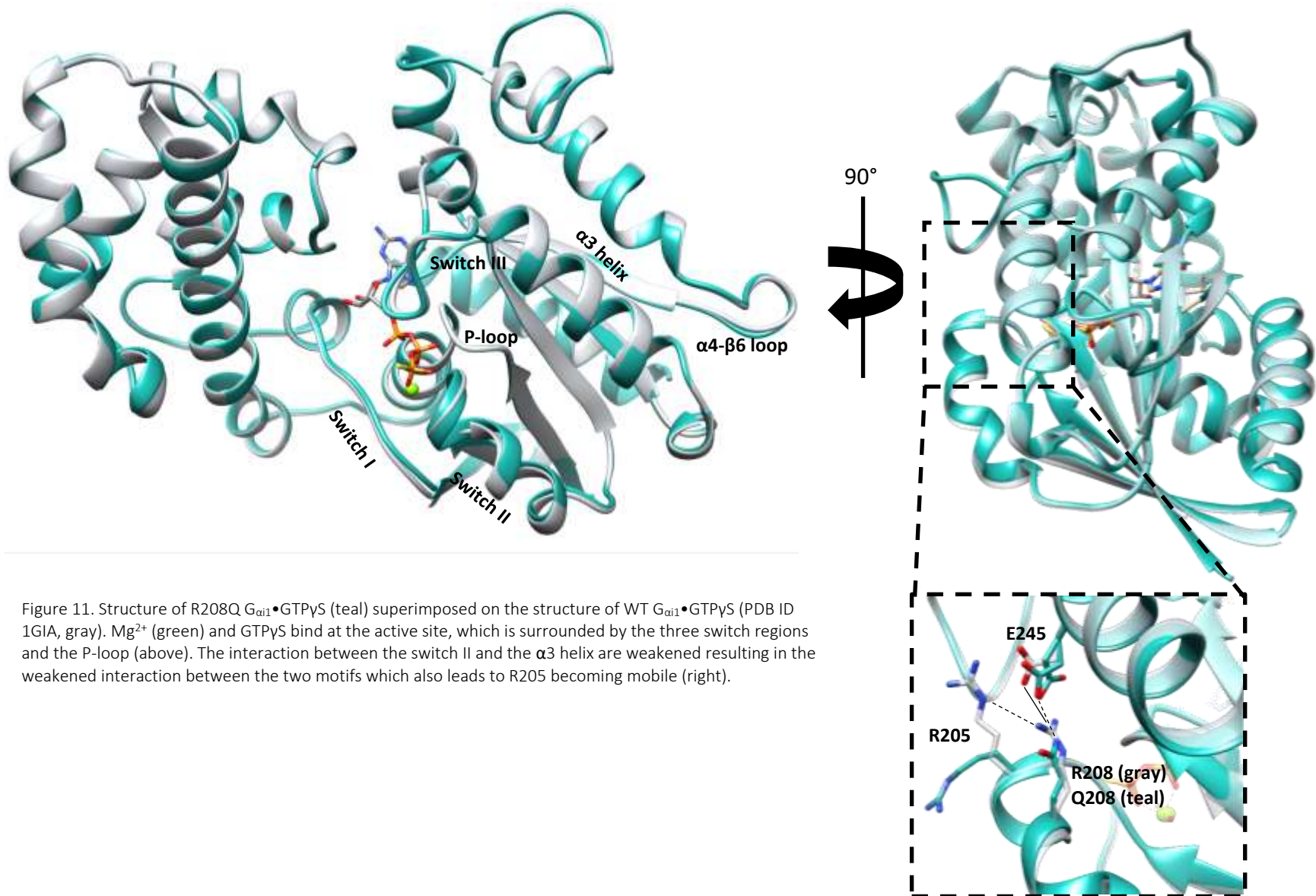
^bThe values for the highest-resolution bin are in parentheses.

^cPrecision-indicating merging R

^dPearson correlation coefficient of two "half" data

^eR_{work} = $\sum |F_{obs} - F_{calc}| / \sum F_{obs}$

^fFive percent of the reflection data were selected at random as a test set, and only these data were used to calculate R_{free}.



Computer Modeling of Intermolecular Interactions

G-proteins are highly conserved proteins both at the primary and the secondary structure levels. Key residues for GTP hydrolysis by $G_{\alpha 1}$ have been identified: R242 (123), E43 (123), and S47 (124) (Figure 12). These residues are known to make up an intricate network involving hydrogen bonds, electrostatic interactions, and hydrophobic forces. R178 has been shown to be directly involved in hydrolysis by stabilizing the negative charge on the γ - PO_4^{2-} (16). Solving the crystal structure for the R208Q $G_{\alpha 1}$ mutant provided the opportunity for using computer modeling to probe intermolecular interactions in a dynamic state. It has been reported that the R208A $G_{\alpha 1}$ mutant has an insignificant effect on GTP hydrolysis (36). This mutant proved to be useful in understanding the interactions present in GTP hydrolysis. We were able to model the R208A $G_{\alpha 1}$ mutant after the previously solved WT $G_{\alpha 1}$ structure (16). Although we were unable to obtain crystals for the R231H $G_{\alpha s}$ protein, the mutation was also simulated from the previously solved WT structure (52).

As WT $G_{\alpha 1} \bullet GTP\gamma S$ shifts into the active conformation, a π -cation interaction is formed between R208 and W211, which contributes to the stability of the switch II region (85, 95). A similar interaction in WT $G_{\alpha s}$ occurs between the corresponding R231 and W234 residues. Following our MD simulation, the RMSD between the C α of the 208 residue in $G_{\alpha 1}$ became 3.82 Å and 1.3 Å for the corresponding 231 position in $G_{\alpha s}$, which suggests that the region around the mutation has become unstable in the $G_{\alpha 1}$ but much less so in $G_{\alpha s}$.

We calculated interaction energies to determine if the destabilization of the switch II region propagated to the switch I and the $\alpha 3$ helix regions and, if present, how it affected the

specific interactions involved in GTP hydrolysis (Table 4). R242 in WT $G_{\alpha 1}$ is located at the other end of the $\alpha 3$ helix relative to the affected W258. Its interaction with E43 has been shown to promote the transition to the active state and allow for nucleotide exchange (123). The WT $G_{\alpha 1}$ •GTP γ S had a total interaction energy (sum of electrostatic and van der Waals) of -60.1 kcal* mol^{-1} at a distance of 3.0 Å between R242 and E43, while, for the R208A $G_{\alpha 1}$ mutant, the value was -62.3 kcal* mol^{-1} at a similar distance. The R208Q $G_{\alpha 1}$ mutant exhibited an interaction with a magnitude of approximately half (-30.8 kcal* mol^{-1}) of the WT protein at an increased distance of 5.2 Å (Table 4). The $G_{\alpha s}$ counterparts are R265 and E50. Table 2 shows that the corresponding interactions in $G_{\alpha s}$ remained unchanged as did the inter-residue distances.

The P-loop is located near the β and γ phosphates of GTP and is a critical motif for the transition to the active state. In the inactive GDP-bound conformation, it forms an electrostatic interaction with the catalytic R178 $G_{\alpha 1}$ (R201 $G_{\alpha s}$) that is known to stabilize the leaving P_i in the switch I region (16, 117). A key difference between heterotrimeric G_{α} proteins and their Ras counterpart is the noticeable lack of an equivalent Arg in the latter. Ras proteins have significantly lower rates of basal GTP hydrolysis, however, the rate is dramatically increased by GTPase Activating Proteins (GAP), which contains a functionally equivalent switch I Arg (125). For WT $G_{\alpha 1}$ and R208A $G_{\alpha 1}$ proteins, E43 was at a distance of 4.6 Å or 5.1 Å from R178 and with similar interaction energies. In the R208Q $G_{\alpha 1}$ mutant, E43 was positioned between the nucleotide and R178 at a much shorter distance (1.8 Å), resulting in a strong electrostatic interaction of -92.0 kcal* mol^{-1} (Table 4 and Figure 12A). For WT $G_{\alpha s}$ and R231H $G_{\alpha s}$, both E50 and

R201 remained at comparable distances (Table 4 and Figure 12B) to that between E43 and R178 in WT $G_{\alpha 1}$, 4.0 and 4.8 Å, respectively, vs. 4.6 Å.

Simulating the interaction between the R178 and γ - PO_4^{2-} resulted in an E_i of -100.0 kcal* mol^{-1} for WT $G_{\alpha 1}$ and -72.7 kcal* mol^{-1} for R208A mutant at a distance of 2.8 Å for both. The R208Q interaction was drastically decreased to -27.0 kcal* mol^{-1} at a distance of 5.6 Å (Table 4). Therefore, the increased interaction with E43 hinders R178 from binding to γ - PO_4^{2-} (Figure 12A). $G_{\alpha s}$ experienced the opposite trend where WT interacted with γ - PO_4^{2-} with an E_i of -40.8 kcal* mol^{-1} at a distance of 6.9 Å while the R231H mutant exhibited an attraction of -103.5 kcal* mol^{-1} at a distance of 3.4 Å. In neither case, however, was there any structural hindrance of the Arg residue with γ - PO_4^{2-} , as seen in $G_{\alpha 1}$.

Also in the P-loop are highly conserved Ser residues necessary for Mg^{2+} binding: S47 in $G_{\alpha 1}$ and S54 in $G_{\alpha s}$. Across all three $G_{\alpha 1}$ simulations, this interaction was minimally altered: -38.9 kcal* mol^{-1} for WT $G_{\alpha 1}$, -30.2 kcal* mol^{-1} for R208Q $G_{\alpha 1}$, and -30.3 kcal* mol^{-1} for R208A $G_{\alpha 1}$, and the difference in the movement was 0.1 Å (Table 4 and Figure 12A). $G_{\alpha s}$ underwent a more drastic change in which the R231H mutant showed an increased affinity for the Mg^{2+} ion with an E_i of -46.9 kcal* mol^{-1} vs -29.7 kcal* mol^{-1} seen in the WT protein. GTPase activity has been shown to be regulated by Mg^{2+} concentration (126), therefore the increased affinity for Mg^{2+} could be contributing to the higher rate of GTP hydrolysis seen in the R231H mutant. The R208Q mutation affected $G_{\alpha 1}$ through perturbations in the $\alpha 3$ helix, and propagated to the P-loop and the switch I region, which ultimately prevented R178 from interacting with γ - PO_4^{2-} . Conversely, the $\alpha 3$ helix

was not affected significantly in the R231H $G_{\alpha s}$ mutant, however, R201 in the switch I region and in the S54P-loop moved closer to the γ - PO_4^{2-} and Mg^{2+} , respectively.

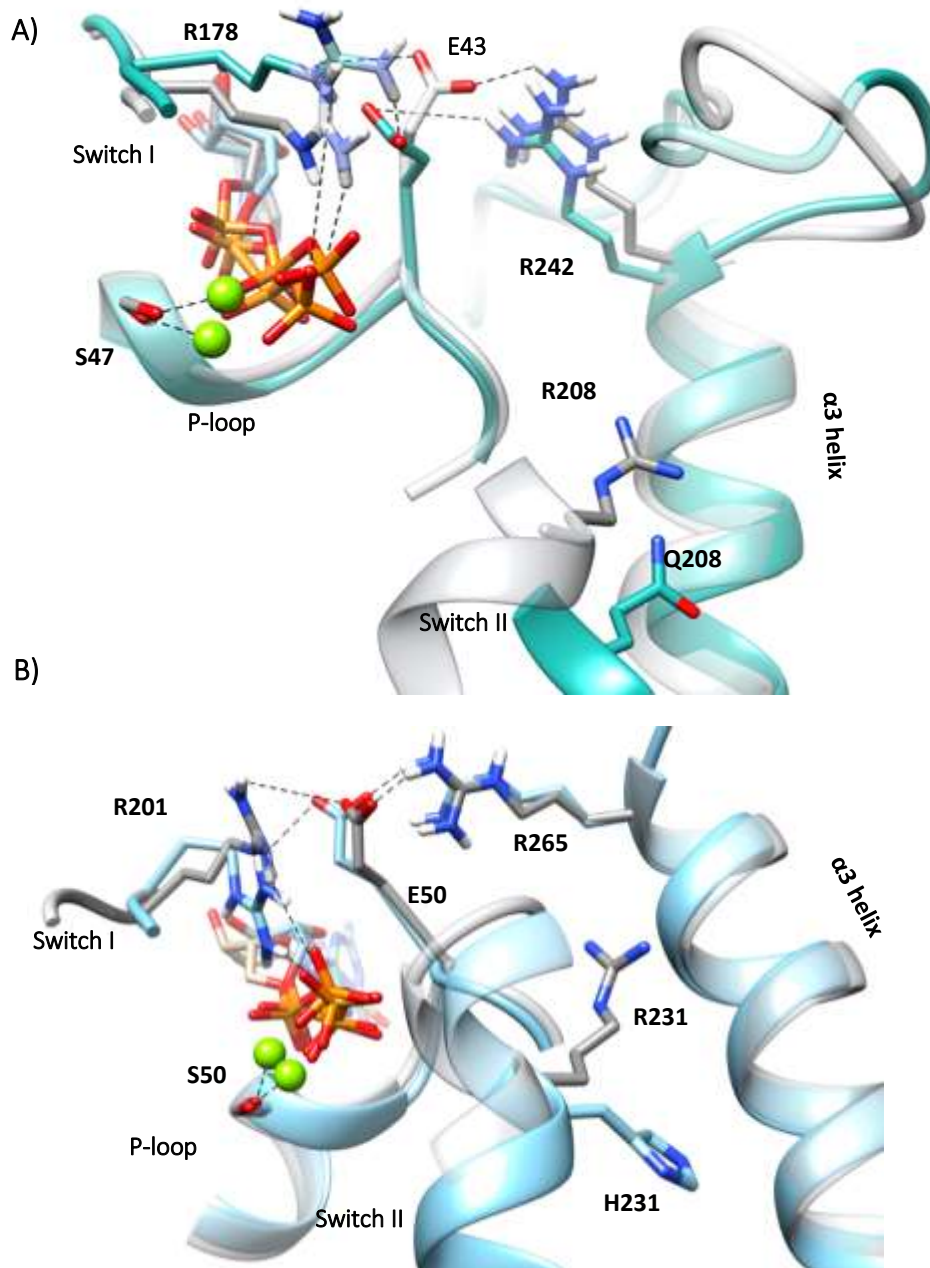


Figure 12. Superposition of the WT and mutant nucleotide binding sites after simulation. **(A)** R208Q $G_{\alpha i1}$ mutant (teal) and WT $G_{\alpha i1}$ (gray). **(B)** R231H $G_{\alpha s}$ mutant (blue) and WT $G_{\alpha s}$ (gray). Mg^{2+} is shown in green and the phosphates of the nucleotide are depicted in orange.

Table 4. Interaction energies and distances between networking residues that are involved in GTP hydrolysis. Interaction energies calculated are a combination of electrostatic and Van der Waals interactions

$G_{\alpha 1}$				$G_{\alpha s}$							
Interaction	Interaction Energy			Distance (Å)			Interaction	Interaction Energy		Distance (Å)	
	WT	R208Q	R208A	WT	R208Q	R208A		WT	R231H	WT	R231H
R242 - E43	-60.1	-30.8	-62.3	3.0	5.2	2.0	R265 - E50	-87.2	-84.6	2.1	2.0
E43 - R178	-33.0	-92.0	-32.0	4.6	1.8	5.1	E50 - R201	-34.6	-32.0	4.0	4.8
R178 - γPO_4^{2-}	-100.0	-27.0	-72.7	2.8	5.6	2.8	R201 - γPO_4^-	-40.8	-103.5	6.9	3.4
Mg ²⁺ - S47	-38.9	-30.2	-30.3	2.2	2.3	2.1	Mg ²⁺ - S54	-29.7	-46.9	2.2	2.0

Interaction Energy reported in kcal* mol^{-1}

Within the switch II region, an interaction between F215 and W258 in the WT $G_{\alpha 1}$ seems to be missing in the R208Q mutant, which causes the $\alpha 3$ helix to shift away compared to WT. This interaction is not found in WT $G_{\alpha s}$ and therefore the $\alpha 3$ helix is left largely unperturbed.

In both proteins, Q204 in $G_{\alpha 1}$ (Q227 in $G_{\alpha s}$) is believed to be crucial for hydrolysis to occur *via* interactions with a nucleophilic water (6). Our simulations are inconclusive as to whether the catalytic Q204 is affected by the R208Q mutation because this residue may orient the nucleophilic water but cannot be observed in a water box and remain in the nucleotide binding site. We attempted to use the nucleotide as a reference point but the modeled R208A $G_{\alpha 1}$ interaction energies were not significantly different from those for the R208Q $G_{\alpha 1}$ mutant, which is not consistent with the known similarity of the rates of GTP hydrolysis of WT and R208A proteins.

There are currently no crystal structures of $G_{\alpha 1}$ in complex with AC but the contact residues have been identified as E207, R208, K209, and I212 from the switch II region, and K312, R313, K314, K315, T316, and E318 of the $\alpha 4$ - $\beta 6$ loop (52). To determine if the oncogenic phenotype is a result of an inability to properly bind AC, the surface accessible surface area (SASA) values for the $G_{\alpha s}$ -AC complex interface were compared to those for WT $G_{\alpha 1}$ and its R208Q $G_{\alpha 1}$ mutant alone (Figure 13A). Of these, only the R313 and K314 residues have significantly different SASA values. WT R313 has a SASA value of $156.9 \pm 13.4 \text{ \AA}^2$ and is less exposed to solvent than R313 in the R208Q mutant, which has a SASA of $178.5 \pm 12.6 \text{ \AA}^2$. The SASA value of K314 in WT $G_{\alpha 1}$ was $56.5 \pm 8.2 \text{ \AA}^2$ vs $102.3 \pm 12.6 \text{ \AA}^2$ in the R208Q mutant. The difference in SASA between the WT and R208Q proteins is -34.9 \AA^2 , suggesting that the interface

between the R208Q $G_{\alpha 1}$ – AC would be largely left unaltered, and the interaction with AC would be similarly efficient. Using the overall SASA values to estimate the relative strengths of the WT $G_{\alpha 1}$ – AC and R208Q $G_{\alpha 1}$ – AC interfaces is limited by the fact that the calculations are based on models rather than on actual structures of $G_{\alpha 1}$ complexes. This assessment also fails to take into account the post-translational myristoylation at glycine 2 that has been shown to be necessary for $G_{\alpha 1}$ to bind AC (22).

Although $G_{\alpha s}$ undergoes a post-translational lipidation in which a palmitoyl group is added to the N-terminus that allows it to bind the membrane, however, it is not necessary to bind AC (23). A crystal structure of $G_{\alpha s}$ in complex with AC has been solved (PDB ID 1AZS) and the interface is known. R231, R232, W234, Q236, N239, L272, N279, R280, W281, L282, R283, and T284 have been shown to interact with the C2 domain of AC (54). *In vivo* studies have previously shown that the R231H $G_{\alpha s}$ mutation decreases cAMP accumulation (118, 127). Furthermore, it has been shown that the R231H mutation does not inhibit binding of $G_{\alpha s}$ to AC (118). Using the structure of WT $G_{\alpha s}$ complexed with AC (54), we were able to confirm these results by modeling the interface residues. The sum of the interactions between interface residues was $-192.9 \text{ kcal} \cdot \text{mol}^{-1}$ for WT $G_{\alpha s}$ and $-191.5 \text{ kcal} \cdot \text{mol}^{-1}$ for the R231H mutant (Figure 14). Additionally, the SASA of $G_{\alpha s}$ alone was comparable to the results seen in $G_{\alpha 1}$, the surface area of all the residues that contact AC was not changed significantly (Figure 13B). These calculations agree with those findings by showing that since the R231H $G_{\alpha s}$ mutant shows an increased rate of GTP hydrolysis, the overall duration of the stimulating $G_{\alpha s}$ – AC interaction would be shorter, therefore, resulting

in decreased cAMP production by AC. Conversely, the lower GTPase activity of $G_{\alpha i1}$ results in a longer inhibiting $G_{\alpha i1}$ – AC interaction that would also lead to lower cAMP concentrations.

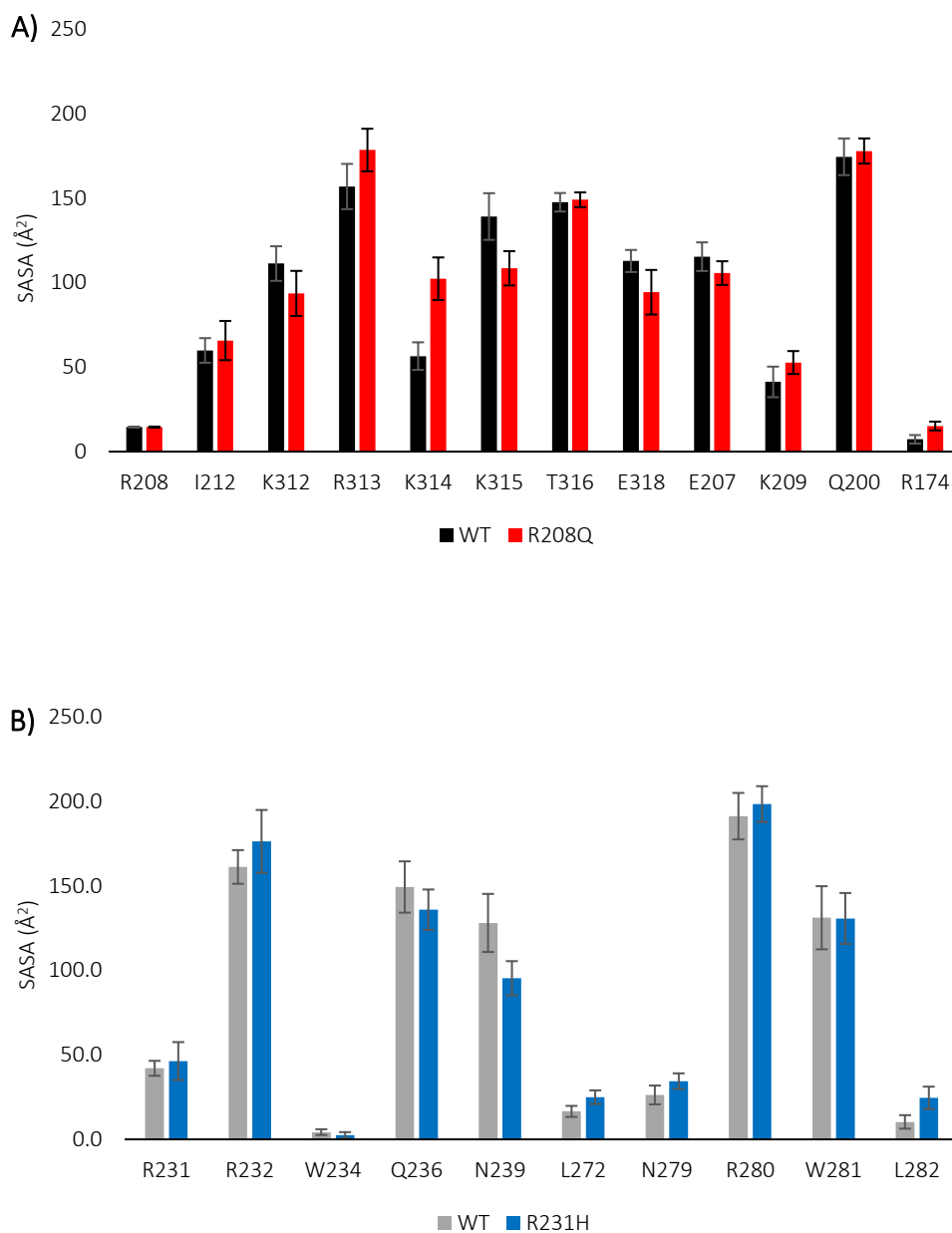


Figure 13. SASA of the residues that interact with the C1 domain of AC. **A)** WT $G_{\alpha i1}$ (black) vs R208Q $G_{\alpha i1}$ (red) **B)** WT $G_{\alpha s}$ (gray) vs R231H $G_{\alpha s}$ (blue). Values given in Å², and errors reported as standard deviation.

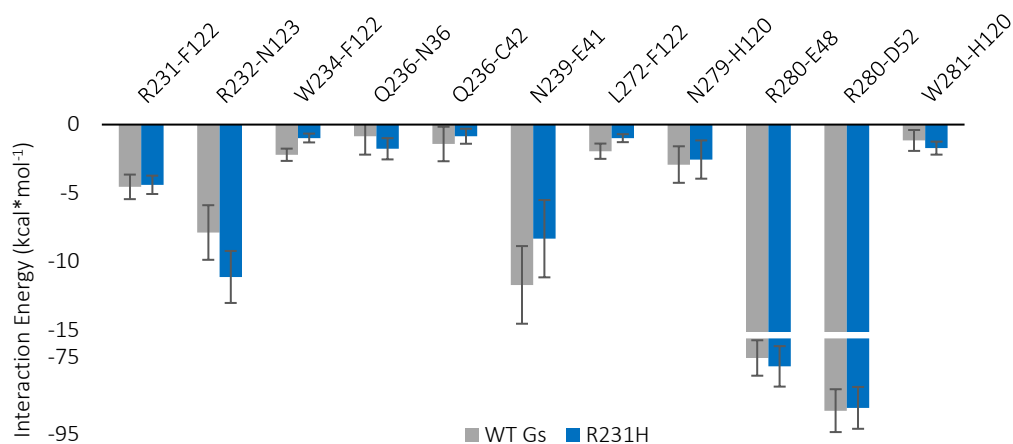


Figure 14. Interaction energies between $G_{\alpha s}$ and AC modeled from 1AZS structure. WT $G_{\alpha s}$ (gray) vs simulated R231H $G_{\alpha s}$ (blue). Units of kcal*mol⁻¹, errors reported as standard deviations.

Conclusion

The crystal structure of the R208Q $G_{\alpha i1}$ mutant is similar to the WT but important differences in the switch regions likely affect the function of the protein. Using two indirect experimental approaches, we showed that the GTPase activity is decreased in the $G_{\alpha i1}$ mutant but increased in the $G_{\alpha s}$ mutant. MD simulations suggest that the microenvironments in the vicinity of the mutations are altered thereby affecting the interaction of key residues in the nucleotide binding site. In R208Q $G_{\alpha i1}$, the energy of the interaction between E43 and R178 increased hindering catalysis by preventing the guanidinium group of the R178 from stabilizing the negative charge on the leaving P_i . R231H $G_{\alpha s}$ is affected in the opposite manner with an increase in E_i between the comparable R201 and γ - PO_4^{2-} compared to the WT protein, which is amplified by the increased E_i seen between S50 and the Mg^{2+} cofactor. Modeling the binding site of G_{α} proteins and AC shows that the interface is minimally affected suggesting that the

differences in cAMP accumulation reported by *in vivo* studies are primarily a result of changes in the rates of GTP hydrolysis.

CHAPTER THREE

PROTEIN FOLDING OF THE R208Q MUTANT

Guanine nucleotide-binding proteins (G-proteins) are regulatory membrane-bound proteins that play an indispensable role in transferring extracellular information across the cell membrane to affect intracellular events. G-proteins are heterotrimeric in that they are composed of an α subunit (G_α), which regulates the activity of the effector protein, and a $\beta\gamma$ subunit complex (4). Inactive G_α subunits are complexed with G-protein coupled receptors, that, once activated by specific ligands, induce conformational changes in the G_α subunits, which prompt the exchange of guanosine 5'-diphosphate (GDP) for guanosine 5'-triphosphate (GTP) and the dissociation of the $\beta\gamma$ dimer (128-130). An α -subunit regulates the appropriate enzyme through direct contact. This process is self-regulated, with hydrolysis of bound GTP to GDP effectively deactivating G_α and reforming the heterotrimeric G-protein (128).

G-proteins are involved in stimulus-sensitive signal transduction pathways that have been fine-tuned to allow the cell to respond to changes in the environment. Disruptions in this balance may lead to disease states. While there are four families of G_α proteins (8), we limited this study to $G_{\alpha i1}$ and $G_{\alpha s}$, which regulate the activity of adenylyl cyclase (AC) (Figure 15) (131). $G_{\alpha s}$, encoded by the *GNAS* gene, up-regulates the synthesis of the secondary messenger cyclic AMP, and the *GNAI1* gene that encodes for $G_{\alpha i1}$, decreases the concentration of cAMP (50). *GNAS* mutations are found in several cancers, including thyroid, large intestine, pituitary, adrenal

glands, biliary tract, pancreas, and the central nervous system (68, 74). Mutations in *GNAI1*, on the other hand, are associated with carcinomas in the large intestine and are found in hematopoietic and lymphoid tissue, and in the upper digestive tract (68). The mutations in *GNAS* and in *GNAI1* genes have been observed in 4.2% and 0.4% of human cancers, respectively (68, 104).

One mutation of interest involves an arginine (Arg) located close to a tryptophan (Trp) in the conserved switch II region of G_{α} subunits (52, 86, 132). Figure 15 shows that the guanidinium group of R231 in G_{α_s} (R208 in $G_{\alpha_{i1}}$) is involved in a π -cation interaction with the indole ring of W234 G_{α_s} (W211 in $G_{\alpha_{i1}}$) when the protein is in the active conformation (13, 15, 17, 85). The oncogenic mutations, R231H in G_{α_s} and R208Q in $G_{\alpha_{i1}}$, disrupt this interaction, which has been shown to be crucial for protein stability (133). Furthermore, it has been reported that the R231H G_{α_s} mutation results in a decrease in cAMP production (118), although the mechanism of action is unknown. Loss of the π -cation interaction could cause changes in the secondary structure by altering the points of contact between G_{α} subunits and AC. Alternatively, these mutations could cause changes in the positions of residues vital to GTPase activity.

The focus of this study is to gain an understanding of the structural differences on the protein stability of the oncogenic R231H in G_{α_s} and R208Q in $G_{\alpha_{i1}}$ mutants. Several biophysical spectroscopic techniques were used for monitoring temperature-induced denaturation. Our results indicate that the Arg mutations that resulted in the loss of the π -cation interaction were not evident in the secondary structures at room temperature, but a decrease in protein stability was observed at higher temperatures. Computational methods were used to interpret the

structural variations in the WT $G_{\alpha s}$ and $G_{\alpha i1}$ proteins and their corresponding mutants.

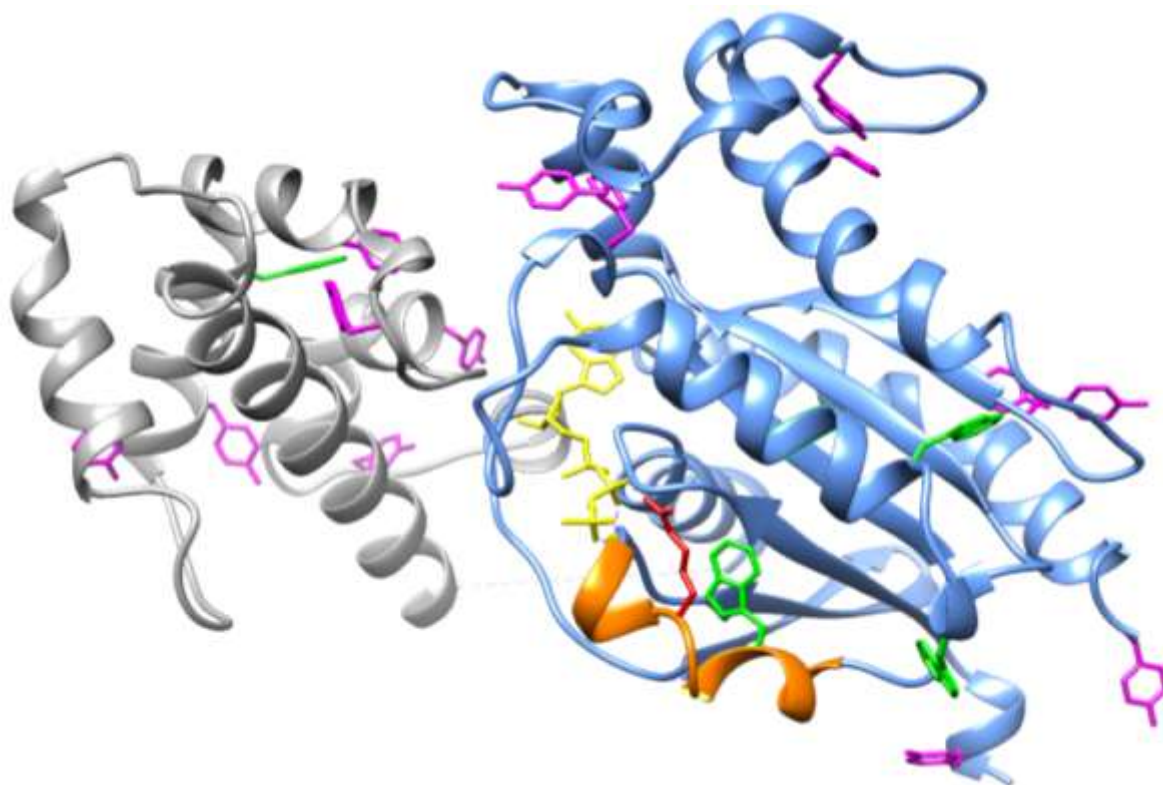


Figure 15. Crystal structure of WT $G_{\alpha s}$ •GTP γ S displaying its four tryptophan residues (green), fourteen tyrosine residues (purple), GTP γ S bound nucleotide (yellow), Mg^{2+} (green sphere), and R234 (red) that is involved in a π -cation interaction with W234. (PDB ID: 1AZT)

Materials and Methods

Expression and Protein Purification

$G_{\alpha i1}$ and $G_{\alpha s}$ were obtained and purified as previously described (95, 107). Arg single-point mutants of $G_{\alpha i1}$ were prepared by site-directed mutagenesis using a Quickchange II kit by Agilent (La Jolla, CA). $G_{\alpha s}$ mutant was purchased from Bio Basic. After purification on a Ni^{2+} affinity column followed by a Superdex 200-pg size exclusion column, the purity of GDP-bound

G_{α} proteins was found to be greater than 95% as estimated by SDS – PAGE. Protein was stored at -80°C in 20 mM Tris, pH 8.0 buffer containing 10% (v/v) glycerol, and 1 mM DTT.

Fluorescence-Monitored GTP γ S Exchange

Experiments were performed with a PTI QuantaMaster fluorimeter (Photon Technologies, Inc., Mirroringham, NJ). Indirect activity assays were conducted with excitation and emission wavelengths set at 280 nm and 340 nm, respectively. Assays were initiated after 60 sec by the addition of 20 μM of GTP γ S to pre-incubated 400 nM $G_{\alpha}\bullet\text{GDP}$ protein samples in buffer containing 50 mM HEPES, pH 7.5, 2 mM MgSO_4 , and 1 mM DTT, and was monitored for 3 hr at 25°C . The GDP- and GTP γ S- bound proteins that were characterized by the activity assays were used in the following denaturation studies.

Fluorescence-Measured Protein Denaturation.

Emission spectra for both GDP- and GTP γ S-bound proteins were recorded over the wavelength range of 300 to 400 nm with the excitation wavelength set at 280 nm. Signal integration time was 0.2 sec with the bandpass for excitation and for emission set at 5 nm. The denaturation experiments started at a temperature of 4°C followed by 4°C increments and concluding at the highest temperature before precipitation occurred. There was a 2 min equilibration period at each set temperature. All T_m values were calculated from fluorescence intensities at the spectral λ_{max} positions for the selected temperatures, using methods adapted from those previously described (134).

UV/Vis-Measured Protein Denaturation

The environments of Tyr (and to a lesser extent Trp) residues in G_{α} proteins were monitored on a Hewlett Packard UV – Vis spectrophotometer. All samples contained 50 mM Tris, pH 7.5, 1 μ M G_{α} •GDP protein, 1 mM DTT, and 2 mM $MgSO_4$. Prior to initiating the experiments, samples were incubated with their respective nucleotide, 2.5 μ M G_{α} •GDP or 20 μ M GTP γ S, at room temperature for 1 hr. The temperature was increased from 20 °C to 80°C, at 0.3 °C*min⁻¹ over 180 mins. For each temperature studied, samples were equilibrated for 1 min and the absorbance was monitored in the wavelength range of 220 – 300 nm. All melting temperatures were calculated from the absorbance values at 280 nm values for the different temperatures, using methods previously described (135).

CD-Measured Protein Denaturation

Experiments were performed using an Olis DSM 20 circular dichroism spectrophotometer. All samples were placed in a cylindrical quartz cuvette with a 1 mm pathlength and contained either 3 μ M G_{α} •GDP or 24 μ M G_{α} •GTP γ S, in 10 mM phosphate, pH 7.5 buffer, 1 mM DTT, and 2 mM $MgSO_4$. Data were collected at 150 V every 1 nm in the wavelength range of 190 nm to 260 nm. The temperature was increased from 20 °C to 100 °C at 4 °C increments with an incubation time of 3 min at each temperature studied. The CONTIN LL algorithm was used to deconvolute the spectra using reference sets with denatured proteins (97) to calculate the percent of each type of secondary structure and T_m values for each protein studied (136, 137).

Results and Discussion

The π -Cation interaction in G_α Subunits:

Upon activation, the Trp located in the switch II region of G_α proteins moves from a less hydrophobic into a more hydrophobic microenvironment, which results in a 30-45% increase in the fluorescence intensity (Figure 16) (85, 95)(80, 95, 138). We observed a red-shift when comparing the differences in wavelengths at maximal emission intensities (λ_{\max}) of the WT $G_{\alpha S}$ and its R231H mutant in the GDP and GTP γ S conformations (Figure 17A). The red-shift was a result from a π -cation interaction between the positively charged guanidinium group of R231 in $G_{\alpha S}$ (R208 in $G_{\alpha i1}$) with the π -electron system of W234 $G_{\alpha S}$ (W211 in $G_{\alpha i1}$) (85, 95). Red-shifts of 3.1 ± 0.3 nm and 3.45 ± 1.0 nm were observed at 20 °C for WT $G_{\alpha S}$ and WT $G_{\alpha i1}$, respectively (Figure 17B and Figure 18). The red-shift for WT $G_{\alpha S}$ gradually decreased up to 52 °C, after which it became a blue-shift until precipitation occurred at 68 °C. This observation signifies that the electrostatic interaction between W234 and R231 weakens as the protein unfolds and severs at higher temperatures resulting in a blue-shift. The R231H $G_{\alpha S}$ mutation afforded a $\Delta\lambda_{\max}$ value of 1.6 ± 0.2 nm (blue-shift) at 20 °C, revealing a disruption of the π -cation interaction when compared to the WT $G_{\alpha S}$ (Figure 17B). R231H $G_{\alpha S}$ is missing the positive charge of the Arg residue, thus the π -electrons of W234 can no longer form electrostatic interactions and instead move into a hydrophobic pocket after activation. With an increase in temperature, the $\Delta\lambda_{\max}$ value of the R231H $G_{\alpha S}$ mutant did not change significantly until R231H $G_{\alpha S}$ •GDP precipitated at 72 °C, indicating that W234 does not form new interactions with other charged residues in the switch II region during thermal denaturation.

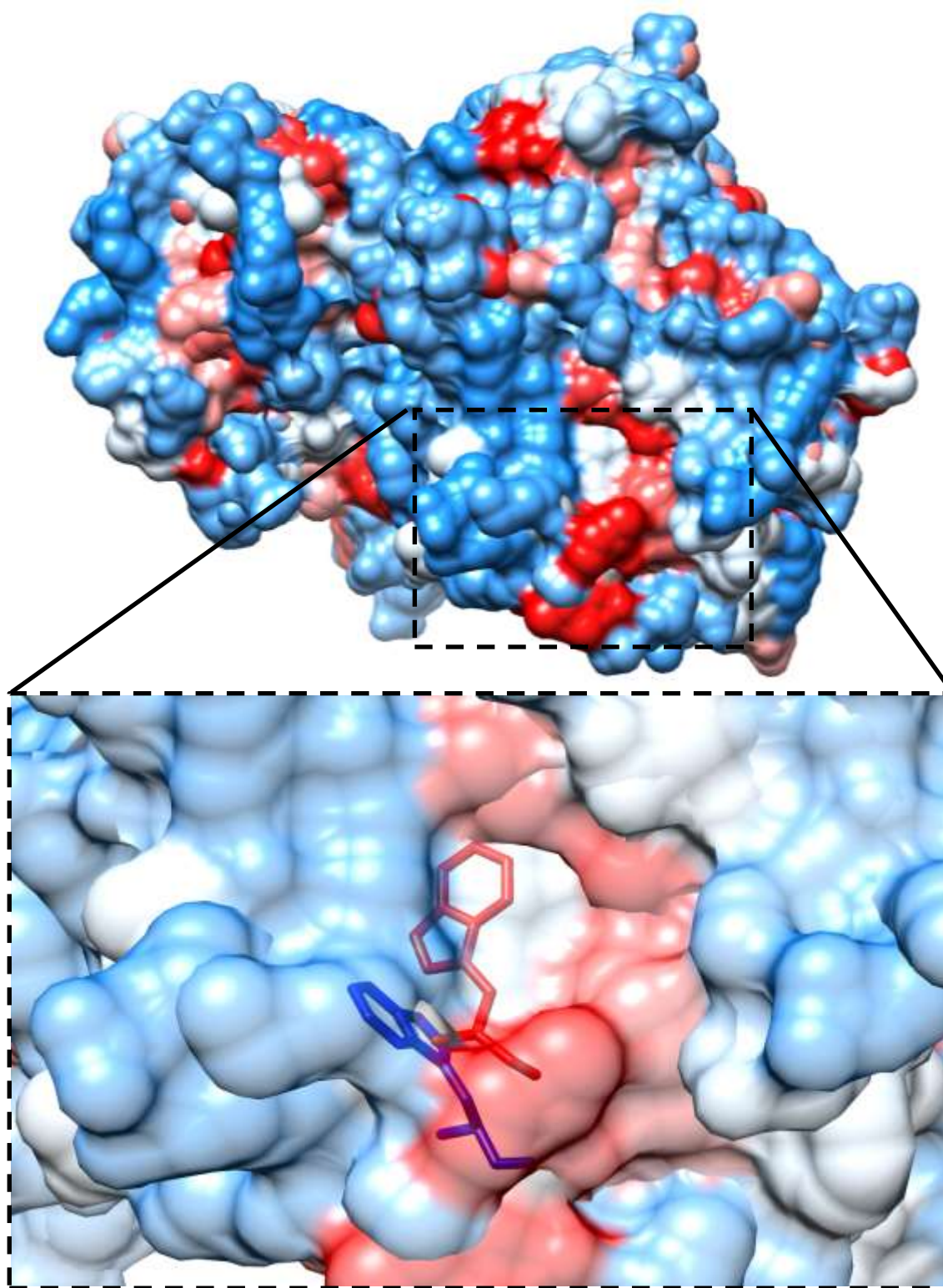


Figure 16. The microenvironment hydrophobicity surrounding W211 as it goes from its inactive to its active conformation. Blue represents a more hydrophilic red represents a more hydrophobic environment. From PDB: 1GIA.

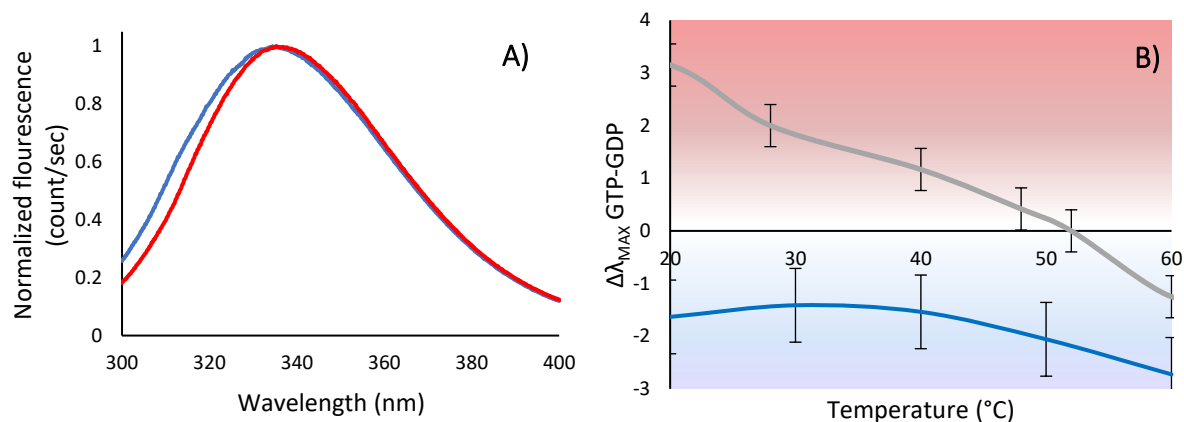


Figure 17. **A)** Normalized emission spectra of WT $G_{\alpha s} \bullet GDP \bullet Mg^{2+}$ before (blue) and after (red) activation with GTP γ S at 20 °C; **B)** Temperature variation of the difference between the λ_{max} values of the GTP γ S and GDP conformations of WT $G_{\alpha s}$ (gray) and $G_{\alpha s}$ R231H (blue).

Similar to the WT $G_{\alpha s}$ protein, the red-shift of WT $G_{\alpha i1}$ was inversely correlated with temperature, but it did not become blue-shifted as the temperature increased (Figure 18). The differences in the two systems could be attributed to the increased stability of the WT $G_{\alpha i1} \bullet GTP\gamma S$ compared to WT $G_{\alpha s} \bullet GTP\gamma S$ (139). The greater stability would require higher temperatures to disrupt non-covalent interactions, protecting the π -cation interaction in the active conformation of WT $G_{\alpha i1}$. As for the behavior of the R231H mutant discussed above, a temperature-dependent decrease in the magnitude of the blue-shift would be expected for the R208Q $G_{\alpha i1}$ mutant. However, a red-shift of 1.7 ± 0.7 nm was observed at 20 °C. The red-shift gradually declined to a negligible $\Delta\lambda_{max}$ value of 0.3 ± 0.8 nm until denaturation occurred at 60 °C (Figure 18). The measured red-shift at 20 °C was unexpected, suggesting the presence of another interaction mechanism for stabilization of π -electrons that was absent in the WT $G_{\alpha i1}$, R208Q $G_{\alpha i1} \bullet GDP$, and $G_{\alpha s}$ systems.

To investigate this possibility, we applied molecular dynamics to WT $G_{\alpha 1}$ and R208Q $G_{\alpha 1}$. To determine the conformation-dependent intermolecular changes that give rise to the red shift, we used the inactive protein as a reference to calculate the differences in the electrostatic interaction energies of the GTPyS and GDP conformations. For WT $G_{\alpha 1}$ the difference in interaction energy between the W211 and the R208 residues is $-3.98 \text{ kcal}\cdot\text{mol}^{-1}$, while, for the R208Q mutant, the W211-Q208 interaction is weakened to $-0.84 \text{ kcal}\cdot\text{mol}^{-1}$ (Table 5) indicating that, because there is a weaker interaction with W211, the red-shift is unlikely due to an interaction between these residues (140). Further examination revealed that, for the mutant, Q208 has a weaker electrostatic interaction with E245 ($-1.22 \text{ kcal}\cdot\text{mol}^{-1}$) at the end of the $\alpha 3$ helix, than R208 in WT $G_{\alpha 1}$ •GTPyS ($-79.75 \text{ kcal}\cdot\text{mol}^{-1}$), thus perturbing both the $\alpha 3$ helix and the switch II region (141). These disruptions propagate outwards towards F215 and orient it into a position that can interact with F199 (Figure 19). A T-oriented π - π stacking with Van der Waals interaction energy of $-1.59 \text{ kcal}\cdot\text{mol}^{-1}$ is formed in the active conformation, which is not found in the WT $G_{\alpha s}$, R231H $G_{\alpha s}$, and WT $G_{\alpha i 1}$ systems.

In addition to calculating interactions energies (Table 5), changes in surface area solvent accessibility area (SASA) when GDP is exchanged for GTP (Table 6) were also determined to gain

Table 5. Interaction energies within residues from the WT $G_{\alpha i 1}$ and Arg mutants

	Electrostatic		VdW		Total		Distances	
	WT	R208Q	WT	R208Q	WT	R208Q	WT	R208Q
W211-R208(Q)	-3.98	-0.84	-6.24	0.99	-10.22	0.15	4.42	6.13
R208(Q)-E245	-79.75	-1.22	2.28	0.04	-77.47	-1.18	2.61	5.07
F215-F199	0.04	-0.01	-0.16	-1.59	-0.12	-1.6	8.93	4.83
W258-F259	1.9	-1.05	-0.16	-0.27	1.73	-1.31	6.05	5.2

Calculated interaction are in kcal/mol

Distances measured in Å

insight into the interactions in these proteins. The change in SASA value for W211 in WT $G_{\alpha 1}$ was -121 \AA^2 compared to -57 \AA^2 in R208Q, but for W258, it decreased to -98 \AA^2 in the R208Q protein from -37 \AA^2 in the WT $G_{\alpha 1}$ (Table 6). Therefore, as an

Table 6. Change in SASA (\AA^2) exposure of W residues in WT $G_{\alpha 1}$ and R208Q Mutant

	WT	R208Q
W211	-121	-57
W258	-37	-98

interaction between F199 and F215 is formed during activation, a gap opens up between the switch II region and $\alpha 3$ helix, allowing water to enter, thereby reducing the contribution of W211 the fluorescence intensity as measured by an increase in SASA. The changes in SASA values indicate that W258 becomes the primary contributor towards fluorescence intensity at 350 nm as well as explains the lower intensity observed in the R208Q mutant (Figure 20). In both WT and R208Q proteins, the W258 residue interacts with F259 in a π - π interaction. In WT and R208Q $G_{\alpha 1}$ proteins, the calculated total interaction energies are relatively strong -18.47 and -16.46

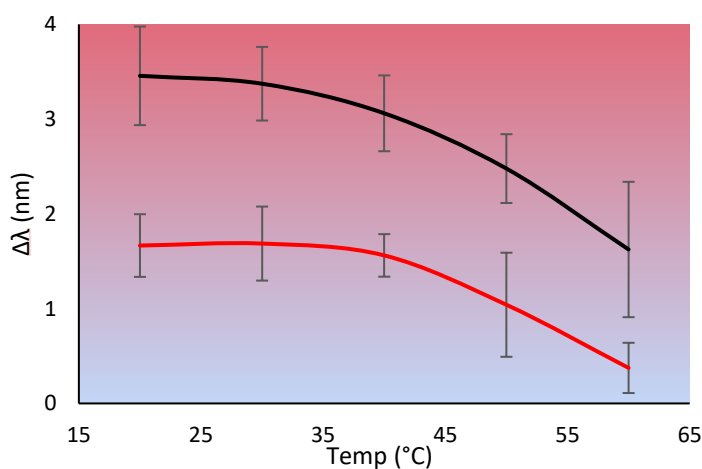


Figure 18. Temperature variation of the difference between the λ_{\max} values of the $GTP\gamma S$ and GDP conformations of various WT $G_{\alpha 1}$ (black) and $G_{\alpha 1}$ R208Q (red).

kcal* mol^{-1} , respectively (Table 5). Therefore, when W258 in the R208Q moves into a hydrophobic environment, a red shift is predicted as observed at 20 °C (Figure 18).

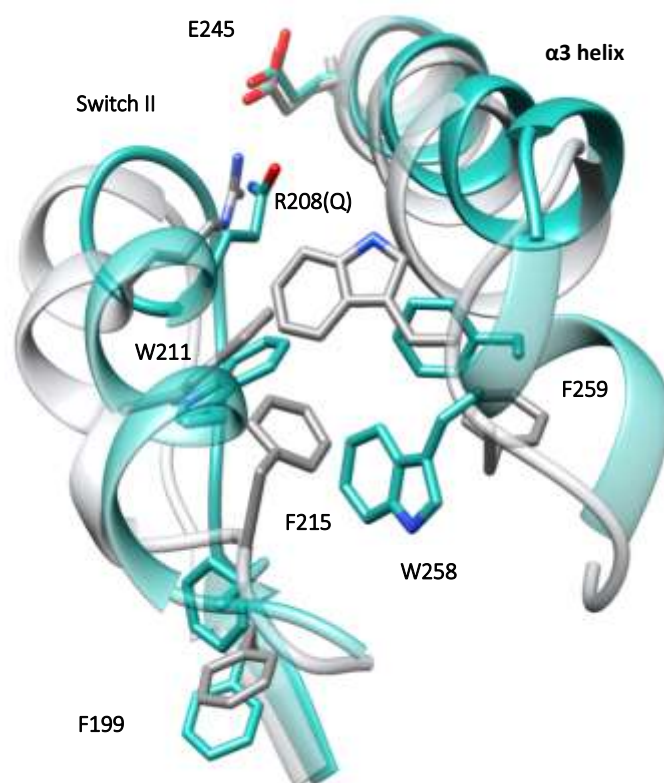


Figure 19. Relative interresidue interactions in WT $G_{\alpha i1}$ (gray) and in R208Q (green) in the GTPyS conformation.

Temperature Denaturation of G_{α} Proteins:

Cation- π interactions contribute to protein stability and previous experiments suggest that disruptions in mutant proteins can propagate through networks of non-covalent interaction (87, 133, 142, 143). To gain a complete picture of the impact of disrupting π -cation interactions, thermal denaturation experiments were used to test the structural stability of the WT and mutant proteins. The melting temperatures (T_m) values were estimated for the active and

inactive conformations of the Arg mutants and compared to the respective WT proteins.

Denaturation was measured via the changes in fluorescence intensity and UV absorbance

resulting from changes in the solvent exposure of Trp and from tyrosine (Tyr) residues, and from

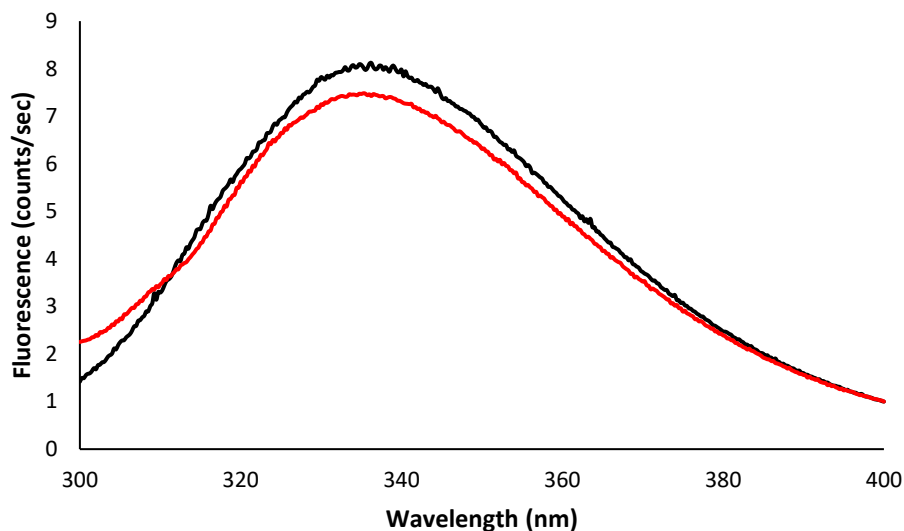


Figure 20. Emission Spectra of WT (black) and R208Q (red) $G_{\alpha i1}$ proteins in the GTP γ S conformations

the change in the percent secondary structure.

Solvent Exposure of Trp residues:

The fluorescence emission spectra profile of the oncogenic mutants was measured between 20 - 80 °C. The decrease in fluorescence intensity due to the exposure of Trp to increasingly hydrophilic environments during unfolding was used to estimate melting temperatures for WT $G_{\alpha s}$, R231H $G_{\alpha s}$, WT $G_{\alpha i1}$, and R208Q $G_{\alpha i1}$ proteins (Figure 21A, Table 7).

The fluorescence intensity of WT $G_{1\alpha 1}$ •GDP decreased by 53% as the protein was heated from 20 °C to 50 °C (Figure 22A), and continued declining until 70 °C, at which point there was no change in intensity and the protein was fully unfolded. A T_m value of 41.1 ± 3.0 °C was previously

determined for WT $G_{\alpha s}$ •GDP and the 39.0 ± 1.1 °C for WT $G_{\alpha i1}$ •GDP (Table 7) (139). The observed fluorescence T_m values for the R231H $G_{\alpha s}$ •GDP and R208Q $G_{\alpha i1}$ •GDP mutants were not significantly different (0.2 to 0.9 °C lower) when compared to their WT counterparts (Table 7), which is reflected in 52% decreases in fluorescence intensity for both mutants in the GDP conformation (Figure 22 A and C). The π -cation interaction only forms in the active conformation and the Arg residue is not involved in structurally significant interactions in the GDP conformation. Therefore, the loss of the stabilizing effect from the π -cation interaction would not be evident in non-covalent interactions in the inactive conformation (139). Although the T_m measurements are technique-dependent, there were no significant differences between the

Table 7. Estimated melting temperature (°C) for G_{α} WT and mutant proteins using three spectroscopic methods.

Protein variant	Fluorescence		Circular Dichroism		UV/Vis Spectroscopy	
	GDP	GTP γ S	GDP	GTP γ S	GDP	GTP γ S
$G_{s\alpha}$ WT	41.1 ± 1.7	38.7 ± 1.0	51.9 ± 2.0	$57.4 \pm 1.5^*$	53.5 ± 1.4	63.7 ± 1.1
$G_{s\alpha}$ R231H	$38.8 \pm 0.5^\dagger$	$34.8 \pm 0.8^*$	50.9 ± 2.7	$56.4 \pm 2.4^*$	$50.5 \pm 1.8^\dagger$	$54.9 \pm 0.9^*$
$G_{i\alpha 1}$ WT	39.0 ± 0.6	$48.7 \pm 2.0^*$	44.2 ± 0.5	$70.9 \pm 2.0^*$	47.6 ± 0.1	$66.5 \pm 0.2^*$
$G_{i\alpha 1}$ R208Q	$35.1 \pm 2.5^\dagger$	$36.9 \pm 0.3^{*\dagger}$	44.1 ± 2.1	$56.8 \pm 1.8^{*\dagger}$	46.6 ± 0.1	$59.5 \pm 0.2^{*\dagger}$

* = $P \leq 0.05$ vs GDP-bound conformation

† = $P \leq 0.05$ vs WT in the same conformation

mutant and their respective WT protein in the GDP conformation (Table 7) (139).

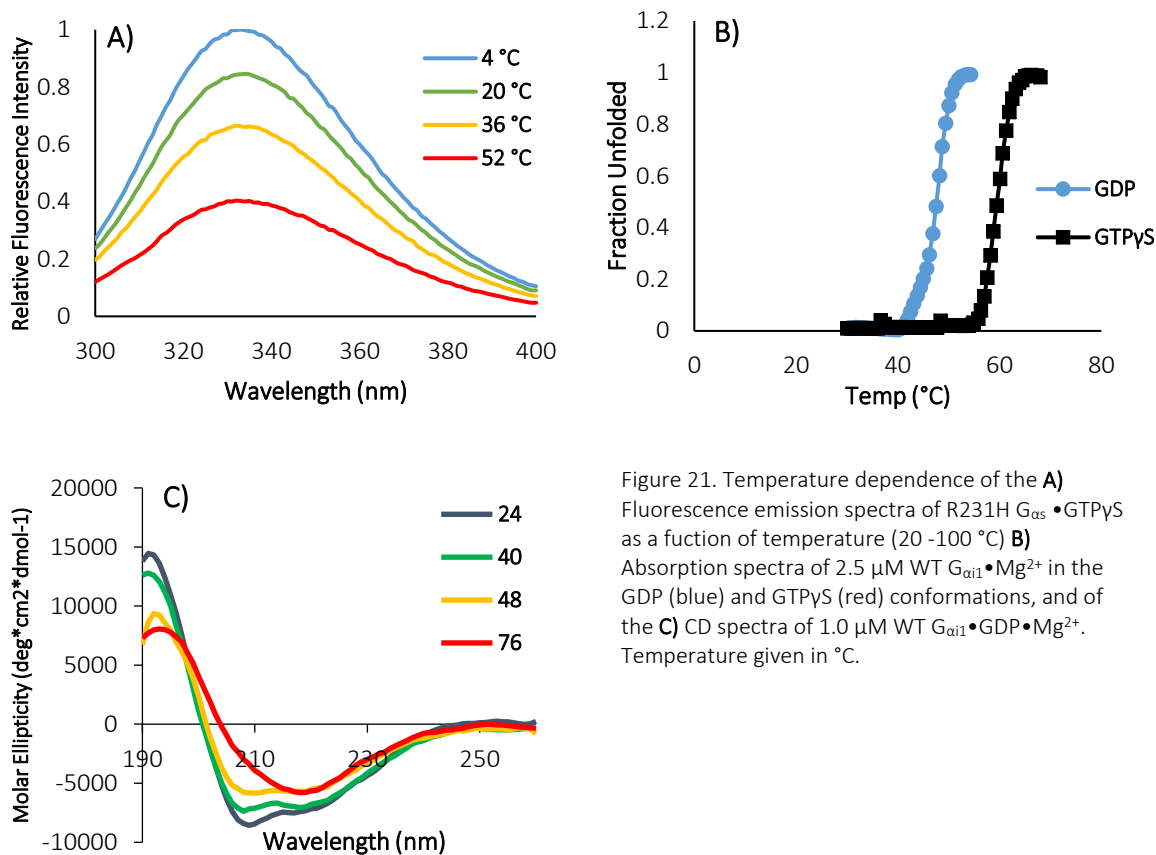


Figure 21. Temperature dependence of the **A)** Fluorescence emission spectra of R231H $G_{\alpha s}$ •GTP γ S as a function of temperature (20-100 °C) **B)** Absorption spectra of 2.5 μ M WT $G_{\alpha i1}$ •Mg $^{2+}$ in the GDP (blue) and GTP γ S (red) conformations, and of the **C)** CD spectra of 1.0 μ M WT $G_{\alpha i1}$ •GDP•Mg $^{2+}$. Temperature given in °C.

In the case of the active conformation, the melting temperature profiles for WT and mutant proteins are different. The T_m value for the R231H $G_{\alpha s}$ •GTP γ S mutant is significantly lower than that of the WT in the active and inactive conformations. The T_m values for the R208Q $G_{\alpha i1}$ mutant was 11.8 °C lower compared to the WT. The larger ΔT_m observed for the $G_{\alpha i1}$ protein is consistent with the propagation of the destabilizing effect of the R208Q $G_{\alpha i1}$ mutation as evidenced by the continued presence of a red-shift, corroborating the changes to the non-covalent interactions. A comparison of the fluorescence intensities at 20 °C and 50 °C for R208Q $G_{\alpha i1}$ •GTP γ S and WT $G_{\alpha i1}$ •GTP γ S illustrates the drastic difference in Trp microenvironments at

higher temperatures. A 62% decrease in fluorescence intensity (Figure 22D) was observed for R208Q $G_{\alpha 1}$ •GTP γ S compared to 33% decrease for WT $G_{\alpha 1}$ •GTP γ S (Figure 22B).

Solvent Exposure of Tyr residues and temperature dependence of secondary structure:

Analogous to the fluorescence experiments, the estimated T_m values from UV/Vis spectrophotometry and from the secondary structures for the mutants were significantly lower than the respective WT proteins in the GTP γ S conformation (Table 7). The ΔT_m occurred only for the active conformation, whereas the R231H $G_{\alpha s}$ mutant was 8.8 °C lower (Figure 21B) and the R208Q $G_{\alpha 1}$ was 7.0 °C lower for UV/Vis, and, for circular dichroism (CD), R231H $G_{\alpha s}$ mutant was 4.0 °C lower (Figure 21C) and the R208Q $G_{\alpha 1}$ was 14.2 °C lower for CD than their WT counterparts (Table 7). These calculations support the hypothesis that the π -cation interaction is integral to the stability of G_{α} subunits in the active conformation and that, at higher temperatures, its disruption propagates outward, thereby altering the non-covalent interactions in the overall protein structure.

Interestingly, the loss of the π -cation interaction results in a change in the unfolding progression. For the active conformation of WT $G_{\alpha s}$, the calculated T_m values indicate that the denaturation initiates at the hydrophobic Trp microenvironments and then radiates toward the secondary structure, followed by the Tyr residues at the surface. In contrast, for the WT $G_{\alpha 1}$, the disruption begins in the Trp environments, though the unfolding around Tyr residues precedes the loss of the secondary structure. However, both Arg mutants deviate from these paths. Starting from the local Trp environments, the secondary structure and the outer surface unfold

simultaneously, indicating that the lack of the π -cation interaction changes the propagation of the non-covalent network within the mutant proteins (144, 145).

Secondary Structure Content:

Circular dichroism was also used to probe the secondary structure content of the inactive and active conformations at various temperatures. The measured R231H $G_{\alpha s}$ •GDP α -helical content at 20 °C was 32.7 ± 1.2 % vs. 34.8 ± 1.6 % in WT $G_{\alpha s}$ •GDP, showing an insignificant difference in the secondary structure compared to literature values (13, 52, 86, 139). Like the inactive conformations, GTP γ S-bound proteins exhibited an α -helical content of 33.0 ± 1.7 % for R231H $G_{\alpha s}$ •GTP γ S vs. 36.0 ± 2.7 % for WT $G_{\alpha s}$ •GTP γ S at 20 °C. The R208Q $G_{\alpha i1}$ mutation resulted in similarly insignificant differences in α -helical content for the active and inactive conformations of the WT and mutant $G_{\alpha s}$ proteins. These results were unexpected given that there was a significant decrease in the stability of the arginine mutants. This suggests that, although there is a change in protein stability, the arginine mutation may not change the interaction with the AC effector. The change in the cAMP production caused by the arginine mutation is more likely due to a change in the rate of hydrolysis of the GTP nucleotide.

When the temperature was increased from 36 °C to 64 °C for the active conformations of WT as well as for the $G_{\alpha s}$ and $G_{\alpha i1}$ mutant proteins, the CD spectra showed a dramatic change in secondary structure, with a 15% – 20 % decrease in the amount of α helices. The primarily α – helical proteins became increasingly dominated by β – sheets, increasing from 10 % to 30 % (Figure 23). Temperatures above 64 °C displayed little change in the spectra and the protein eventually precipitated at 84 °C.

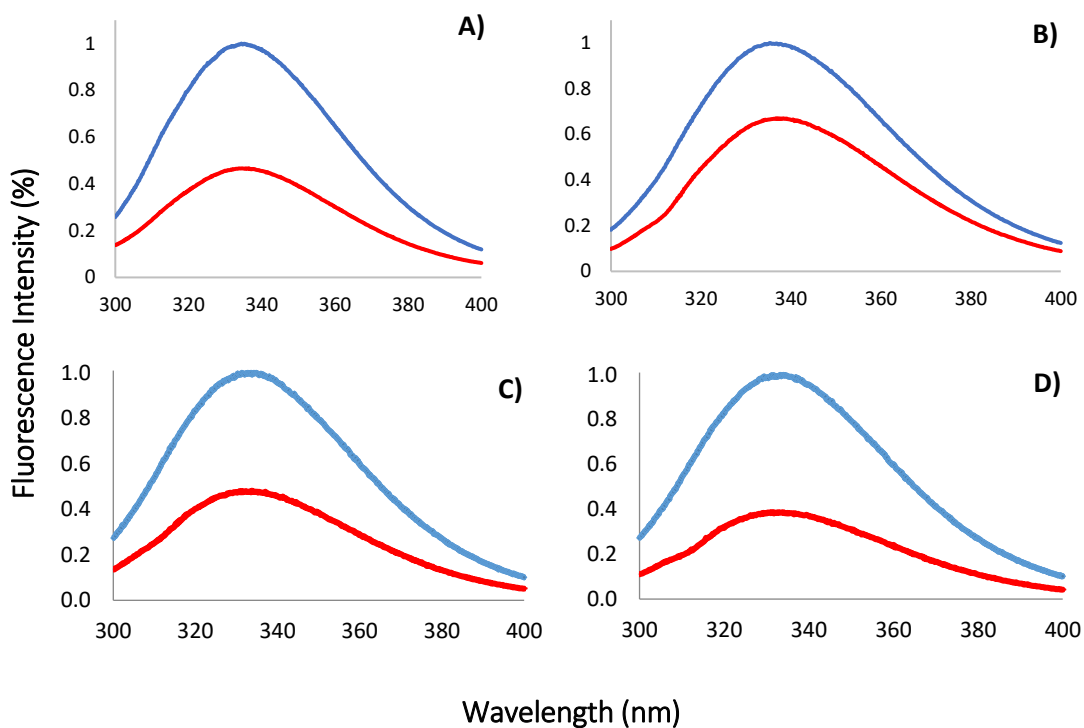


Figure 22. Intrinsic Trp fluorescence of WT and R208Q $G_{\alpha i1}$ proteins. Emission spectra of 0.4 μM of $G_{\alpha i1} \cdot \text{Mg}^{2+}$ at 20 °C (blue) and 50 °C (red) of WT in the **A)** GDP or **B)** GTP γ S conformations, and of R208Q in the **C)** GDP or **D)** GTP γ S conformations.

Neither mutation significantly diverged from their WT counterpart, as was expected from the previously discussed stability study.

In the case of the active GTP γ S conformations, the secondary structure of the WT and mutants of $G_{\alpha s}$ and $G_{\alpha i1}$ proteins did not significantly diverge in the temperature range 20 °C to 40 °C, but for temperatures between 32 °C and 64 °C a dramatic deviation from WT $G_{\alpha s}$ was observed in the α – helical content of R231H $G_{\alpha s}$ (Figure 23) and R208Q $G_{\alpha i1}$ mutants (data not shown). The occurrence of unfolding in the α -helical structure at different temperatures may be related to the lack of the π -cation interaction in the mutant proteins.

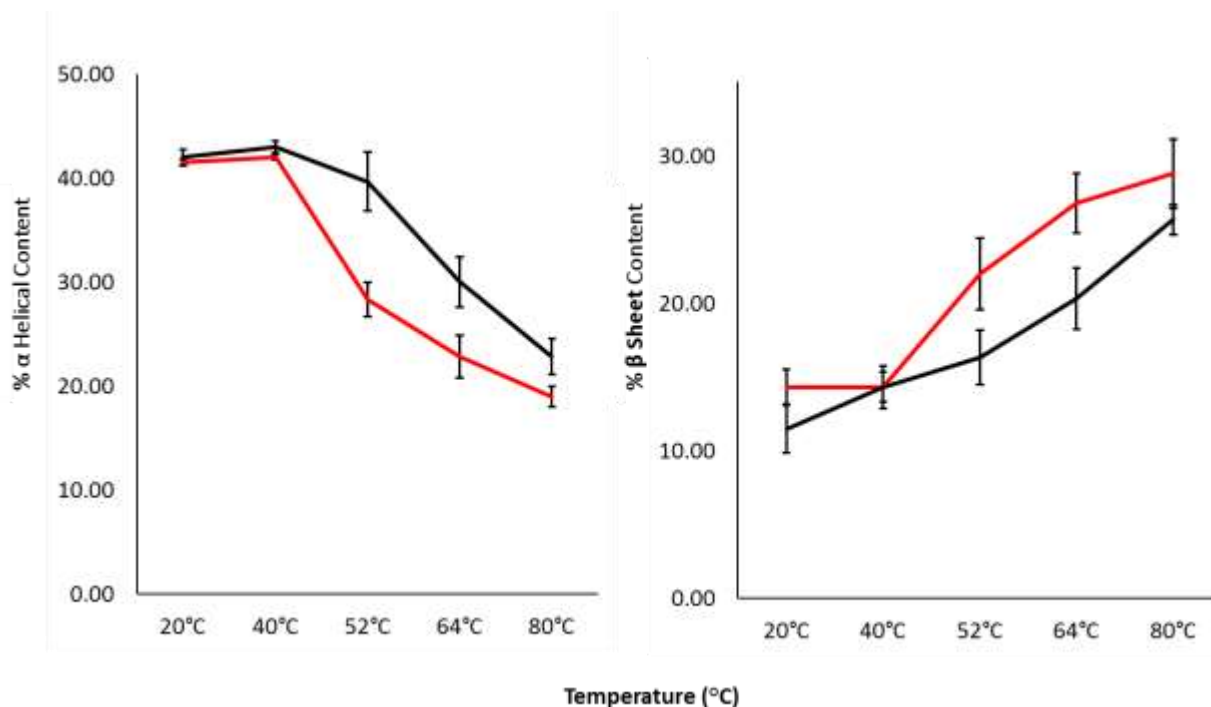


Figure 23. Calculated % secondary structure of **A)** α - helices and **B)** β - sheets in the GTP γ S conformations of WT G α_{i1} (black) and R208Q (red) as a function of temperature.

Conclusion

This study highlights the importance of the π -cation interaction towards protein stability. Mutations of an essential Arg residue involved in the interaction leads to a destabilization of the switch II region and the complete loss of the red-shift in the case of R231H G α_s . The R208Q mutation in G α_{i1} did not abolish the red-shift with an increase in temperature, leading us to conclude that the decreased interaction between residues Q208 and E245 results in the weakening the structural integrity in the immediate vicinity of the residues. The weak Q208-E245 interaction propagated outward, leading to the formation of an F199-F215 π - π interaction in R208Q G α_{i1} •GTP γ S. As a result, the W258 residue, which is involved in a π - π stacking interaction with F259, moves into a more hydrophobic microenvironment thus accounting for a red-shift.

Although the mutations alter the position of several residues, they do not change the secondary or tertiary structures at room temperature as measured by CD. These results suggest that the differences in production of cAMP between WT and mutant proteins are not a consequence of changes in the contact points between AC and G_{α} subunits (118). While the structures are not changed at room temperatures, at higher temperatures there are significant decreases in the percent of α – helices. The cleavage of the π -cation interaction most likely does not directly modulate the levels of cAMP by altering the secondary structure, but the changes in the non-covalent interaction network could translate in functional modifications at the level of GTP hydrolysis.

APPENDIX A

EFFECT OF A DOUBLE MUTANT ON THE SWITCH II REGION

Chapter 3 investigated the π - cation interaction between W211 and R208 present in the active conformations of $G_{\alpha 1}$ proteins (85) where we demonstrated that disrupting this interaction had consequences for stability as measured by relative T_m values. We further explored this feature to determine if the proximal R205 residue can interact with W211 to create the π - cation interaction seen in WT and R208Q proteins. By using the same spectroscopic techniques as in chapter 3, we investigated whether the double mutant (R205A/R208Q) can act as a substitute for a π -cation interaction.

The crystal structures of the $G_{\alpha 1}$ proteins in the inactive GDP-bound conformation (86), active conformation using GTP γ S (a non-hydrolyzable GTP analog) (16), as well as in the AlF_4^- (a γ -phosphate mimetic) (120), have been solved. G_{α} is composed of two domains: the α -helical domain and the GTPase domain. In the GTPase domain there are switch regions known as switch I, switch II, and switch III that are located near the nucleotide-binding site. The switch regions undergo a drastic structural change when going from the inactive GDP-bound conformation to the active GTP-bound conformation (146). In the GDP-bound state, switch II and switch III are unordered, but, upon activation, they become ordered around the γ -phosphate of GTP.

The R208Q mutation in $G_{\alpha 1}$ is observed in intestinal cancers (68). However, the mechanism by which this mutation contributes to tumor progression is not known. The Arg in the switch II region of the GTPase domain is involved in two events during the hydrolysis of GTP. First, the formation of a π -cation interaction formed with W211 (Figure 24), promoting a conformational change to the active state. Secondly, R208 represents an important member in a network of residues necessary for the binding and stabilization of GTP and magnesium (Mg^{2+}).

This arginine plays a central role in the function of $G_{\alpha 1}$. Further analysis of the structure reveals a similarly positioned R205 residue which is also part of a random coil in the switch II region, giving it the freedom to rotate freely. R205, therefore, could be a potential π -acceptor, allowing the π -cation interaction to form and further stabilize the protein. The double mutant $G_{\alpha 1}$ R205A/R208Q was prepared to test this hypothesis.

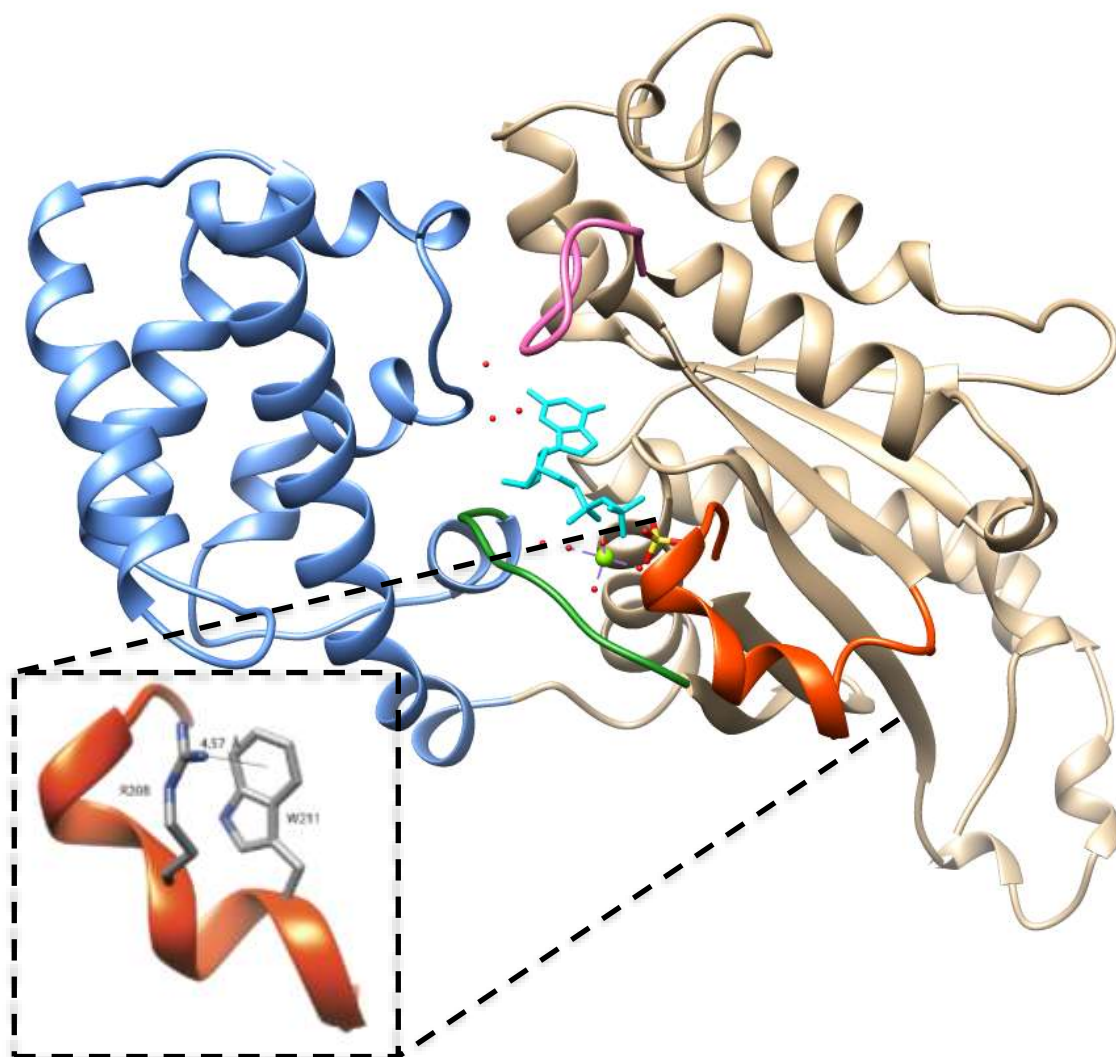


Figure 24. WT $G_{\alpha 1}$ structure. Switch I (green) switch II (orange) and switch III (pink) undergo significant structural changes upon activation. This brings R208 near W211 which creates a π -cation interaction causing a red shift.

The focus of this study was to determine if R205 could be used as a substitute to R208 in the π -cation interaction in the active conformation and to compare the stability of the WT $G_{\alpha 1}$ to a double mutant of the $G_{\alpha 1}$ protein carrying both R205A and R208Q. We did this from different vantage points including inside the core of the protein to its surface of the protein and overall secondary structure. The structural stability of WT was compared to the oncogenic R208Q and the R205A/R208Q double mutant by measuring melting temperatures (T_m) calculated from several biophysical techniques.

Gilman and colleagues have reported that fluorescence could be used as an indirect tool to monitor the GTPase activity of G_{α} -proteins (80, 81). As the protein moves into the active conformation, the intrinsic tryptophan fluorescence increases, while the net tryptophan movement is to a more hydrophobic environment. Gilman and colleagues found that a properly functioning $G_{\alpha 1}$ should see a ~40% increase in fluorescence of upon activation. Unbound tetrafluoroaluminate (III) (AlF_4^-) resembles a phosphate in size and geometry however upon binding, switches from a tetrahedral to square planar geometry. AlF_4^- activation does not require GDP exchange resulting in the first order reaction rate which mimics the transition state and can be measured with fluorescence. Using this technique for WT $G_{\alpha 1}$, we also report an ~40% increase in following the addition of AlF_4^- (Figure 25), which is in agreement with the results found by Gilman (80). Activation of the R208Q and the R205A/R208Q double mutant resulted in significantly smaller changes in fluorescence, an approximately 28.5% change for both mutant proteins (Figure 25).

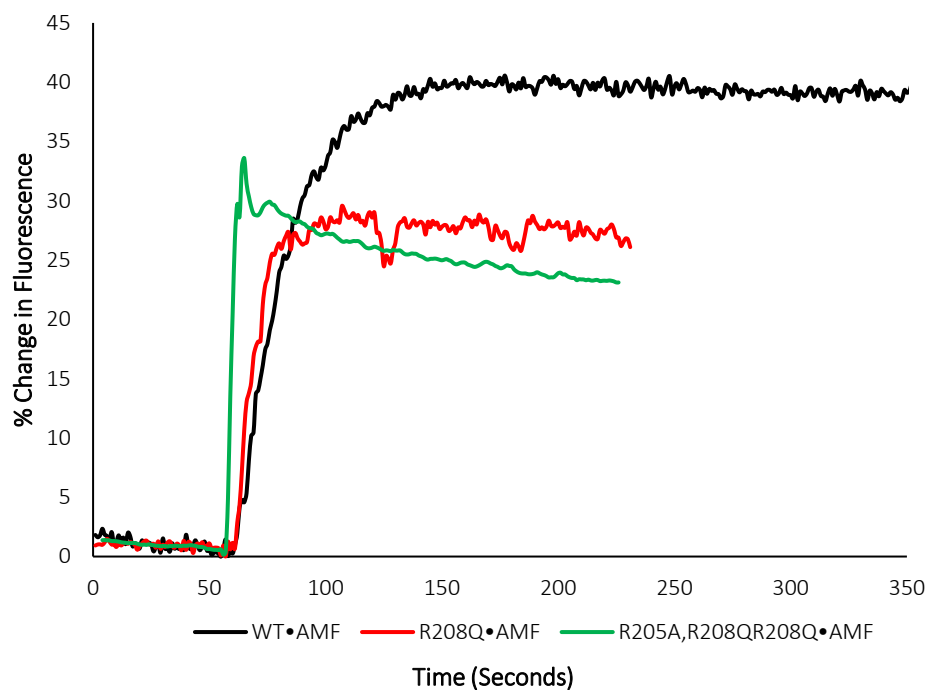


Figure 25: Activation with AlF_4^- of WT $\text{G}_{\alpha i1}$ (black), R208Q $\text{G}_{\alpha i1}$ proteins (red), and the R205A/R208Q double mutant (green).

Hamm and colleagues (85) described a red shift upon activation due to the interaction between R208 and W211 in the wild-type $\text{G}_{\alpha i1}$ protein. We wished to expand on this by determining how the R208Q mutation would affect the red shift. We observed similar results for WT proteins at room temperature (with shifts of 3.45 ± 1.04 nm for GTP γ S and 2.93 ± 1.25 nm for AMF, respectively). The red shift became progressively smaller as the temperature increased (Figure 26) and at 60 °C, still existed for GTP γ S activation, which was 1.63 ± 1.24 nm. In contrast, a 0.67 ± 1.06 nm blue shift formed with AMF activation, indicating that W211 had moved to a more hydrophobic environment, ceasing the π – cation interaction. When measuring the red shift at room temperature in the R208Q mutant, the red shift persisted regardless of whether AlF_4^- (0.88 ± 0.81 nm) or GTP γ S (1.67 ± 0.66 nm, chapter three) was used to activate the protein

(Figure 25). Furthermore, both the AMF and GTP γ S induced red shifts disappeared at higher temperatures, albeit at different temperatures (Figure 26A vs B). The AMF red shift disappeared by 50 °C and continued to shift to a lower wavelength (blue shift) until 60 °C when the blue shift was 1.56 ± 0.97 nm at which point the protein became unstable. The R208Q mutant lacks the key arginine residue necessary for providing the positive charge needed for the π -cation interaction, and thus, the existence of a red shift was unexpected.

We created the R205A/R208Q double mutant to further explore the continued red shift observed in the R208Q mutant. The double mutant allows us to determine if the observed red shift was due to this proximal Arg residue in the 205 position. Eliminating both arginine residues abolished the red shift and gave rise to a -2.0 to -5.0 nm blue shift at all temperatures for AMF activations. However, for GTP γ S activations, a +1.0 nm red shift persisted at lower temperatures

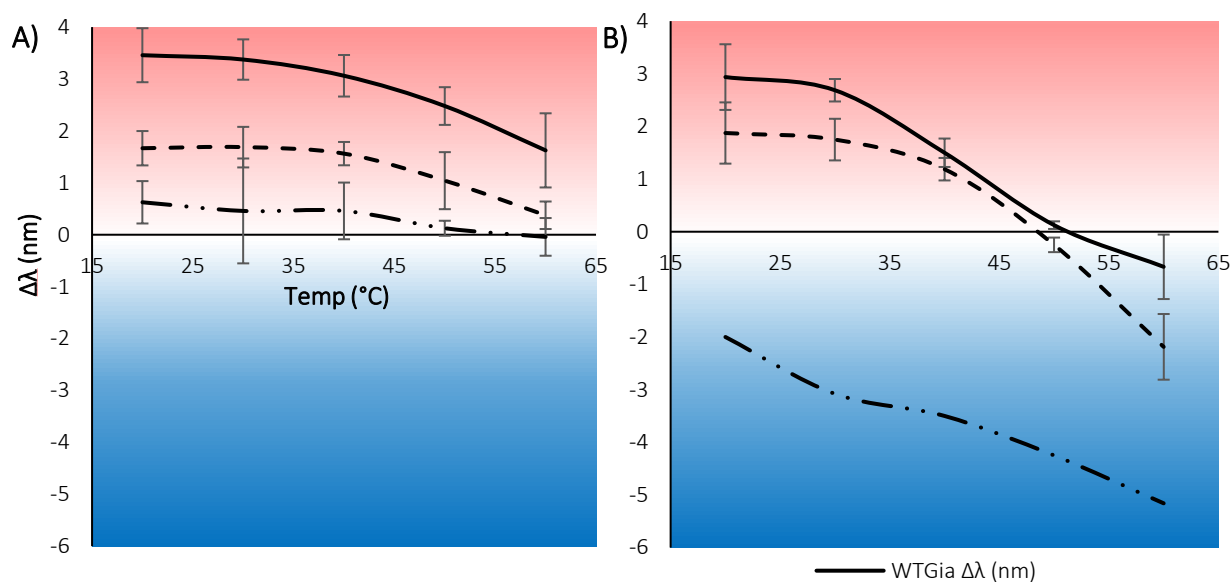


Figure 26. Shift in maximal wavelength at 20 °C λ_{\max} vs temp. **A)** GTP γ S vs GDP bound conformations **B)** AMF vs GDP conformations for WT G α_{i1} , R208Q G α_{i1} and, the double mutant R205A/R208Q G α_{i1} .

and behaved similarly to the R208Q single mutant in that it was a 0.04 ± 0.63 nm blue shift by 60 °C.

To examine the solvent exposure resulting from the conformational change, trypsin digestion was used. Gilman and colleagues first noted the different cleavage patterns between active and inactive WTG $_{\alpha}$ (116). Upon activation of the GTP γ S conformation, rapid cleavage at the N-terminus occurs while the middle of the protein is protected (where R208 is located), resulting in the accumulation of 37 to 39 kDa polypeptides. GDP, on the other hand, is digested into relatively small fragments suggesting that R208 is cleaved only when complexed to GDP while becoming inaccessible in the active conformation. AMF activation leads to partial digestion. It is thought this is a result of increased mobility of the R208 residue causing it to be exposed in short intervals (95).

Surprisingly, similar cleavage patterns were observed for the R208Q mutant, the R205A/R208Q double mutant and the WT. This suggests that R205 is subject to the same environmental changes as R208, resulting in its cleavage when in the GDP-bound conformation, while it remains protected in the GTP γ S conformation (Figure 27, lanes 5-7). The R205A/R208Q double mutant was cleaved at the N-terminus but since both R205 and R208 are no longer cleavable by trypsin, the result is an accumulation of relatively smaller fragments (Figure 27, lanes 8-10).

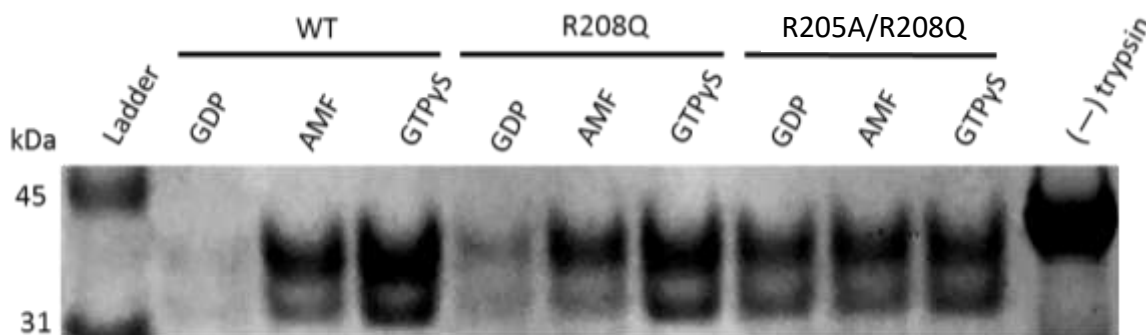


Figure 27. Trypsin digest of G_{α} proteins in the inactive and active conformations.

To investigate the melting properties of the R208Q mutant, and to better understand the roles of R205 and W211, we compared three techniques: fluorescence, CD, and UV/Vis, to obtain a global understanding of the protein's folding. Fluorescence measures the Trp residues at the core of the protein while UV/Vis depends on the Tyr residues at the surface. CD measures the proteins as a whole as the secondary structure changes.

Fluorescence intensity as a function of temperature was used to determine the melting temperature (T_m). As the temperature increased, the fluorescence intensity decreased indicative of protein unfolding. In the inactive conformation, T_m WT is 39.0 °C and the T_m R208Q is 35.1 °C. Surprisingly, activation with AlF_4^- yielded insignificant changes to the T_m ($p = 0.45$), and all three proteins had T_m values around 35 °C (Table 8). Activation with GTP γ S exhibits a stark contrast between the WT and both the R208Q mutant and the R205A/R208Q double mutant where the T_m for the WT protein is 48.7 °C, and the two mutant proteins are 36.9 °C.

Computer algorithms are able to calculate T_m values from the CD spectra. We calculated a T_m value for $WTG_{\alpha i1} \cdot GDP$ of 44.20 °C, $WTG_{\alpha i1} \cdot AMF$ 47.50 °C, $WTG_{\alpha i1} \cdot GTP\gamma S$ of 70.90 °C. The GDP conformation of the R208Q mutant and the R205A/R208Q double mutant were similar to

that of the WT at around 44 °C. For the R208Q mutant, both active conformations show significantly lower melting temperatures compared to the WT protein of the same conformation with the AMF conformation having a T_m of 39.33 °C and the GTP γ S of 56.75 °C (Table 8). The R205A/R208Q double mutant also had a lower T_m value compared to WT and to the R208Q mutant (Table 8).

In both the inactive conformations and in the AMF active conformations of all three proteins, the T_m values were similar and around 47 °C (Table 8). When activating with GTP γ S the same trend was observed; T_m of WT $G_{\alpha 1}$ was the highest followed by the R208Q mutant and the R205A/R208Q double mutant was the smallest (Table 8).

In a study of Trp mutants done previously in this lab by Najor et al (95), the W211F mutant was characterized. Since the π -cation interaction is thought to occur between R208 and W211, we thought it would be interesting to compare the results of the W211F mutant to the R208Q mutant. Using fluorescence, the W211F mutant had a T_m of 35.30 °C in the GDP conformation, 34.10 °C in the AMF conformation and 37.20 °C in the GTP γ S conformation. CD yielded results that were inconsistent with both WT and the R208Q mutants, 54.30 °C for the GDP, 57.00 °C for the AMF and 56.50 °C for the GTP γ S (Table 8). These results are uncharacteristically high for $G_{\alpha 1}$ and may need to be reevaluated at a later time. Regardless, it is important to note that both active conformations are not significantly different than the GDP-bound conformation. UV/Vis calculations are consistent with fluorescence results with T_m calculations of 46.80 °C, 45.78 °C, and 52.30 °C, respectively, for GDP, AMF and GTP γ S conformations.

Table 8. T_m estimates using three spectroscopic techniques for all three proteins in the inactive and both active conformations.

$G_{\alpha 1}$ variant	Fluorescence			CD			UV/Vis		
	GDP	AMF	GTP γ S	GDP	AMF	GTP γ S	GDP	AMF	GTP γ S
WT	39.00	38.30	48.70*	44.20	47.50*	70.90*	47.60	48.60*	66.50*
R208Q	38.1	36.41	36.89†	44.10	39.33†	56.75*†	46.60	46.55†	59.52*†
R205A; R208Q	34.80	35.01	36.92†	44.05	—	48.56*†‡	46.33†	45.07*†	51.47*†‡
W211F	35.30	34.10	37.20†	54.30†‡	57.00†‡	56.50†	46.80†	45.78†	52.30†

S.E.M. ≤ 3 , $n \geq 3$ for all measurements

* = $P \leq 0.05$ vs GDP-bound conformation

† = $P \leq 0.05$ vs WT in the same conformation

‡ = $P \leq 0.05$ vs R208Q in the same conformation

— = Data not collected

The R205A/R208Q double mutant behaves similarly to the R208Q mutant, confirming that the π -cation reaction does contribute a significant amount toward the overall stability of the protein. However, the R205A/R208Q $G_{\alpha 1}$ double mutant follows a similar trend as the R208Q mutant and is similar to the R208Q mutant despite technique used leading us to believe that R205 is not additionally stabilizing the protein in the active conformation. Future *in silico* experiments to determine the role of the R205 residue in the stability and/or activity of the protein would include interaction energies of R205 with nearby residues that have been shown to be important for GTP hydrolysis, similar to those done in chapter 2.

APPENDIX B

GLYCOGEN SYNTHASE KINASE 3 β

Glycogen Synthase Kinase 3 β (GSK3 β) is a constitutively active serine/threonine kinase, which was named so because it originally was shown to regulate cellular glycogen levels through inhibition of glycogen synthase (GS), and is itself inhibited by insulin among others (147). Extensive studies have provided evidence that GSK-3 functions as an important regulatory kinase for at least 50 targets and is involved in a number of important roles including inflammation, apoptosis, embryonic development, heart function, and synaptic transmission in neurons (148-153). Similar to G-proteins, GSK-3 has been shown to provide important regulation in an array of signaling pathways vital for homeostasis.

There are two GSK-3 isoforms, GSK-3 α (51kDa) and GSK-3 β (47kDa), which are expressed by the *GSK3A* and *GSK3B* genes, respectively. GSK-3 β exists in two different splice variants GSK-3 β 1 and GSK-3 β 2, where GSK-3 β 1 is a shorter variant and lacks exon 9 (a 13 residue exon) while GSK-3 β 2 is longer and does contain the 13-residue exon 9 in the catalytic domain. While GSK-3 β 1 is expressed in tissues ubiquitously, GSK-3 β 2 is expressed exclusively in the central nervous system (CNS). The function of exon 9 in GSK-3 β 2 is still largely unknown, therefore unless otherwise stated, the rest of this section will be referring to GSK-3 β 1.

Serine/threonine kinases typically utilize an alpha helix and a beta sheet, which must be aligned into a specific conformation for activity. While GSK-3 does contain this secondary structure, the mechanism by which they are aligned is unique (Figure 28). Most kinases use phosphorylated residues in an activation domain to achieve an active conformation. GSK-3 is more tightly regulated and phosphorylation may inhibit or activate it depending on the phosphorylation site. GSK-3 is inactivated when phosphorylated at the amine terminal serine (S)

9 (GSK-3 β) or S21 (GSK-3 α). When phosphorylated at these residues, a primed pseudo-substrate is formed in the active site, which acts as a competitive inhibitor (Figure 28) (154). In contrast, phosphorylation at Tyrosine (Y) 216 or Y279 in GSK-3 β or GSK-3 α , respectively, seems to promote activity but because GSK-3 is a constitutively active enzyme, it is unknown how important this phosphorylation actually is for activity.

Crystal structure analysis shows GSK-3 prefers a phosphoserine on the substrate. More specifically, GSK-3 β recognizes the sequence S/TXXXS, in which the P + 4 serine has been previously phosphorylated by another kinase. When the substrate has been “primed” by a prior phosphorylation event, GSK-3 β is found to be exponentially more efficient (155). Similar to G α proteins, GSK-3 activity must be closely regulated. Cells have four mechanisms for regulating GSK-3: phosphorylation of GSK-3 itself, phosphorylation of the substrate, subcellular localization, and the formation of protein complexes (156). Natively, the most effective mechanism of regulation is through phosphorylation of key residues of GSK-3. Hyperactive GSK-3 has been linked to several devastating illnesses, including Alzheimer’s (149), diabetes (150), and cancer (148, 157). Inhibition of GSK-3 has, therefore, become a critical research topic. Li⁺ has been shown to inhibit GSK-3 and is effective in the 1-2 mM range (158, 159), therefore at physiologically-relevant concentrations, inhibition is minimally effective. Like many enzymes, GSK-3’s active site requires a Mg²⁺ cofactor to function (Figure 28). Li⁺ is a noncompetitive inhibitor of GSK-3 with respect to the substrate but evidence has shown that Li⁺ is a competitive

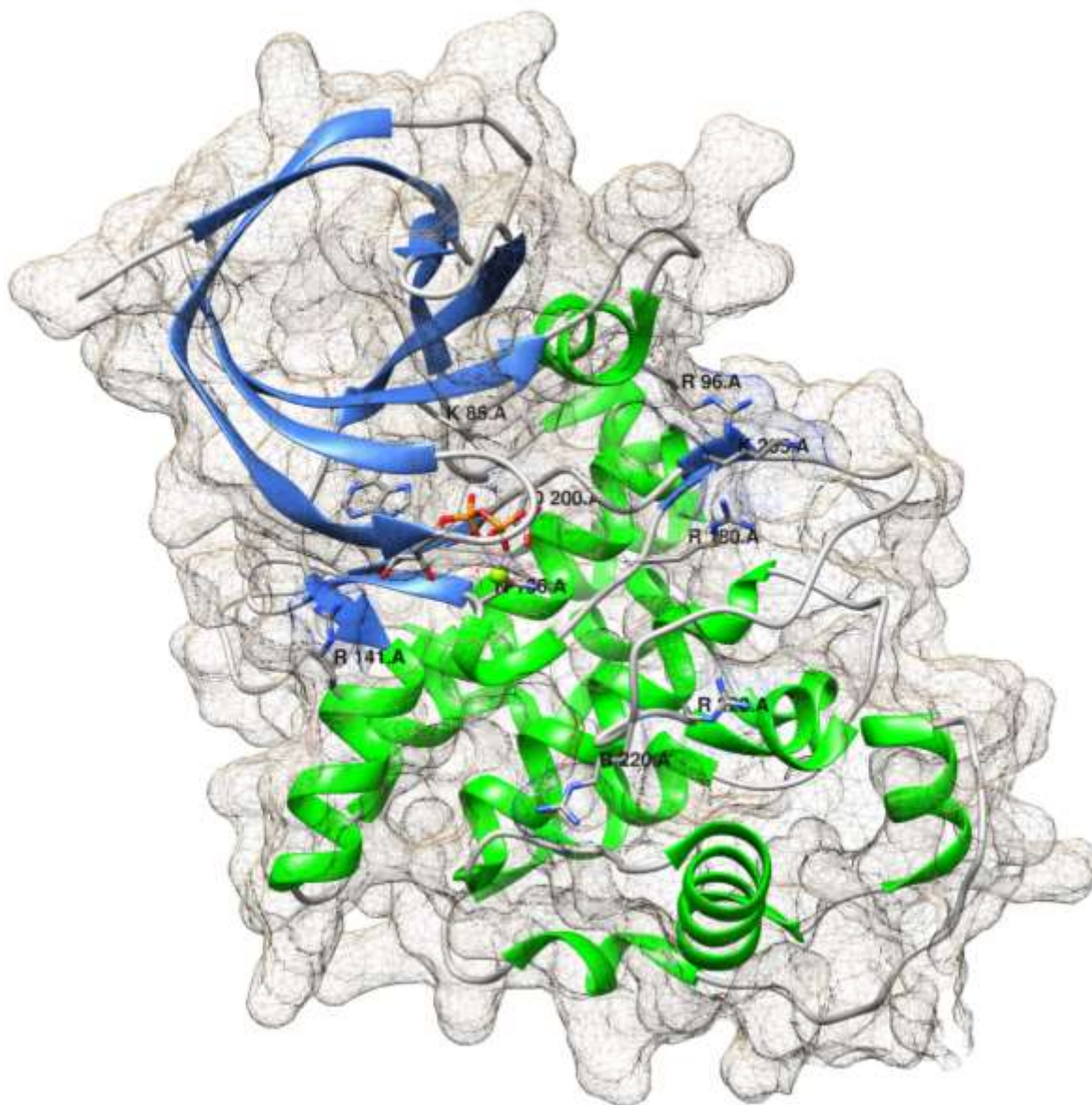


Figure 28. The crystal structure of GSK-3 β has been solved. An ADP molecule is located in the active site situated around the Mg²⁺ cofactor. The basic arginine and lysine residues just next to the active site explain GSK-3 β 's preference for "primed" substrates. PDB ID: 1J1C

inhibitor with respect to Mg²⁺ (160, 161). This is a fairly unusual mechanism in that Li⁺ binds the enzyme-substrate complex by displacing the Mg²⁺ cofactor from the active site. Mechanistically, it is a plausible hypothesis because Li⁺ can compete with the native Mg²⁺ cofactor in the active site (162-164). Because both Li⁺ and Mg²⁺ are similar in atomic radius, and both are positively

charged, Li^+ is thought to be able to fit in the active site and displace the Mg^{2+} ion. Because Li^+ is a monovalent cation, as opposed to Mg^{2+} , a divalent cation, Li^+ is unable to interact with ATP in the same manner, thus, inhibiting the enzyme.

Conflicting evidence suggests that GSK-3 β may have two Mg^{2+} binding sites (164). Inhibition of GSK-3 β with a second and more potent inhibitor beryllium (Be^{2+}) show a further reduced activity of GSK-3 β . This “dual inhibition analysis” hints that there are two active sites present in GSK-3 β but only one is sensitive to Li^+ . It is important to note that these studies also suggest that Be^{2+} binds to both the Mg^{2+} and an ATP molecule in the active site whereas Li^+ does not interact with ATP (164).

The goal of this research was to enhance our understanding of Li^+ as a pharmaceutical agent by 1) gaining better insight into the effects of Li^+ on the enzyme and the mechanism of GSK-3 β and 2) to better understand the structural significance of GSK-3 β and the relationship to Li^+ .

We were able to successfully amplify both the long and short splice variants of human GSK-3 β using PCR with DNA from the H1299 cell line (generously provided by Dr. Abde Abukhdeir from Rush University). The recombinant *GSK3B* gene was transformed into a bacmid in DH10Bac cells. The bacmid was transformed into sf-9 insect cells to generate baculovirus containing either the *GSK3B1* or *GSK3B2* gene, which was then used to infect naïve sf-9 cells at ~50 % confluency for 5 days at 37 °C to create the P0 stock (Figure 29). Infected cells can be visually inspected as the radius of infected cells grows to be twice the size of non-infected cells

(Figure 30). A viral plaque assay was used to quantify the baculovirus titer. Once a high-titer baculovirus stock (with a multiplicity of infection (MOI) $\geq 1.0 \times 10^8$ pfu) had been generated, the *Sf9* cells were infected and further cultured on a larger scale to create the P1 stocks which can be harvested for recombinant protein production (and Figure 31).

Unfortunately, we were unable to scale up production to express large enough quantities of protein to use for further biophysical studies. Future experiments would need to determine a cost-effective method for gaining high-yield protein preparations. It would then be possible to investigate GSK-3 β activity by the efficiency of transfer of [γ - 32 P]-ATP to a synthetic GSM peptide substrate. Li $^+$ vs. Mg $^{2+}$ would then be used to compare the effect of Li $^+$ on the

activity of GSK-3 β . Furthermore, folding studies in conjunction with X-ray crystallography might provide ample information with regard to the structure of GSK-3 β . Although the structure has previously been solved, all existing X-ray structures show only one Mg $^{2+}$ binding site. We would be able to compare the electron density at the metal binding site(s) of GSK-3 β by conducting a crystallographic titration with Mg $^{2+}$ in the presence and absence of Li $^+$. The hypothesis is that the

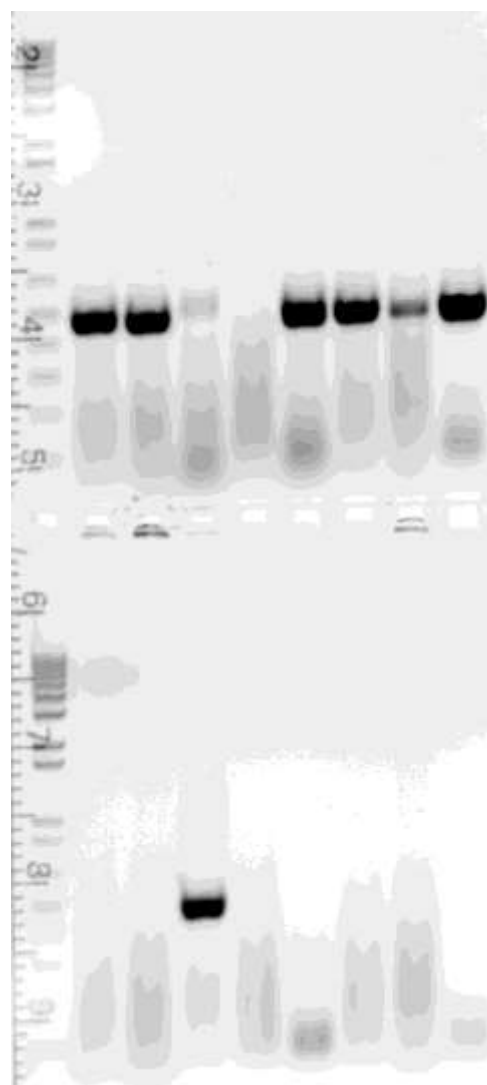


Figure 29. PCR analysis of bacterial colonies. Colonies at the top are expressing GSK-3 β 2 while the ones on the bottom are expressing GSK-3 β 1.

existing crystal structures only capture one Mg^{2+} binding site because the second binding site may have a much lower affinity for Mg^{2+} , which can be displaced by Li^+ under crystallization conditions.

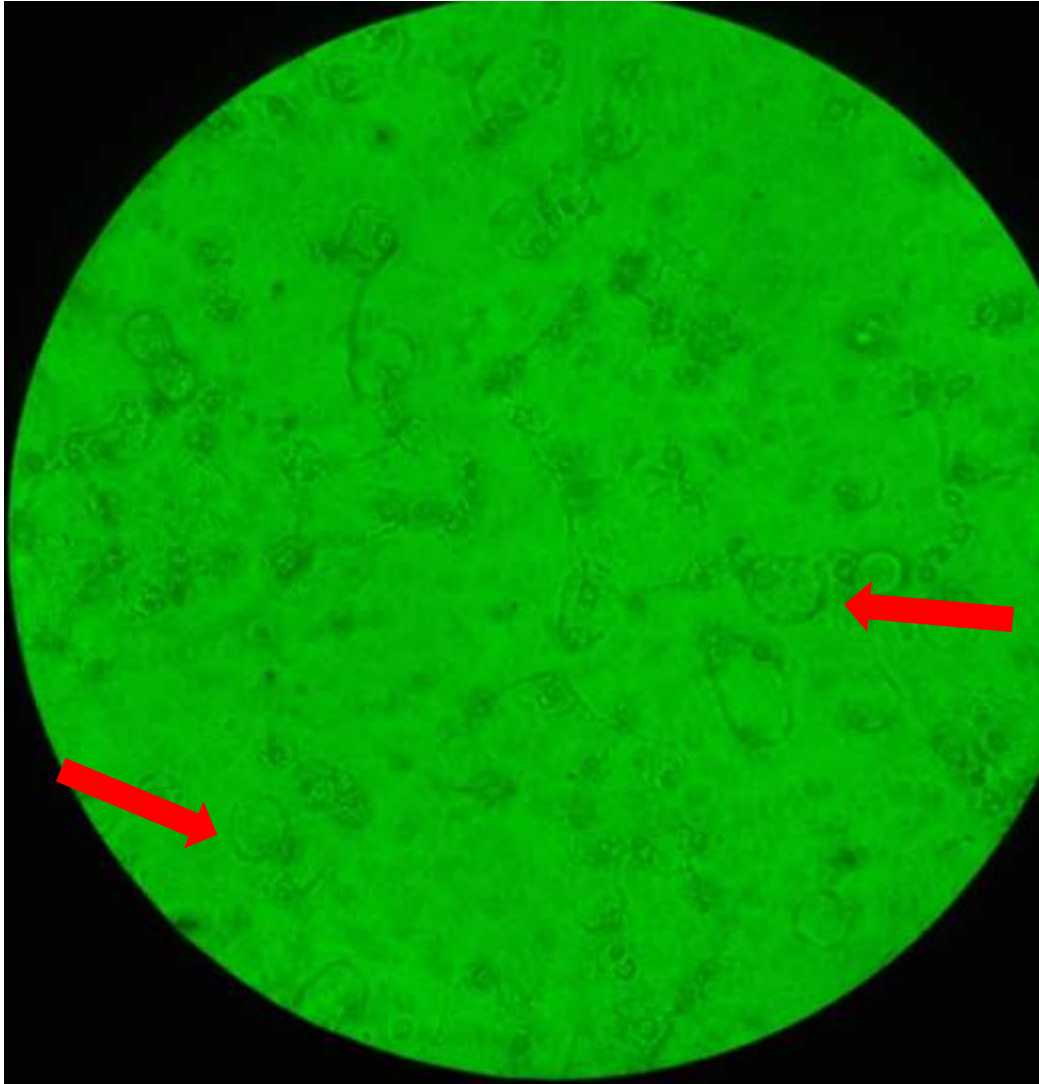


Figure 30. Transfected *Sf-9* Cells under a light microscope magnified 100x. The red arrows show examples of infected cells which show a significant increase in cell diameter.

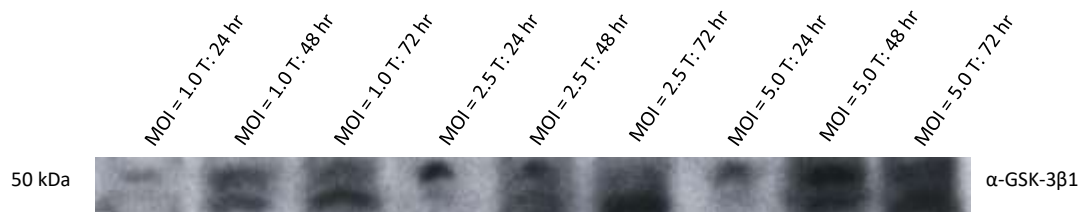


Figure 31. Western blot analysis confirms the presence of GSK-3 in Sf-9 whole cell lysate. This blot compares different MOI and incubation times to determine the optimal incubation conditions.

REFERENCES

1. Gilman A. G. 1995. Nobel lecture. G proteins and regulation of adenylyl cyclase. *Biosci Rep.* 15:65-97.
2. Rodbell M. 1995. Nobel lecture. signal transduction: Evolution of an idea. *Biosci Rep.* 15:117-133.
3. Ringertz N, editor. Nobel lectures in physiology or medicine 1991-1995. Singapore: World Scientific Publishing Company; 1997.
4. Oldham W. M., Hamm H. E. 2006. Structural basis of function in heterotrimeric G proteins. *Q Rev Biophys.* 39:117-166.
5. Oldham W. M., Hamm H. E. 2008. Heterotrimeric G protein activation by G-protein-coupled receptors. *Nat Rev Mol Cell Biol.* 9:60-71.
6. Sprang S. R. 2016. Invited review: Activation of G proteins by GTP and the mechanism of G α -catalyzed GTP hydrolysis. *Biopolymers.* 105:449-462.
7. Fredriksson R., Schioth H. B. 2005. The repertoire of G-protein-coupled receptors in fully sequenced genomes. *Mol Pharmacol.* 67:1414-1425.
8. Wettschureck N., Offermanns S. 2005. Mammalian G proteins and their cell type specific functions. *Physiol Rev.* 85:1159-1204.
9. Perrault R., Zahradka P. 2014. Atypical G α_i signal transduction. *Curr Vasc Pharmacol.* 12:258-270.
10. The UniProt Consortium. 2017. UniProt: The universal protein knowledgebase. *Nucleic Acids Res.* 45:D158-D169.
11. Neves S. R., Ram P. T., Iyengar R. 2002. G protein pathways. *Science.* 296:1636-1639.
12. Lokits A. D., Indrischek H., Meiler J., Hamm H. E., Stadler P. F. 2018. Tracing the evolution of the heterotrimeric G protein α subunit in metazoa. *BMC Evol Biol.* 18:51-018-1147-8.

13. Lambright D. G., Noel J. P., Hamm H. E., Sigler P. B. 1994. Structural determinants for activation of the α -subunit of a heterotrimeric G protein. *Nature*. 369:621-628.
14. Mixon M. B., Lee E., Coleman D. E., Berghuis A. M., Gilman A. G., Sprang S. R. 1995. Tertiary and quaternary structural changes in $G_{i\alpha 1}$ induced by GTP hydrolysis. *Science*. 270:954-960.
15. Noel J. P., Hamm H. E., Sigler P. B. 1993. The 2.2 Å crystal structure of transducin- α complexed with GTP γ S. *Nature*. 366:654-663.
16. Coleman D. E., Berghuis A. M., Lee E., Linder M. E., Gilman A. G., Sprang S. R. 1994. Structures of active conformations of $G_{i\alpha 1}$ and the mechanism of GTP hydrolysis. *Science*. 265:1405-1412.
17. Lambright D. G., Sondek J., Bohm A., Skiba N. P., Hamm H. E., Sigler P. B. 1996. The 2.0 Å crystal structure of a heterotrimeric G protein. *Nature*. 379:311-319.
18. Tang W. J., Gilman A. G. 1991. Type-specific regulation of adenylyl cyclase by G protein $\beta\gamma$ subunits. *Science*. 254:1500-1503.
19. Katz A., Wu D., Simon M. I. 1992. Subunits $\beta\gamma$ of heterotrimeric G protein activate β 2 isoform of phospholipase C. *Nature*. 360:686-689.
20. Mirshahi T., Mittal V., Zhang H., Linder M. E., Logothetis D. E. 2002. Distinct sites on G protein $\beta\gamma$ subunits regulate different effector functions. *J Biol Chem*. 277:36345-36350.
21. Chen C. A., Manning D. R. 2001. Regulation of G proteins by covalent modification. *Oncogene*. 20:1643-1652.
22. van Keulen S. C., Rothlisberger U. 2017. Effect of N-terminal myristoylation on the active conformation of $G_{i\alpha 1}$ -GTP. *Biochemistry*. 56:271-280.
23. Wedegaertner P. B., Chu D. H., Wilson P. T., Levis M. J., Bourne H. R. 1993. Palmitoylation is required for signaling functions and membrane attachment of $G_{q\alpha}$ and $G_{s\alpha}$. *J Biol Chem*. 268:25001-25008.
24. Preininger A. M., Van Eps N., Yu N. J., Medkova M., Hubbell W. L., Hamm H. E. 2003. The myristoylated amino terminus of $G_{i\alpha 1}$ plays a critical role in the structure and function of $G_{i\alpha 1}$ subunits in solution. *Biochemistry*. 42:7931-7941.
25. Janz J. M., Farrens D. L. 2004. Rhodopsin activation exposes a key hydrophobic binding site for the transducin α -subunit C terminus. *J Biol Chem*. 279:29767-29773.

26. Kisselev O. G., Kao J., Ponder J. W., Fann Y. C., Gautam N., Marshall G. R. 1998. Light-activated rhodopsin induces structural binding motif in G protein alpha subunit. *Proc Natl Acad Sci U S A*. 95:4270-4275.
27. Liu W., Clark W. A., Sharma P., Northup J. K. 1998. Mechanism of allosteric regulation of the rod cGMP phosphodiesterase activity by the helical domain of transducin α subunit. *J Biol Chem*. 273:34284-34292.
28. Kaya A. I., Lokits A. D., Gilbert J. A., Iverson T. M., Meiler J., Hamm H. E. 2014. A conserved phenylalanine as a relay between the $\alpha 5$ helix and the GDP binding region of heterotrimeric G_i protein α subunit. *J Biol Chem*. 289:24475-24487.
29. Abdulaev N. G., Mao X., Ramon E., Ngo T., Mysliwy J., Marino J. P., Ridge K. D. 2009. Designing point mutants to detect structural coupling in a heterotrimeric G protein α -subunit by NMR spectroscopy. *Photochem Photobiol*. 85:431-436.
30. Remmers A. E., Engel C., Liu M., Neubig R. R. 1999. Interdomain interactions regulate GDP release from heterotrimeric G proteins. *Biochemistry*. 38:13795-13800.
31. McCudden C. R., Hains M. D., Kimple R. J., Siderovski D. P., Willard F. S. 2005. G-protein signaling: Back to the future. *Cell Mol Life Sci*. 62:551-577.
32. Berman D. M., Wilkie T. M., Gilman A. G. 1996. GAIP and RGS4 are GTPase-activating proteins for the G_i subfamily of G protein α subunits. *Cell*. 86:445-452.
33. Mukhopadhyay S., Ross E. M. 1999. Rapid GTP binding and hydrolysis by G_q promoted by receptor and GTPase-activating proteins. *Proc Natl Acad Sci U S A*. 96:9539-9544.
34. Carvalho A. T., Szeler K., Vavitsas K., Aqvist J., Kamerlin S. C. 2015. Modeling the mechanisms of biological GTP hydrolysis. *Arch Biochem Biophys*. 582:80-90.
35. Li G., Zhang X. C. 2004. GTP hydrolysis mechanism of ras-like GTPases. *J Mol Biol*. 340:921-932.
36. Thomas C. J., Du X., Li P., Wang Y., Ross E. M., Sprang S. R. 2004. Uncoupling conformational change from GTP hydrolysis in a heterotrimeric G protein α -subunit. *Proc Natl Acad Sci U S A*. 101:7560-7565.
37. Zurita A., Zhang Y., Pedersen L., Darden T., Birnbaumer L. 2010. Obligatory role in GTP hydrolysis for the amide carbonyl oxygen of the Mg²⁺-coordinating Thr of regulatory GTPases. *Proc Natl Acad Sci U S A*. 107:9596-9601.

38. Nishina H., Nimota K., Kukimoto I., Maehama T., Takahashi K., Hoshino S., Kanaho Y., Katada T. 1995. Significance of Thr182 in the nucleotide-exchange and GTP-hydrolysis reactions of the α subunit of GTP-binding protein G_{i2} . *J Biochem.* 118:1083-1089.
39. Clapham D. E., Neer E. J. 1993. New roles for G-protein $\beta\gamma$ -dimers in transmembrane signalling. *Nature.* 365:403-406.
40. Smrcka A. V. 2008. G protein $\beta\gamma$ subunits: Central mediators of G protein-coupled receptor signaling. *Cell Mol Life Sci.* 65:2191-2214.
41. Pronin A. N., Gautam N. 1992. Interaction between G-protein β and γ subunit types is selective. *Proc Natl Acad Sci U S A.* 89:6220-6224.
42. Spring D. J., Neer E. J. 1994. A 14-amino acid region of the G protein γ subunit is sufficient to confer selectivity of γ binding to the β subunit. *J Biol Chem.* 269:22882-22886.
43. Kim J. H., Roy A., Jouandot D., 2nd, Cho K. H. 2013. The glucose signaling network in yeast. *Biochim Biophys Acta.* 1830:5204-5210.
44. Rolland F., Winderickx J., Thevelein J. M. 2001. Glucose-sensing mechanisms in eukaryotic cells. *Trends Biochem Sci.* 26:310-317.
45. Roscioni S. S., Elzinga C. R., Schmidt M. 2008. Epac: Effectors and biological functions. *Naunyn Schmiedebergs Arch Pharmacol.* 377:345-357.
46. Almahariq M., Mei F. C., Cheng X. 2014. Cyclic AMP sensor EPAC proteins and energy homeostasis. *Trends Endocrinol Metab.* 25:60-71.
47. Kumar N., Prasad P., Jash E., Saini M., Husain A., Goldman A., Sehrawat S. 2018. Insights into exchange factor directly activated by cAMP (EPAC) as potential target for cancer treatment. *Mol Cell Biochem.* Available from <https://doi.org/10.1007/s11010-018-3294-z>. Epub ahead of print.
48. Cheng X., Ji Z., Tsalkova T., Mei F. 2008. Epac and PKA: A tale of two intracellular cAMP receptors. *Acta Biochim Biophys Sin (Shanghai).* 40:651-662.
49. Takahashi H., Honma M., Miyauchi Y., Nakamura S., Ishida-Yamamoto A., Iizuka H. 2004. Cyclic AMP differentially regulates cell proliferation of normal human keratinocytes through ERK activation depending on the expression pattern of B-raf. *Arch Dermatol Res.* 296:74-82.
50. Halls M. L., Cooper D. M. 2017. Adenylyl cyclase signalling complexes - pharmacological challenges and opportunities. *Pharmacol Ther.* 172:171-180.

51. Berlot C. H., Bourne H. R. 1992. Identification of effector-activating residues of $G_{s\alpha}$. *Cell*. 68:911-922.
52. Sunahara R. K., Tesmer J. J., Gilman A. G., Sprang S. R. 1997. Crystal structure of the adenylyl cyclase activator $G_{s\alpha}$. *Science*. 278:1943-1947.
53. Dessauer C. W., Tesmer J. J., Sprang S. R., Gilman A. G. 1998. Identification of a $G_{i\alpha}$ binding site on type V adenylyl cyclase. *J Biol Chem*. 273:25831-25839.
54. Tesmer J. J., Sunahara R. K., Gilman A. G., Sprang S. R. 1997. Crystal structure of the catalytic domains of adenylyl cyclase in a complex with $G_{s\alpha}$ GTP γ S. *Science*. 278:1907-1916.
55. Frauenfelder H., Sligar S. G., Wolynes P. G. 1991. The energy landscapes and motions of proteins. *Science*. 254:1598-1603.
56. Englander S. W., Mayne L. 2014. The nature of protein folding pathways. *Proc Natl Acad Sci U S A*. 111:15873-15880.
57. Radford S. E. 2000. Protein folding: Progress made and promises ahead. *Trends Biochem Sci*. 25:611-618.
58. Baldwin R. L., Rose G. D. 2013. Molten globules, entropy-driven conformational change and protein folding. *Curr Opin Struct Biol*. 23:4-10.
59. Bhattacharyya S., Varadarajan R. 2013. Packing in molten globules and native states. *Curr Opin Struct Biol*. 23:11-21.
60. Selkoe D. J. 2003. Folding proteins in fatal ways. *Nature*. 426:900-904.
61. Ross C. A., Poirier M. A. 2004. Protein aggregation and neurodegenerative disease. *Nat Med*. 10 Suppl:S10-7.
62. Riek R., Eisenberg D. S. 2016. The activities of amyloids from a structural perspective. *Nature*. 539:227-235.
63. Shortle D., Chan H. S., Dill K. A. 1992. Modeling the effects of mutations on the denatured states of proteins. *Protein Sci*. 1:201-215.
64. Calloni G., Zoffoli S., Stefani M., Dobson C. M., Chiti F. 2005. Investigating the effects of mutations on protein aggregation in the cell. *J Biol Chem*. 280:10607-10613.

65. National Center for Health Statistics. Health, United States, 2016: With chartbook on long-term trends in health. Washington, DC 20402: U.S. Government Printing Office; 2017.
66. Stratton M. R., Campbell P. J., Futreal P. A. 2009. The cancer genome. *Nature*. 458:719-724.
67. Garraway L. A., Lander E. S. 2013. Lessons from the cancer genome. *Cell*. 153:17-37.
68. O'Hayre M., Vazquez-Prado J., Kufareva I., Stawiski E. W., Handel T. M., Seshagiri S., Gutkind J. S. 2013. The emerging mutational landscape of G proteins and G-protein-coupled receptors in cancer. *Nat Rev Cancer*. 13:412-424.
69. Berrettini W. H., Vuoristo J., Ferraro T. N., Buono R. J., Wildenauer D., Ala-Kokko L. 1998. Human G(olf) gene polymorphisms and vulnerability to bipolar disorder. *Psychiatr Genet*. 8:235-238.
70. Jope R. S., Nemeroff C. B. 2013. The ups and downs of bipolar disorder research. *Biol Psychiatry*. 73:597-599.
71. Friedman E., Wang H. Y. 1996. Receptor-mediated activation of G proteins is increased in postmortem brains of bipolar affective disorder subjects. *J Neurochem*. 67:1145-1152.
72. Weinstein L. S., Shenker A., Gejman P. V., Merino M. J., Friedman E., Spiegel A. M. 1991. Activating mutations of the stimulatory G protein in the McCune-albright syndrome. *N Engl J Med*. 325:1688-1695.
73. Dhanasekaran N., Heasley L. E., Johnson G. L. 1995. G protein-coupled receptor systems involved in cell growth and oncogenesis. *Endocr Rev*. 16:259-270.
74. Dorsam R. T., Gutkind J. S. 2007. G-protein-coupled receptors and cancer. *Nature reviews cancer*. 7:79-94.
75. Wilson C. H., McIntyre R. E., Arends M. J., Adams D. J. 2010. The activating mutation R201C in GNAS promotes intestinal tumorigenesis in *apc(min/+)* mice through activation of wnt and ERK1/2 MAPK pathways. *Oncogene*. 29:4567-4575.
76. Malumbres M., Barbacid M. 2003. RAS oncogenes: The first 30 years. *Nat Rev Cancer*. 3:459-465.
77. Bull S. C., Doig A. J. 2015. Properties of protein drug target classes. *PLoS One*. 10:e0117955.
78. Weber G., Laurence D. J. 1954. Fluorescent indicators of adsorption in aqueous solution and on the solid phase. *Biochem J*. 56:151-156.

79. Lakowicz J. Principles of fluorescence spectroscopy. 3rd ed. Boston, MA: Springer USA; 2006.
80. Higashijima T., Ferguson K. M., Sternweis P. C., Ross E. M., Smigel M. D., Gilman A. G. 1987. The effect of activating ligands on the intrinsic fluorescence of guanine nucleotide-binding regulatory proteins. *J Biol Chem.* 262:752-756.
81. Higashijima T., Ferguson K. M., Smigel M. D., Gilman A. G. 1987. The effect of GTP and Mg^{2+} on the GTPase activity and the fluorescent properties of G_o . *J Biol Chem.* 262:757-761.
82. Stryer L. 1968. Fluorescence spectroscopy of proteins. *Science.* 162:526-533.
83. Antonny B., Chabre M. 1992. Characterization of the aluminum and beryllium fluoride species which activate transducin. analysis of the binding and dissociation kinetics. *J Biol Chem.* 267:6710-6718.
84. Faurobert E., Otto-Bruc A., Chardin P., Chabre M. 1993. Tryptophan W207 in transducin T_α is the fluorescence sensor of the G protein activation switch and is involved in the effector binding. *EMBO J.* 12:4191-4198.
85. Hamm H. E., Meier S. M., Liao G., Preininger A. M. 2009. Trp fluorescence reveals an activation-dependent cation- π interaction in the switch II region of $G_{\alpha i}$ proteins. *Protein Sci.* 18:2326-2335.
86. Coleman D. E., Sprang S. R. 1998. Crystal structures of the G protein $G_{i\alpha 1}$ complexed with GDP and Mg^{2+} : A crystallographic titration experiment. *Biochemistry.* 37:14376-14385.
87. Dougherty D. A. 2013. The cation- π interaction. *Acc Chem Res.* 46:885-893.
88. Dougherty D. A. 2007. Cation- π interactions involving aromatic amino acids. *J Nutr.* 137:1504S-1508S; discussion 1516S-1517S.
89. Gallivan J. P., Dougherty D. A. 1999. Cation- π interactions in structural biology. *Proc Natl Acad Sci U S A.* 96:9459-9464.
90. Ma J. C., Dougherty D. A. 1997. The cation- π interaction. *Chem Rev.* 97:1303-1324.
91. Riley K. E., Tran K. A. 2017. Strength and character of R-X... π interactions involving aromatic amino acid sidechains in protein-ligand complexes derived from crystal structures in the protein data bank. *Crystals.* 7:273.
92. Burley S. K., Petsko G. A. 1986. Amino-aromatic interactions in proteins. *FEBS Lett.* 203:139-143.

93. Borozan S. Z., Zlatovic M. V., Stojanovic S. D. 2016. Anion- π interactions in complexes of proteins and halogen-containing amino acids. *J Biol Inorg Chem*. 21:357-368.
94. Wheeler S. E., Bloom J. W. 2014. Anion- π interactions and positive electrostatic potentials of N-heterocycles arise from the positions of the nuclei, not changes in the π -electron distribution. *Chem Commun (Camb)*. 50:11118-11121.
95. Najor M. S., Olsen K. W., Graham D. J., Mota de Freitas D. 2014. Contribution of each Trp residue toward the intrinsic fluorescence of the G $_{\alpha 1}$ protein. *Protein Sci*. 23:1392-1402.
96. Wilkins M. R., Gasteiger E., Bairoch A., Sanchez J. C., Williams K. L., Appel R. D., Hochstrasser D. F. 1999. Protein identification and analysis tools in the ExPASy server. *Methods Mol Biol*. 112:531-552.
97. Provencher S. W., Glockner J. 1981. Estimation of globular protein secondary structure from circular dichroism. *Biochemistry*. 20:33-37.
98. Hauryliuk V., Hansson S., Ehrenberg M. 2008. Cofactor dependent conformational switching of GTPases. *Biophys J*. 95:1704-1715.
99. Davidi D., Noor E., Liebermeister W., Bar-Even A., Flamholz A., Tummeler K., Barenholz U., Goldenfeld M., Shlomi T., Milo R. 2016. Global characterization of in vivo enzyme catalytic rates and their correspondence to in vitro k_{cat} measurements. *Proc Natl Acad Sci U S A*. 113:3401-3406.
100. Zhang B., Sun N., Mu X., Zhi L., Zhai L., Jiang Y., Fu Z., Yao Z. 2017. G protein αS subunit promotes cell proliferation of renal cell carcinoma with involvement of protein kinase A signaling. *DNA Cell Biol*. 36:237-242.
101. Hanahan D., Weinberg R. A. 2011. Hallmarks of cancer: The next generation. *Cell*. 144:646-674.
102. Fajardo A. M., Piazza G. A., Tinsley H. N. 2014. The role of cyclic nucleotide signaling pathways in cancer: Targets for prevention and treatment. *Cancers (Basel)*. 6:436-458.
103. Alakus H., Babicky M. L., Ghosh P., Yost S., Jepsen K., Dai Y., Arias A., Samuels M. L., Mose E. S., Schwab R. B., Peterson M. R., Lowy A. M., Frazer K. A., Harismendy O. 2014. Genome-wide mutational landscape of mucinous carcinomatosis peritonei of appendiceal origin. *Genome Med*. 6:43.
104. Pugh T. J., Weeraratne S. D., Archer T. C., Pomeranz Krummel D. A., Auclair D., Bochicchio J., Carneiro M. O., Carter S. L., Cibulskis K., Erlich R. L., Greulich H., Lawrence M. S., Lennon N. J.,

McKenna A., Meldrim J., Ramos A. H., Ross M. G., Russ C., Shefler E., Sivachenko A., Sogoloff B., Stojanov P., Tamayo P., Mesirov J. P., Amani V., Teider N., Sengupta S., Francois J. P., Northcott P. A., Taylor M. D., Yu F., Crabtree G. R., Kautzman A. G., Gabriel S. B., Getz G., Jager N., Jones D. T., Lichter P., Pfister S. M., Roberts T. M., Meyerson M., Pomeroy S. L., Cho Y. J. 2012.

Medulloblastoma exome sequencing uncovers subtype-specific somatic mutations. *Nature*. 488:106-110.

105. Carter S. G., Karl D. W. 1982. Inorganic phosphate assay with malachite green: An improvement and evaluation. *J Biochem Biophys Methods*. 7:7-13.

106. Wu Z. L. 2011. Phosphatase-coupled universal kinase assay and kinetics for first-order-rate coupling reaction. *PLoS One*. 6:e23172.

107. Lee E., Linder M. E., Gilman A. G. 1994. Expression of G-protein α subunits in escherichia coli. *Methods Enzymol*. 237:146-164.

108. Morikawa T., Muroya A., Nakajima Y., Tanaka T., Hirai K., Sugio S., Wakamatsu K., Kohno T. 2007. Crystallization and preliminary X-ray crystallographic analysis of the receptor-uncoupled mutant of $G_{\alpha i1}$. *Acta Crystallogr Sect F Struct Biol Cryst Commun*. 63:139-141.

109. Adams P. D., Grosse-Kunstleve R. W., Hung L. W., Ioerger T. R., McCoy A. J., Moriarty N. W., Read R. J., Sacchettini J. C., Sauter N. K., Terwilliger T. C. 2002. PHENIX: Building new software for automated crystallographic structure determination. *Acta Crystallogr D Biol Crystallogr*. 58:1948-1954.

110. Pettersen E. F., Goddard T. D., Huang C. C., Couch G. S., Greenblatt D. M., Meng E. C., Ferrin T. E. 2004. UCSF chimera--a visualization system for exploratory research and analysis. *J Comput Chem*. 25:1605-1612.

111. Berman H. M., Westbrook J., Feng Z., Gilliland G., Bhat T. N., Weissig H., Shindyalov I. N., Bourne P. E. 2000. The protein data bank. *Nucleic Acids Res*. 28:235-242.

112. Arnold K., Bordoli L., Kopp J., Schwede T. 2006. The SWISS-MODEL workspace: A web-based environment for protein structure homology modelling. *Bioinformatics*. 22:195-201.

113. Sonddek J., Lambright D. G., Noel J. P., Hamm H. E., Sigler P. B. 1994. GTPase mechanism of G proteins from the 1.7-A crystal structure of transducin α -GDP- AlF_4^- . *Nature*. 372:276-279.

114. Humphrey W., Dalke A., Schulten K. 1996. VMD: Visual molecular dynamics. *J Mol Graph*. 14:33-8, 27-8.

115. Phillips J. C., Braun R., Wang W., Gumbart J., Tajkhorshid E., Villa E., Chipot C., Skeel R. D., Kale L., Schulten K. 2005. Scalable molecular dynamics with NAMD. *J Comput Chem.* 26:1781-1802.
116. Kleuss C., Raw A. S., Lee E., Sprang S. R., Gilman A. G. 1994. Mechanism of GTP hydrolysis by G-protein α subunits. *Proc Natl Acad Sci U S A.* 91:9828-9831.
117. Thaker T. M., Sarwar M., Preininger A. M., Hamm H. E., Iverson T. M. 2014. A transient interaction between the phosphate binding loop and switch I contributes to the allosteric network between receptor and nucleotide in $G_{\alpha 1}$. *J Biol Chem.* 289:11331-11341.
118. Iiri T., Farfel Z., Bourne H. R. 1997. Conditional activation defect of a human $G_{s\alpha}$ mutant. *Proc Natl Acad Sci U S A.* 94:5656-5661.
119. Lambert N. A., Johnston C. A., Cappell S. D., Kuravi S., Kimple A. J., Willard F. S., Siderovski D. P. 2010. Regulators of G-protein signaling accelerate GPCR signaling kinetics and govern sensitivity solely by accelerating GTPase activity. *Proc Natl Acad Sci U S A.* 107:7066-7071.
120. Tesmer J. J., Berman D. M., Gilman A. G., Sprang S. R. 1997. Structure of RGS4 bound to AlF_4^- -activated $G_{i\alpha 1}$: Stabilization of the transition state for GTP hydrolysis. *Cell.* 89:251-261.
121. Berman D. M., Kozasa T., Gilman A. G. 1996. The GTPase-activating protein RGS4 stabilizes the transition state for nucleotide hydrolysis. *J Biol Chem.* 271:27209-27212.
122. Graziano M. P., Gilman A. G. 1989. Synthesis in escherichia coli of GTPase-deficient mutants of $G_{s\alpha}$. *J Biol Chem.* 264:15475-15482.
123. Johnston C. A., Willard F. S., Jczyk M. R., Fredericks Z., Bodor E. T., Jones M. B., Blaesius R., Watts V. J., Harden T. K., Sondek J., Ramer J. K., Siderovski D. P. 2005. Structure of $G_{\alpha 1}$ bound to a GDP-selective peptide provides insight into guanine nucleotide exchange. *Structure.* 13:1069-1080.
124. Slepak V. Z., Katz A., Simon M. I. 1995. Functional analysis of a dominant negative mutant of $G_{\alpha 2}$. *J Biol Chem.* 270:4037-4041.
125. Ahmadian M. R., Stege P., Scheffzek K., Wittinghofer A. 1997. Confirmation of the arginine-finger hypothesis for the GAP-stimulated GTP-hydrolysis reaction of Ras. *Nat Struct Biol.* 4:686-689.
126. Zhang B., Zhang Y., Wang Z., Zheng Y. 2000. The role of Mg^{2+} cofactor in the guanine nucleotide exchange and GTP hydrolysis reactions of Rho family GTP-binding proteins. *J Biol Chem.* 275:25299-25307.

127. Farfel Z., Iri T., Shapira H., Roitman A., Mouallem M., Bourne H. R. 1996. Pseudohypoparathyroidism, a novel mutation in the $\beta\gamma$ -contact region of $G_{s\alpha}$ impairs receptor stimulation. *J Biol Chem.* 271:19653-19655.
128. Syrovatkina V., Alegre K. O., Dey R., Huang X. Y. 2016. Regulation, signaling, and physiological functions of G-proteins. *J Mol Biol.* 428:3850-3868.
129. Higashijima T., Ferguson K. M., Sternweis P. C., Smigel M. D., Gilman A. G. 1987. Effects of Mg^{2+} and the $\beta\gamma$ -subunit complex on the interactions of guanine nucleotides with G proteins. *J Biol Chem.* 262:762-766.
130. Van Eps N., Preininger A. M., Alexander N., Kaya A. I., Meier S., Meiler J., Hamm H. E., Hubbell W. L. 2011. Interaction of a G protein with an activated receptor opens the interdomain interface in the α subunit. *Proc Natl Acad Sci U S A.* 108:9420-9424.
131. Sprang S. R. 1997. G protein mechanisms: Insights from structural analysis. *Annu Rev Biochem.* 66:639-678.
132. Rasmussen S. G., DeVree B. T., Zou Y., Kruse A. C., Chung K. Y., Kobilka T. S., Thian F. S., Chae P. S., Pardon E., Calinski D., Mathiesen J. M., Shah S. T., Lyons J. A., Caffrey M., Gellman S. H., Steyaert J., Skinotitis G., Weis W. I., Sunahara R. K., Kobilka B. K. 2011. Crystal structure of the β_2 adrenergic receptor- G_s protein complex. *Nature.* 477:549-555.
133. Tayubi I. A., Sethumadhavan R. 2010. Nature of cation- π interactions and their role in structural stability of immunoglobulin proteins. *Biochemistry (Mosc).* 75:912-918.
134. Brandts J. F. 1964. The thermodynamics of protein denaturation. I. the denaturation of chymotrypsinogen. *J Am Chem Soc.* 86:4291-4301.
135. Olsen K. W. 1994. Thermal denaturation procedures for hemoglobin. *Methods Enzymol.* 231:514-524.
136. Whitmore L., Wallace B. A. 2008. Protein secondary structure analyses from circular dichroism spectroscopy: Methods and reference databases. *Biopolymers.* 89:392-400.
137. Sreerama N., Venyaminov S. Y., Woody R. W. 2000. Estimation of protein secondary structure from circular dichroism spectra: Inclusion of denatured proteins with native proteins in the analysis. *Anal Biochem.* 287:243-251.
138. Phillips W. J., Cerione R. A. 1988. The intrinsic fluorescence of the α subunit of transducin. measurement of receptor-dependent guanine nucleotide exchange. *J Biol Chem.* 263:15498-15505.

139. Najor M., Leveson B. D., Goossens J. L., Kothawala, S., Olsen, K.W., Freitas D. M. Submitted. Folding of G α subunits: Implications for disease states. *Submitted*.
140. Piovesan D., Minervini G., Tosatto S. C. 2016. The RING 2.0 web server for high quality residue interaction networks. *Nucleic Acids Res.* 44:W367-74.
141. Warner D. R., Romanowski R., Yu S., Weinstein L. S. 1999. Mutagenesis of the conserved residue Glu259 of G α demonstrates the importance of interactions between switches 2 and 3 for activation. *J Biol Chem.* 274:4977-4984.
142. Pinheiro S., Soteras I., Gelpi J. L., Dehez F., Chipot C., Luque F. J., Curutchet C. 2017. Structural and energetic study of cation- π -cation interactions in proteins. *Phys Chem Chem Phys.* 19:9849-9861.
143. Dougherty D. A. 1996. Cation- π interactions in chemistry and biology: A new view of benzene, phe, tyr, and trp. *Science.* 271:163-168.
144. Cockroft S. L., Hunter C. A. 2007. Chemical double-mutant cycles: Dissecting non-covalent interactions. *Chem Soc Rev.* 36:172-188.
145. Carter P. J., Winter G., Wilkinson A. J., Fersht A. R. 1984. The use of double mutants to detect structural changes in the active site of the tyrosyl-tRNA synthetase (bacillus stearothermophilus). *Cell.* 38:835-840.
146. Bae H., Anderson K., Flood L. A., Skiba N. P., Hamm H. E., Graber S. G. 1997. Molecular determinants of selectivity in 5-hydroxytryptamine_{1B} receptor-G protein interactions. *J Biol Chem.* 272:32071-32077.
147. Embi N., Rylatt D. B., Cohen P. 1980. Glycogen synthase kinase-3 from rabbit skeletal muscle. separation from cyclic-AMP-dependent protein kinase and phosphorylase kinase. *Eur J Biochem.* 107:519-527.
148. McCubrey J. A., Steelman L. S., Bertrand F. E., Davis N. M., Sokolosky M., Abrams S. L., Montalto G., D'Assoro A. B., Libra M., Nicoletti F., Maestro R., Basecke J., Rakus D., Gizak A., Demidenko Z. N., Cocco L., Martelli A. M., Cervello M. 2014. GSK-3 as potential target for therapeutic intervention in cancer. *Oncotarget.* 5:2881-2911.
149. Martin L., Latypova X., Wilson C. M., Magnaudeix A., Perrin M. L., Yardin C., Terro F. 2013. Tau protein kinases: Involvement in Alzheimer's disease. *Ageing Res Rev.* 12:289-309.

150. Amar S., Belmaker R. H., Agam G. 2011. The possible involvement of glycogen synthase kinase-3 (GSK-3) in diabetes, cancer and central nervous system diseases. *Curr Pharm Des.* 17:2264-2277.
151. Gao C., Holscher C., Liu Y., Li L. 2011. GSK3: A key target for the development of novel treatments for type 2 diabetes mellitus and alzheimer disease. *Rev Neurosci.* 23:1-11.
152. Lal H., Ahmad F., Woodgett J., Force T. 2015. The GSK-3 family as therapeutic target for myocardial diseases. *Circ Res.* 116:138-149.
153. Llorens-Martin M., Jurado J., Hernandez F., Avila J. 2014. GSK-3 β , a pivotal kinase in Alzheimer disease. *Front Mol Neurosci.* 7:46.
154. Cohen P., Frame S. 2001. The renaissance of GSK3. *Nat Rev Mol Cell Biol.* 2:769-776.
155. Dajani R., Fraser E., Roe S. M., Young N., Good V., Dale T. C., Pearl L. H. 2001. Crystal structure of glycogen synthase kinase 3 β : Structural basis for phosphate-primed substrate specificity and autoinhibition. *Cell.* 105:721-732.
156. Jope R. S., Yuskaitis C. J., Beurel E. 2007. Glycogen synthase kinase-3 (GSK3): Inflammation, diseases, and therapeutics. *Neurochem Res.* 32:577-595.
157. Maurer U., Preiss F., Brauns-Schubert P., Schlicher L., Charvet C. 2014. GSK-3 - at the crossroads of cell death and survival. *J Cell Sci.* 127:1369-1378.
158. Schou M. Clinical aspects of lithium in psychiatry. In: Schou M, editor. *Lithium and the Cell: Pharmacology and Biochemistry.* San Diego: Academic Press; 1991. p. 1-6.
159. Gustin J. P., Karakas B., Weiss M. B., Abukhdeir A. M., Luring J., Garay J. P., Cosgrove D., Tamaki A., Konishi H., Konishi Y., Mohseni M., Wang G., Rosen D. M., Denmeade S. R., Higgins M. J., Vitolo M. I., Bachman K. E., Park B. H. 2009. Knockin of mutant PIK3CA activates multiple oncogenic pathways. *Proc Natl Acad Sci U S A.* 106:2835-2840.
160. Srinivasan C., Toon J., Amari L., Abukhdeir A. M., Hamm H., Geraldles C. F., Ho Y. K., Mota de Freitas D. 2004. Competition between lithium and magnesium ions for the G-protein transducin in the guanosine 5'-diphosphate bound conformation. *J Inorg Biochem.* 98:691-701.
161. Dudev T., Lim C. 2011. Competition between Li⁺ and Mg²⁺ in metalloproteins. implications for lithium therapy. *J Am Chem Soc.* 133:9506-9515.
162. Klein P. S., Melton D. A. 1996. A molecular mechanism for the effect of lithium on development. *Proc Natl Acad Sci U S A.* 93:8455-8459.

163. Ryves W. J., Harwood A. J. 2001. Lithium inhibits glycogen synthase kinase-3 by competition for magnesium. *Biochem Biophys Res Commun.* 280:720-725.
164. Ryves W. J., Dajani R., Pearl L., Harwood A. J. 2002. Glycogen synthase kinase-3 inhibition by lithium and beryllium suggests the presence of two magnesium binding sites. *Biochem Biophys Res Commun.* 290:967-972.

VITA

Jesse Lee Goossens was born October 12, 1986, in Denver, CO. He began his undergraduate in August of 2005 at the University of Colorado in Boulder, CO. Here he double majored in biochemistry and molecular, cellular, developmental biology with a minor in chemistry. He began working in the lab of Dr. Dylan Taatjes, in the Department of Chemistry and Biochemistry at the University of Colorado, in his second year of school. He obtained his Bachelors of Arts degree and graduated with departmental honors *Cum Laude* from the department of chemistry and biochemistry in December of 2009. While continuing to work in Dr. Taatjes' lab, he was able to collaborate with Dr. Richard Young of MIT where they were able to publish "Mediator and Cohesin connect gene expression and chromatin architecture" in *Nature* in 2011.

In August of 2012, Jesse began the chemistry Ph.D. program at Loyola University Chicago. He was awarded a graduate fellowship from August 2012 to July 2015 and an NIH research fellowship from August 2015 to August 2018.